Master's thesis in Geography

Geoinformatics

Assessing the cooling impact of tree canopies in an intensively modified tropical landscape

Iris Aalto

2020

Supervisors:

Petri Pellikka
Eduardo Maeda
Janne Heiskanen

Master's Programme in Geography

Faculty of Science

HELSINGIN YLIOPISTO
HELSINGFORS UNIVERSITET
UNIVERSITY OF HELSINKI

Tiedekunta – Fakultet – Faculty	Osasto – Institution – Department
Faculty of Science	Department of Geosciences and Geography

Tekijä – Författare – Author

Iris Aalto

Tutkielman otsikko – Avhandlings titel – Title of thesis

Assessing the cooling impact of tree canopies in an intensively modified tropical landscape

Koulutusohjelma ja opintosuunta – Utbildningsprogram och studieinriktning – Programme and study track

Master's programme in geography, Geoinformatics

Tutkielman taso – Avhandlings nivå – Level of the thesis	Aika – Datum – Date	Sivumäärä – Sidoantal – Number of pages
Master's thesis, 30 credits	6/2020	78 + appendices

Tiivistelmä – Referat – Abstract

Global warming is expected to have detrimental consequences on fragile ecosystems in the tropics and to threaten both the global biodiversity as well as food security of millions of people. Forests have the potential to buffer the temperature changes, and the microclimatic conditions below tree canopies usually differ substantially from the ambient macroclimate. Trees cool down their surroundings through several biophysical mechanisms, and the cooling benefits occur also with trees outside forest. Remote sensing technologies offer new possibilities to study how tree cover affects temperatures both in local and regional scales.

The aim of this study was to examine canopy cover's effect on microclimate and land surface temperature (LST) in Taita Hills, Kenya. Temperatures recorded by 19 microclimate sensors under different canopy covers in the study area and LST estimated by Landsat 8 thermal infrared sensor (TIRS) were studied. The main interest was in daytime mean and maximum temperatures measured with the microclimate sensors in June-July 2019. The Landsat 8 imagery was obtained in July 4, 2019 and LST was retrieved using the single-channel method. The temperature records were combined with high-resolution airborne laser scanning (ALS) data of the area from years 2014 and 2015 to address how topographical factors and canopy cover affect temperatures in the area. Four multiple regression models were developed to study the joint impacts of topography and canopy cover on LST.

The results showed a negative linear relationship between daytime mean and maximum temperatures and canopy cover percentage (R^2 = 0.6–0.74). Any increase in canopy cover contributed to reducing temperatures at all microclimate measuring heights, the magnitude being the highest at soil surface level. The difference in mean temperatures between 0% and 100% canopy cover sites was 4.6–5.9 ˚C and in maximum temperatures 8.9–12.1 ˚C. LST was also affected negatively by canopy cover with a slope of 5.0 ˚C. It was found that canopy cover's impact on LST depends on altitude and that a considerable dividing line existed at 1000 m a.s.l. as canopy cover's effect in the highlands decreased to half compared to the lowlands.

Based on the results it was concluded that trees have substantial effect on both microclimate and LST, but the effect is highly dependent on altitude. This indicates trees' increasing significance in hot environments and highlights the importance of maintaining tree cover particularly in the lowland areas. Trees outside forests can increase climate change resilience in the area and the remaining forest fragments should be conserved to control the regional temperatures.

Avainsanat – Nyckelord – Keywords

agroforestry, airborne laser scanning, canopy cover, Landsat 8, land surface temperature, microclimate, remote sensing

Säilytyspaikka – Förvaringställe – Where deposited

University of Helsinki electronic theses library E-thesis/HELDA

Muita tietoja – Övriga uppgifter – Additional information

HELSINGIN YLIOPISTO
HELSINGFORS UNIVERSITET
UNIVERSITY OF HELSINKI

Tiedekunta – Fakultet – Faculty	Osasto – Institution – Department
Matemaattis-luonnontieteellinen tiedekunta	Geotieteiden ja maantieteen laitos

Tekijä – Författare – Author

Iris Aalto

Tutkielman otsikko – Avhandlings titel – Title of thesis

Assessing the cooling impact of tree canopies in an intensively modified tropical landscape

Koulutusohjelma ja opintosuunta – Utbildningsprogram och studieinriktning – Programme and study track

Maantieteen maisteriohjelma, geoinformatiikka

Tutkielman taso – Avhandlings nivå – Level of the thesis	Aika – Datum – Date	Sivumäärä – Sidoantal – Number of pages
Maisterintutkielma, 30 op.	6/2020	78 + liitteet

Tiivistelmä – Referat – Abstract

Ilmastonmuutoksella on ennustettu olevan kohtalokkaita seurauksia trooppisten alueiden hauraille ekosysteemeille, ja se uhkaa sekä maailmanlaajuista biodiversiteettiä että miljoonien ihmisten ruokaturvaa. Metsien on havaittu puskuroivan ilmaston lämpenemistä, ja mikroilmastolliset olosuhteet puiden latvustojen alla eroavat merkittävästi ympäröivästä makroilmastosta. Puut viilentävät lähiympäristöään monien biofysikaalisten mekanismien avulla, ja viilentävä vaikutus on havaittavissa myös metsän ulkopuolella kasvavilla puilla. Kaukokartoitus tarjoaa uusia mahdollisuuksia tutkia, kuinka topografia ja latvuspeite vaikuttavat lämpötiloihin sekä paikallisesti että alueellisesti.

Tämän tutkimuksen tarkoituksena oli tutkia latvuspeitteen vaikutusta mikroilmastoon ja maan pinnan lämpötilaan Kenian Taitavuorilla. Eri latvuspeiton omaaville paikoille asennettiin 19 mikroilmaston mittaamiseen tarkoitettua sensoria, jotka tallensivat lämpötilaa. Lisäksi käytettiin Landsat 8 lämpöinfrapunasensorin (TIRS) tallentamaa dataa maan pinnan lämpötilasta (LST). Tutkimuksessa keskityttiin erityisesti päiväsajan keski- ja maksimilämpötiloihin, jotka mitattiin lämpötilasensoreilla kesä-heinäkuussa 2019. LST oli tallennettu 4. heinäkuuta 2019 ja laskettiin käyttämällä single-channel -metodia (SC). Lämpötiloja verrattiin korkean resoluution laserkeilausaineistoon (ALS) vuosilta 2014 ja 2015, jotta topografian ja latvuspeitteen vaikutuksia alueen lämpötiloihin voitaisiin tarkastella. Monimuuttujaregressiomallilla tutkittiin topografian ja latvuspeitteen yhteisvaikutuksia.

Tulokset osoittavat negatiivisen lineaarisen suhteen päiväsaikaisten keski- ja maksimilämpötilojen ja latvuspeitteen välillä (R^2 = 0.6–0.74). Kaikki lisäys latvuspeitteen määrään vaikutti negatiivisesti lämpötiloihin jokaisella mittauskorkeudella, vaikutuksen ollessa suurin pintalämpötiloihin. Ero 0 % ja 100 %:n latvuspeitteen alueilla oli keskilämpötiloissa 4.6–5.9 ˚C ja maksimilämpötiloissa 8.9–12.1 ˚C. Latvuspeite vaikutti negatiivisesti myös LST:en kulmakertoimella 5.0 ˚C. Latvuspeitteen vaikutus LST:en oli riippuvainen korkeudesta, ja merkittävä jakolinja löydettiin 1000 metrin korkeudelta, jossa latvuspeitteen vaikutus vuorilla laski puoleen verrattuna alankoihin.

Tulosten perusteella voitiin päätellä, että puilla on merkittävä vaikutus sekä mikroilmastoon että maan pinnan lämpötilaan, mutta on riippuvainen korkeudesta. Tämä osoittaa, että puiden merkitys kasvaa mitä kuumemmasta ympäristöstä on kyse, ja että puuston säilyttäminen olisi erityisen tärkeää alankoalueilla. Metsän ulkopuolella kasvavat puut voivat lisätä kestävyyttä ilmastonmuutoksen edessä tutkimusalueella, ja jäljellä olevat metsäsirpaleet on syytä säilyttää alueellisen lämpötilan hallitsemiseksi.

Avainsanat – Nyckelord – Keywords

kaukokartoitus, Landsat 8, laserkeilaus, latvuspeite, maanpinnan lämpötila, mikroilmasto, peltometsäviljely

Säilytyspaikka – Förvaringställe – Where deposited

Helsingin yliopiston digitaaliset opinnäytteet E-thesis/HELDA

Muita tietoja – Övriga uppgifter – Additional information

Table of contents

List of figures

List of tables

List of abbreviations

ALS	Airborne laser scanning
CC	Canopy cover
DEM	Digital elevation model
DN	Digital Number
FAO	Food and Agriculture Organization of the United Nations
HP	Hemispherical photograph
IPCC	Intergovernmental Panel on Climate Change
LAI	Leaf Area Index
LSE	Land surface emissivity
LST	Land surface temperature
LST’	Topographically corrected land surface temperature
LULCC	Land use and land cover change
LUMO	Lualenyi, Mramba Communal Grazing Area, and Oza Group Ranch
MODIS	Moderate Resolution Imaging Spectroradiometer
NDVI	Normalized Difference Vegetation Index
OLI	Operational Land Imager
MWA	Mono-window algorithm
SC	Single-channel method
SLCA	Stray light correction algorithm
SWA	Split-window algorithm
T	Temperature
T’	Topographically corrected temperature
T_{air}	Temperature measured 15 cm above ground
T_{soil}	Temperature measured 6 cm below ground
$T_{surface}$	Temperature measured 2 cm above ground
TIRS	Thermal infrared sensor
TOF	Trees outside forest

USGS	United States Geological Survey
UTC	Coordinated Universal Time
WGS-84	World Geodetic System

1. Introduction

Food and Agriculture Orgnization of the United Nations (FAO) defines a forest as a land area of at least 0.5 hectares with a minimum canopy cover of 10 percent and trees higher than 5 meters (FAO, 2015). Forests cover a little under 4 billion hectares of Earth's surface, but the number is decreasing, tropical forests experiencing highest rates of forest loss mainly due to agricultural expansion, especially in Africa (FAO, 2016). All trees are not classified as forest. The single trees that are not part of a forest are commonly called trees outside forest (TOF) and by the definition of FAO (2000) include trees on farmland, in cities, along roads and other locations that are not defined as forest. Others define TOF not with FAO's limitations for forests but rather as trees that do not fall into the local perception of forests (Schnell, et al., 2015).

Trees are providers of vital ecosystem services including water regulation, air purification, carbon sequestration, climate regulation and are a source of goods for humans (Martínez, et al., 2018). The provision of ecosystem services is most apparent in forests, but TOF provide the same benefits, yet in a smaller scale. Many ecosystem services take place in the understories where tree canopies are the modifiers of microclimates essential for these functions, such as nutrient cycling and pollination (De Frenne, et al., 2013). In the climate discussion, the role of trees in carbon sequestration is highly emphasized (e.g. Baccini, et al., 2017; Pellikka, et al., 2018), but recent research has shown that the effect of trees in either cooling or warming the climate should be highlighted even more than trees' ability to sequester carbon (Ellison, et al., 2017; Abera, et al., 2020). Carbon sequestration is an indirect way in which trees cause climate cooling, yet an individual tree's direct ability to transpire water and cool the air can equal the power of several air conditioners (Ellison, et al., 2017).

Temperature's relationship with vegetation has been studied extensively. In urban areas, trees are widely studied because of their ability to decrease the urban heat island effect. Methods for quantification of the cooling effect exist and are applied in the studies of urban vegetation (Rogan, et al., 2013; Barbierato, et al., 2019; Ziter, et al., 2019). In rural settings, particulalrly in Africa, the research on trees' local cooling potential is however lacking, in spite of vast amount of studies about forests in general. Forest understories stay cooler in hot macroclimates and warmer when the surrounding temperatures are cold. The effect has different magnitudes in different latitudes, tropical forests experiencing the greatest cooling (Li, et al., 2015; Wanderley, et al., 2019). In forests, the understory microclimate affects the biota more than ambient temperatures outside the forest (De Frenne, et al., 2019; Ellison, et al., 2017). The

temperature buffering provided by tree cover may protect ecosystems from climate change consequences (Zomer, et al., 2016; Ellison, et al., 2017; De Frenne, et al., 2019; Wanderley, et al., 2019), but the magnitude of the buffering is highly affected by the forest area (Ewers & Banks-Leite, 2013). In time, forest microclimates will likely warm like the macroclimate around them, and fragmentation will potentially speed up this process (Ewers & Banks-Leite, 2013; Li, et al., 2016a).

Forests' response to climate warming has mostly been studied at macroscale, despite that the microclimatic impacts of forest canopies are known and recognized (Robinette, 1972; Belsky, et al., 1989; De Frenne, et al., 2019). Microclimate may however be a more beneficial variable when approaching forests' attenuation of macroclimate warming (De Frenne, et al., 2013). Due to the importance of microclimatic conditions in especially tropical species' survival in the facing of climate change, more studies focused below tree canopies are needed (Jucker, et al., 2018). Microclimatic studies require however vast amounts of field measurements which makes them sometimes unpractical or imprecise if applied in larger scale (Prata, et al., 1995). Satellite-derived land surface temperature (LST) is a beneficial method when point-wise field measurements are simply insufficient since it has high spatial coverage and is correlated with air temperature (Jin & Dickinson, 2010; Li, et al., 2013), yet it cannot provide information in the smallest relevant scales (Potter, et al., 2013; Jucker, et al., 2018). Due to the complexity of the issue with climate change, research in both spatial resolutions are needed and so far, the tropical rural areas have been widely underrepresented.

In estimations of vegetation amounts, land cover and land use types or vegetation indices such as the normalized vegetation index (NDVI) or leaf area index (LAI) are common approaches in previous research (Nemani, et al., 1993; Kim, 2013; He, et al., 2019), but recently airborne laser scanning (ALS) has proved to be a more effective method in the computation of structural variables such as canopy height, canopy cover and above-ground biomass (Griffin, et al., 2008; Heiskanen, et al., 2015a; Heiskanen, et al., 2015b; Jucker, et al., 2018). Canopy cover is the most important variable used in defining forests or other land with tree cover (FAO, 2015). With these new technologies, trees can be assessed more precisely in large scale compared to field measurements, and hence together with either field based or remotely sensed temperatures trees' contribution to temperature regulation can be studied in a new way of detailed yet large scale.

Climate change and its consequences are a risk for Taita Hills and the surroundings. Temperatures in Kenya are expected to increase by 2–4 °C by the end of the century (Adhikari,

et al., 2015), and changes in precipitation that will increase the moisture stress of crops are projected as well (MoALF, 2016). Dry spells, heat stress and extreme rain events pose a threat to the area's agricultural production. These phenomena cause crop failure and low yields and hence affect the livelihoods of people (Adhikari, et al., 2015; MoALF, 2016). Farmers in the area have already noticed climate fluctuations that affect their crops and livestock as well (Mwalusepo, et al., 2015). Agroforestry, the combination of trees with agricultural production, is a common practice in the area and has huge potential in increasing climate change resilience (Mbow, et al., 2014; Kuyah, et al., 2019). The preserving of trees in these vulnerable ecosystems is therefore of major importance.

In this thesis, the cooling impact of trees in an intensively modified tropical landscape was studied. The primary aim of this study was to examine the impact of canopy cover percentage on temperature in Taita Hills, Kenya. From the microclimate perspective, the relationship was studied using microclimatological measurements and ALS data. Since microclimate sensors cannot entirely catch the spatial variability of temperatures, satellite thermal data and ALS data were analyzed to examine the relationship between canopy cover and LST. The study aimed to answer the following research questions:

1. What is the magnitude of canopy cover influence on the microclimate in a heterogeneous tropical landscape?
2. What amount of canopy cover is needed for a considerable effect on local land surface temperature?
3. Is the cooling impact of trees the same across altitudinal and macroclimate gradients?

Based on previous research, it is hypothesized that trees do affect temperatures inversely with increasing canopy cover and that the effect is most notable in mean and maximum temperatures.

2. Background

2.1 Trees and climate

2.1.1 Forests, microclimates and climate change

Climatic conditions below forest canopies can differ substantially from the ambient macroclimate and can furthermore be spatially variable within the forest (Chen, et al., 1999). Microclimate means the climatic conditions with low spatiotemporal resolution, usually near the ground or along forest vertical profile, with a scale from centimeters to meters (Zellweger, et al., 2019). Temperatures close to the ground are modified mostly by topographic factors and vegetation structure that produce local microclimates through shading, mixing of air and evapotranspiration in contrast to free air temperatures that are highly controlled by elevation and atmospheric processes (Das, et al., 2015; Zellweger, et al., 2020). The great differences between forest microclimates and the macroclimate outside the forest leads to the forest biota being adapted to the distinct climate conditions prevailing under canopies, microclimate affecting several ecological processes related with species' behavior, distribution and development (Chen, et al., 1999). Near-ground environments, surface air and soil, are also where several ecosystem services by forests take place, such as tree generation, nutrient cycling, and pollination (Chapman, 2012; De Frenne, et al., 2013). In the research on climate change, most observations are based on air temperature measurements at 2 m height in open areas regardless of the fact that these environments differ notably from the habitats occupied by most terrestrial organisms (De Frenne, et al., 2019). Land use and land cover change (LULCC) including deforestation and partial canopy cover loss accelerate effects of climate warming by affecting evapotranspiration, precipitation and carbon balance (Alkama & Cescatti, 2016; FAO, 2016; Ellison, et al., 2017). LULCC has been found to be one of the major drivers of the climate warming both globally and in Africa, and the connection has been studied extensively (Brink & Eva, 2009; Luyssaert, et al., 2014; Alkama & Cescatti, 2016; Li, et al., 2016b; IPCC, 2018; Pellikka & Hakala, et al., 2019; Abera, et al., 2020).

The enhanced greenhouse effect warms the global temperatures, but the impact on microclimates is less understood due to their complexity. Yet, microclimates are affecting the biota in many cases more than the air temperature (De Frenne, et al., 2019). Climate warming changes the composition of organism communities, a phenomenon called "thermophilization", describing the shift from species adapted to lower temperatures to species adapted to higher

temperatures (De Frenne, et al., 2013; Zellweger, et al., 2020). Species with low tolerance for thermal variation in their environment are in high risk of suffering critically of climate warming, which threatens biodiversity especially as majority of the species are tropical (Deutsch, et al., 2008). In several habitats there has been discovered to exist a lag in the response of organisms to climate warming, and recent research has found this to be due to the buffering effect of forest canopies: tree crowns act as an insulation layer that separates the microclimate inside the forest from the ambient air temperatures. (De Frenne, et al., 2013; Zellweger, et al., 2020). Canopy cover's role in increasing climate change resilience of forest floor biota and decreasing the climatic debt can thus be of major importance in conserving forest biodiversity and ecosystem services.

2.1.2 Cooling effect of trees

Trees cool down their surroundings through several biochemical and biophysical mechanisms. All vegetation sequesters carbon in photographsynthesis where the plant takes in CO_2 from the atmosphere and uses the carbon for building material. Forests act as global carbon sinks, meaning that they sequester carbon more than emit. In a global scale, forests affect the atmospheric CO_2 concentrations: deforestation causes the carbon that trees have contained to be released to the atmosphere and the sequestration to stop, which increases the atmospheric CO_2 levels and causes warming (Malhi, et al., 2002). Afforestation and reforestation in turn cause trees to sequester and store more carbon than a site without trees, which decreases the CO_2 in the atmosphere and induce cooling. Locally, trees' cooling effect works mainly through biophysical mechanisms evapotranspiration and albedo (Li, et al., 2016a). In addition, the shading caused by tree canopies intercepting solar radiation affects the microclimates near the ground as the sun flecks move on the forest floor (Chen, et al., 1999; Zellweger, et al., 2020). Albedo describes the ratio of reflected and incoming solar radiation and its effect on climate depends on the surrounding environment and surface reflectance: in most cases in the tropics, trees appear darker than the ground and therefore albedo warms the atmosphere (Li, et al., 2015; Li, et al., 2016).

Evapotranspiration means two processes that happen simultaneously and are difficult to separate: transpiration and evaporation. Transpiration is the chain of events where the plant takes up water from the soil and transpires it through leaf stomata by turning liquid water into water vapor. Transpiration keeps the water flowing through the stem from the roots and transports minerals from the soil at the same time. The sun warms the leaf causing the water inside the leaf to turn into water vapor: this process requires energy that the plant absorbs from

the atmospheric heat, which causes the surrounding air to cool (Allen, et al., 1998). Transpiration cools down also the plant since the water vapor contains heat and when it escapes the heat escapes as well. Evaporation means the transforming of liquid water to water vapor at any given surface, for instance rain droplets from tree stems. Meteorological factors impact evaporation primarily, but vegetation cover is the most important non-meteorological factor to influence the rate of evaporation locally (Jensen, 2007; Li, et al., 2015; Gkatsopoulos, 2017; Abera, et al., 2020). Together these processes are called evapotranspiration. Evapotranspiration rate is affected by soil moisture availability, air and water vapor pressure, wind speed and surrounding temperature. Trees also provide shade that cools down the ground and under-canopy atmosphere, but it is not possible to measure effects of the two phenomena separately. Trees' cooling power varies in time and different latitudes, being the greatest in the tropics near the equator (van Noordwijk, et al., 2014; Li, et al., 2015; Wanderley, et al., 2019) with notable diurnal differences (Belsky, et al., 1989; Bouka Biona, et al., 2001; Li, et al., 2015).

2.1.3 Trees outside forests: agroforestry

In agriculture, the potential of trees has been recognized for thousands of years. This integration of trees with agriculture or animal husbandry is called agroforestry (Figure 1) (Zomer, et al., 2014). Agroforestry is widely practiced in the tropical areas around the world and its ecological and economic benefits are known well: carbon sequestration (Zomer, et al., 2016; Pellikka, et al., 2018), soil quality improvement (e.g. Chander et al., 1998; Dollinger & Jose, 2018), erosion and runoff control (Naharuddin, et al., 2018) and product variability (Leakey, et al., 2005), among others. Agroforestry can decrease rates of deforestation by providing fuel wood grown in the farm and by decreasing the needed land area for agricultural practices (Unruh, et al., 1993). Deforestation is a major problem in Africa, where together with South America forest loss is the highest in the world despite the recent slowing down of the phenomenon (FAO, 2016). Reasons for deforestation in the drylands of Africa is mostly the gathering of fuel wood for household use and the expansion of agriculture (Abdelgalil, 2004). Deforestation accelerates climate change (Fearnside, 2000) which puts the ecosystems and people's livelihoods under threat (IPCC, 2018). The consequences of climate change have been estimated to be most drastic in tropical areas in terms of environment, economy and food security (IPCC, 2018). Agroforestry's potential in climate change buffering has been documented by van Noordwijk, et al. (2014) and more precisely in the African context by Mbow, et al. (2014) who concluded that agroforestry has major potential in moderating extreme climates and improving food security. Yet, agroforestry practices are widely unexploited in many sub-Saharan regions in

Figure 1. Agroforestry farm in Taita Hills, Kenya, combines *Grevillea robusta* with maize.

Africa (Mbow, et al., 2014), and farms with tree cover have decreased remerkably between years 2000 and 2010 (Zomer, et al., 2014). Lack of support and knowledge are the major reasons for the reluctance to establish agroforestry systems (Kuyah, et al., 2019).

Economic and direct benefits are a greater motivation for farmers to adopt agroforestry strategies than environmental benefits like carbon sequestration (Mbow, et al., 2014). People do however recognize that trees impact the surrounding temperatures (Meijaard, et al., 2013). Agroforestry trees provide shade for both livestock and crops (Wilson & Lovell, 2016), but the research on the cooling effect is focused on the impact of shading on crop productivity (Boffa, 1999), and the potential to cool locally is less studied. Belsky et al. (1989) studied the microclimate under the canopies of two different tree species, *Acacia tortillis* and *Adasonia digitala,* in Tsavo National Park (West), close to Taita Hills, and found soil temperature in 5 cm depth to be 5–11 °C and surface temperature even 20 °C lower compared to open grassland. Kohli and Saini (2003) recorded a 10.7 °C amplitude in open field compared to 5.6 °C in forests in India, different agroforestry systems having temperatures somewhere in between. Same pattern was recognized in below-ground measurements with even greater difference. In semi-arid sub-Saharan Africa, Boffa (1999) summarizes that tree cover of common agroforestry tree species has been proved to decrease the temperatures underneath. The behavior of the cooling

impact along the canopy cover gradient is yet not addressed widley. Agroforestry's potential in decreasing climate change vulnerability, of which temperature buffering is an important component, is fortunately emerging more and more as a vital topic in research (Mbow, et al., 2014; Kuyah, et al., 2019).

2.1.4 Canopy cover and canopy closure

There is a variety of terms describing canopies of which some are indistinguishable and some not. Canopy cover and canopy closure have different meanings despite being used as synonyms (Gonsamo, et al., 2013). Jennings et al. (1999) define canopy closure as "the proportion of the sky hemisphere obscured by vegetation when viewed from a single point", while canopy cover is "the proportion of the forest floor covered by the vertical projection of the tree crowns" (Figure 2). (Korhonen, et al., 2006). Therefore, the term canopy closure includes an angular view while for canopy cover it is vertical. This causes using the terms as synonyms is either an under- or overestimation of the other: canopy cover defines a tree canopy as the outer lines of a tree crown, thus ignoring the small gaps within (Korhonen, et al., 2006; Heiskanen, et al., 2015a). Canopy closure instead takes crown gaps into account. Due to the angular view, tree height and slope affect canopy closure unlike canopy cover. In forestry, canopy closure can be stated to often be a more useful measure than canopy cover because it has a direct relationship with light regimen and microclimate (Jennings, et al., 1999; Gonsamo, et al., 2013).

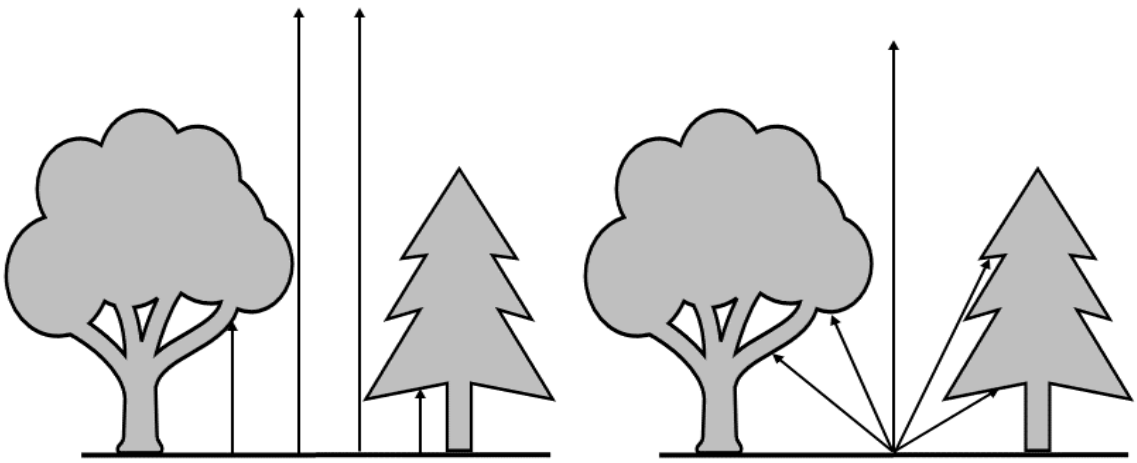

Figure 2. Canopy cover means the vertical projection of tree crowns and canopy closure the proportion of sky hemisphere covered by trees.

Several methods have been established for the estimation of canopy cover and canopy closure in the field, statistics and using remote sensing. These methods include for instance hemispherical photographs, spherical densiometer, crown relascope, Cajanus tube, inventories, ocular inspection and ALS (Jennings, et al., 1999; Korhonen, et al., 2006; Paletto & Tosi, 2009; Heiskanen, et al., 2015a). For an accurate canopy cover or canopy closure, field measurements must always be incorporated in the estimations (Korhonen, et al., 2006).

Hemispherical photographs are images of the sky hemisphere taken with a 180° angular fisheye lens where the pixels are classified using a threshold value into dark and light, namely trees and sky pixels. The proportion of sky (gap fraction) is then calculated from these pixels. Canopy closure can be calculated with 1-gap fraction. (Jennings, et al, 1999). Estimation of canopy cover from hemispherical photographs is also possible. For this, a viewing angle of 30° causes least bias in the estimation (Heiskanen, et al., 2015b). However, it is always an underestimation of canopy cover using hemispherical photographs due to the gaps in tree canopies (Paletto & Tosi, 2009; Heiskanen, et al., 2015a).

ALS suits canopy assessment better in landscape level than time consuming field methods (Alexander, et al., 2013) and gives high accuracies for canopy cover estimations (Heiskanen, et al., 2015a). Depending on pulse density, it suits both canopy cover and canopy closure retrieval, yet failure of detecting all the gaps in canopies results in better accuracies for vertical canopy cover than canopy closure (Alexander, et al., 2013). It may cause a slight overestimation of canopy cover due to the scan angle being off-nadir (Korhonen, et al., 2011).

2.2 Remote sensing of temperature

2.2.1 Principles of electromagnetic radiation and satellite-derived land surface temperature

Satellite-derived LST can be computed from the thermal radiation emitted from the Earth's surface and captured by a thermal infrared (TIR) sensor onboard a satellite (Li, et al., 2013; Simó, et al., 2018). LST has its physical basis on the laws of electromagnetic radiation. A blackbody is a theoretical object that radiates and absorbs energy at maximum rate per unit area at each wavelength at given temperature. The sun can be considered a 6000 K blackbody that acts as the initial source of electromagnetic radiation on Earth (and that is recorded by remote sensing sensors). The kinetic heat that an object produces is converted to radiant energy. The radiant energy exiting an object is called radiant flux (Φ).

The kinetic and radiant temperatures of objects are strongly correlated, meaning that the thermal radiant energy can be measured with remote sensing sensors. The correlation is not perfect, and the radiant temperature is always less than the true temperature of an object. There is no perfect blackbody existing on the Earth, thus the amount of energy that an object radiates depends on the properties of the object. Soil, vegetation, water and buildings have all different amounts of radiated energy (Jensen, 2007). This quality is called emissivity (ε) and is the ratio between the actual radiance emitted and the radiance of a blackbody at the same temperature. Water content is one major factor in determining emissivity because water absorbs strongly thermal radiation. Emissivity of soil depends on soil moisture and increases the most with increasing vegetation cover (Van de Griend & Owe, 1993). Due to this relationship, the Normalized Difference Vegetation Index (NDVI), which is based on the reflectance properties of green vegetation in the red and near-infrared spectral regions and is utilized to quantify vegetation, can be used in estimating effective land surface emissivity in satellite image pixel scale (Van de Griend & Owe, 1993; Valor & Caselles, 1996).

The thermal radiation is emitted as thermal infrared radiation in the spectrum 3.0–14 μm. The atmospheric window for thermal infrared means the region of the spectrum where the atmosphere lets the thermal infrared radiation to transmit with little disturbance by factors such as water vapor, ozone or carbon dioxide (Jensen, 2007). A remote sensing sensor is made sensitive to a part of the window so that most of the emitted radiation can be recorded. Thermal infrared sensors on satellites record usually radiation in the region 10.5–15.5 μm. The dominant wavelength means the wavelength that an object is mostly radiating. Depending on the object or phenomenon to be examined, the sensor's sensitivity to that wavelength should be considered (Jensen, 2007). The retrieval of LST from satellite TIRS is based on the inverse of Planck's law (Jin & Dickinson, 2010).

2.2.2 Land surface temperature in forest studies

Using satellite thermal data in environmental studies roots back to the 1960's and was first used for the estimation of sea surface temperature by McMillin (1975) before the development of algorithms suitable for LST retrieval (McMillin, 1975; Prata, et al., 1995). LST most commonly refers to the skin temperature of the Earth, comprising of the top canopy layer including buildings (Jin & Dickinson, 2010; Bense, et al., 2016). LST signal is affected by canopy properties and ground surface, the canopy top contributing the most (Bense, et al., 2016). LST drives the exchange of long-wave radiation at the Earth's surface and is a paramount factor in the processes of water balance and energy balance as well as evapotranspiration. It affects

directly the surface air temperature, soil moisture and vice versa and consequently the microclimate, which in turn controls the habitat of flora and fauna (De Frenne, et al., 2013; Bense, et al., 2016; Zellweger, et al., 2019). Since LST varies greatly over time and space, ground measurements are not suitable for larger scale evaluation of LST: significant differences can occur just in a scale of centimeters, which causes the spatial sampling often to be too sparse for sufficiently representative measurements (Prata, et al., 1995). For this reason, the thermal infrared bands of satellite sensors, such as Landsat 8 or MODIS, are becoming more prominent when estimating regional and global LST (Prata, et al., 1995; Li, et al., 2013; Li, et al., 2016b). Satellite-derived LST is the average thermal radiation recorded by a sensor in the scale of the sensor's pixel size and separates therefore distinctly from pointwise *in situ* measurements of temperature.

Deforestation and LULCC have been extensively represented in the research on LST (Li, et al., 2015; Li, et al., 2016b; Tran, et al., 2017). Wanderley et al. (2019) used Landsat 5 to study LST's relationship with anthropized area fraction in Brazil. They compared the non-forested area percentage to LST and found that 100 % decrease in anthropized area decreased LST by 3.8 °C. Another study in Brazil by van Leeuwen et al. (2011) computed the difference between 0 % forest cover and 100 % forest cover to be 6.8 °C in their study area and pronounced LST to be a valid variable in land cover change detection. Li et al. (2015) computed a 4.4 °C difference in LST between forest and open land in the tropics in their study on global effect of forests on LST, while Nemani et al. (1993) showed a relationship between NDVI-based canopy cover and LST in North America. In African context, research on trees' potential on LST control has been limited and more studies on the topic are needed. Abera et al. (2019, 2020) found LST consistently increasing after the conversion from forest to cropland, and Mildrexler et al. (2011) discovered both large forests and smaller patches regulate LST in Central Africa. Land cover change in urban context has been studied by Akinyemi et al. (2020), who found LST to increase as a consequence of deforestation.

2.2.3 Landsat 8 land surface temperature

Landsat 8 was launched in 2013 and it orbits the Earth in a sun-synchronous orbit at 705 km. The temporal resolution is 16 days and scene size 185 km x 180 km. It carries two sensors: the Operational Land Imager (OLI) and the Thermal Infrared Sensor (TIRS). OLI sensor has 9 spectral bands (bands 1–9), covering the region of visible light, infrared, middle- and short-wave infrared, as well as has bands designated for cirrus and coastal studies. The spatial resolution is 30 m except the panchromatic band of 15 m resolution. The TIRS sensor has two

thermal infrared bands (bands 10–11) that have a spatial resolution of 100 m. Unfortunately, shortly after the launch a stray light problem was detected with TIRS band 11, and it is thus not recommended by United States Geological Survey (USGS) to use for scientific purposes (USGS, 2017).

Due to the various factors affecting LST, the accurate estimation of LST is a challenge (Simó, et al., 2018; Li, et al., 2013). To retrieve LST from Landsat 8, several methods have been developed. The most general understanding classifies the different methods to single-channel methods (SC), split-window algorithms (SWA) and mono-window algorithms (MWA). The SC was developed by Juan and Sobrino (2003) and improved by Jiménez-Muñoz et al. (2009). This method can be used on sensors with only one thermal band and requires minimum input parameters, namely land surface emissivity (LSE) and water vapor content. The mono-window algorithm was proposed by Qin et al. (2001) and requires only one thermal band like SC. The algorithm works with three parameters: the effective mean atmospheric temperature, LSE and atmospheric transmittance. SWA in turn was developed by McMillin (1975) for the estimation of sea surface temperature and needs two thermal bands. It is not as dependent on atmospheric variables as the other methods, needing only two parameters: atmospheric transmittance and LSE. Rozenstein et al. (2014) improved the algorithm to suit Landsat 8.

Wang et al. (2019) compared the SWA, MWA and SC and recommend the use of split-window algorithm in hot and humid conditions since it is the least sensitive to errors in the input parameters. Meng et al. (2019) conclude that high water vapor contents make the SC perform poorly and recommend the use of SW because in theory it is the most reliable method globally. However, despite Landsat 8 having two thermal infrared channels which would make the use of the split-window algorithm possible, the USGS does not recommend the use of band 11 due to the problems with stray light. Montanaro et al. (2015) developed a stray light correction algorithm (SLCA) for band 11 that the USGS started to implement in the processing of Landsat 8 TIRS data in February 2017 (USGS, 2017). Several studies have verified the results for the SWA (García-Santos, et al., 2018; Meng, et al., 2019; Wang, et al., 2019) but before more research has been done on the accuracy and reliability of SLCA, the use of band 11 remains questionable.

Landsat 8 TIRS has been widely studied using different LST retrieval algorithms (e.g. Jiménez-Muñoz, et al., 2014; García-Santos, et al., 2018; Meng, et al., 2019; Wang, et al., 2019). As is the case with LST product usage in general, also Landsat 8 TIR imagery has mostly been utilized in research on urban heat islands. For example, Barbierato et al. (2019) and Tran et al.

(2017) studied the urban heat island effect with Landsat 8 bands 10 and 11, and band 10, respectively. Studies using Landsat 8 TIRS imagery in rural, tropical environments are so far limited. He et al. (2019) used Landsat 8 imagery to study the effect of topography and vegetation on LST in a mountainous area in China using band 10. Their results showed the altitudinal lapse rate to vary greatly depending on aspect, slope, vegetation cover and season. Abera et al. (2020) studied LST change after the conversion of bushland to cropland in Taita Hills utilizing Landsat 8 TIR data.

2.2.4 Remote sensing of microclimate

Remote sensing of microclimate is challenging due to the coarse resolution of thermal infrared instruments carried by satellites (De Frenne, et al., 2019; Jucker, et al., 2018) and in forested areas the thermal signal consists mostly of the uppermost layer of canopies and hence does not capture the ground temperature signal (Jucker, et al., 2018; Bense, et al., 2016; Mildrexler, et al., 2011). The knowledge about satellite TIR sensors' ability in capturing the prevalent temperatures below canopies is lacking and more research is needed on the topic of satellite imagery's usefulness in microclimate studies (Zellweger, et al., 2019). However, LST can provide valuable information on regional to global scales despite the resolution being too low for studies about the smallest organisms (Potter, et al., 2013).

Microclimate is modified mostly by two variables: topography and vegetation. Despite having been widely used as the indicator for vegetation amounts in studies about vegetation's and temperature's relationship, the NDVI is not the best measure for vegetation quantity (Weng, et al., 2004). Airborne laser scanning has proved to be useful in the mapping of factors affecting microclimate, providing high-resolution, accurate models on the topographic conditions and vegetation structure in the form of different digital terrain models (DTM), such as digital elevation models (DEM), digital surface models (DSM) or canopy height models (CHM) (Zellweger, et al., 2019). These methods provide new ways to study detailed microclimate, yet research on canopy understory circumstances using ALS and temperature data is lacking. One of the pioneering studies by Jucker et al. (2018) used canopy metrics and topographic variables obtained from ALS data to study the impact on field measured air temperature and water vapor and found mean and maximum temperatures to decrease with increasing canopy height. More research on the topic particularly in tropical regions is urgently needed as the fragile ecosystems close to the ground are in high risk of degrading with climate warming.

3. Study area

The Taita Hills are located in the Taita-Taveta County in the Coast Province of south-eastern Kenya, approximately 200 km from Mombasa and 360 km from the capital city Nairobi. The study area comprises of the hills and the lowland areas of Maktau, LUMO Community Wildlife Sanctuary and Taita Hills Wildlife Sanctuary, that were laser scanned in 2014 and 2015 by University of Helsinki for various projects, such as BIODEV and Taitawater (Heiskanen, et al., 2015b; Adhikari, et al., 2017), totaling roughly 1100 km^2 (Figure 3). The elevation in the study area varies from 550 m a.s.l. to the highest peak of the hills, Vuria, at 2208 m a.s.l.

Climate in the study area is mainly semi-arid, the hills receiving more rainfall than the plains. Two rainy seasons control the climate and growing seasons in the area: Long rains from March to June and Short rains from October to December (Pellikka, et al., 2013). According to the Kenya Ministry of Agriculture, Livestock and Fishery (MoALF), annual precipitation averages 650 mm, but differences between highlands and lowlands is notable, lowlands receiving 500 mm annually compared to 1500 mm in the hills (MoALF, 2016). Mean temperature is 23 °C, in the highlands 18 °C (MoALF, 2016).

Agroecologically, Taita-Taveta County is divided into eight zones based on relief and mean annual rainfall (MoALF, 2016). Vegetation in the study area varies from dry savanna and shrubland in the lowlands (Figure 4) to indigenous cloud forests in the upper hills. The landscape in the hills is dominated by intensive agriculture and small forest segments (Figure 5). TOF make up a remarkable amount of the area's total above-ground carbon and play an important part in carbon sequestration in the area (Pellikka, et al., 2018), especially because Taita Hills have experienced massive indigenous forest loss since 1950's (Pellikka, et al., 2009). Yet, due to exotic plantation, the total forest cover has roughly remained the same (Pellikka, et al., 2009). The remaining forest are highly fragmented, area ranging from 1 ha to 200 ha, total forest area in Taita Hills being approximately 6 km^2 (Pellikka, et al., 2009). Forest loss is a major threat to area's biodiversity, as Taita Hills are identified as a biodiversity hotspot (Pellikka, et al., 2013).

Agriculture is the main livelihood in the area and the dominant land use type. Most of the farms in Taita-Taveta County are small-scale subsistence farms sized on average 0.4 to 4.8 ha, lowland farms being bigger than the hill farms (MoALF, 2016). Over 83 % of farms rely solely on one income source, maize being the most common agricultural crop being cultivated in over 90 % of farms (MoALF, 2016). Other important crops are beans, cowpeas, green grams,

sorghum, pigeon peas, cassava and sweet potatoes. Main livestock held is chicken, other important livestock are beef and dairy cattle, sheep, goat, camel and pig (MoALF, 2016). Agroforestry is a common practice in the area.

The cloud forests on the hills act as a water tank for the lowland areas (Pellikka, et al., 2013). According to Erdogan et al. (2011), Taita Hills are predicted to experience tree cover loss in the form of agricultural expansion by 2030, which is a 40 % increase in cropland area from year 2003. The expansion will mostly take place in the lowlands and the foothill (Maeda, et al., 2010a). Soil erosivity has been observed to increase in the Taita Hills between 1987 and 2003, and it is predicted to increase more in the future, especially in the highlands, where availability of topographically favorable spaces for agriculture is decreasing (Maeda, et al., 2010a; Erdogan, et al., 2011). However, based on Pellikka et al. (2018), the land cover change trend seemed to slow down as 2011 and carbon stocks increased from 2003.

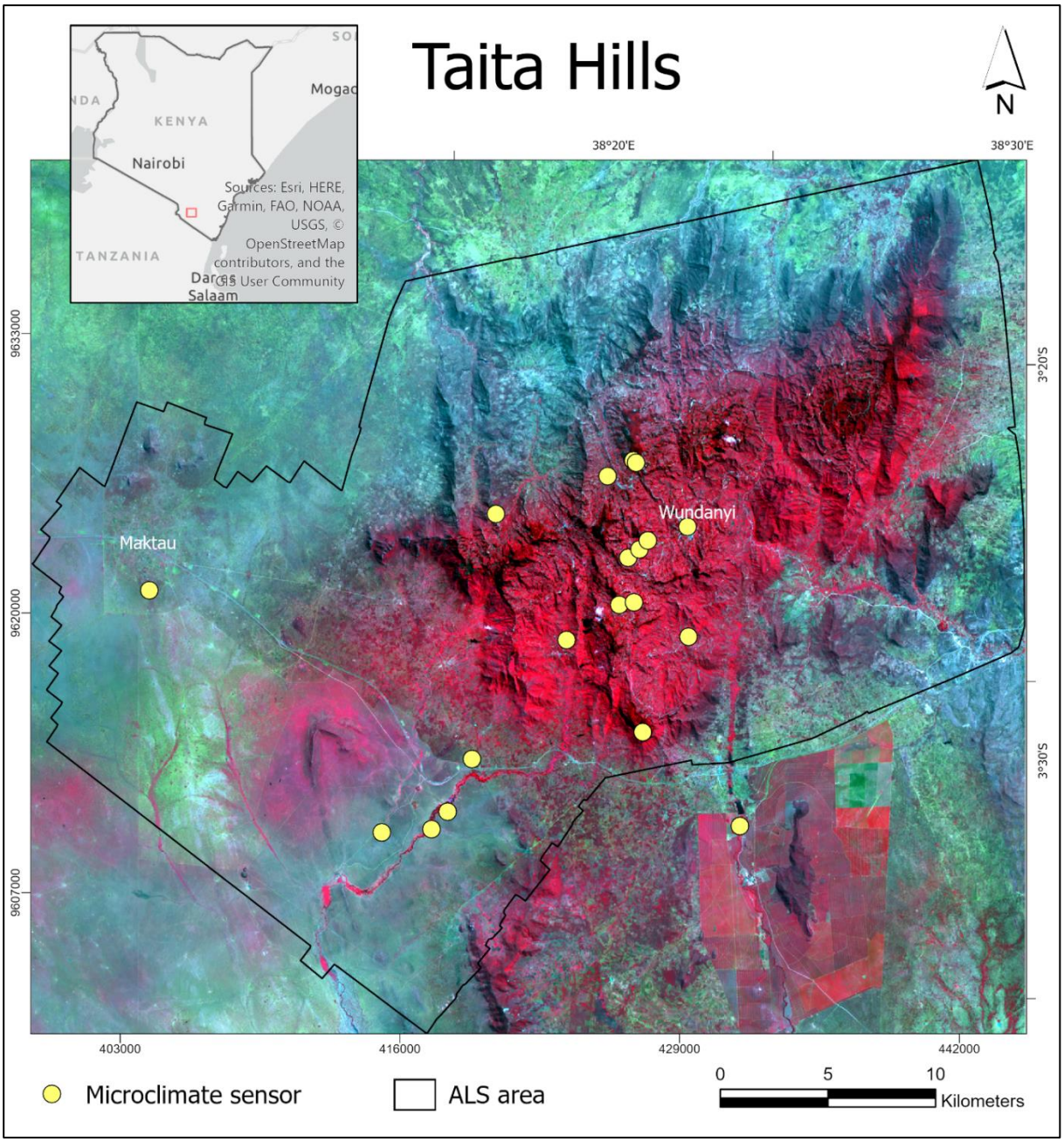

Figure 3. Location of study area and microclimate sensors in Taita Hills. The base map is a false color Landsat 8 OLI image from 4th of July 2019.

Figure 4. Savanna bushland landscape in the lowlands close to Maktau in 1200 m a.s.l.

Figure 5. Highland agriculture and agroforestry in 1560 m a.s.l.

4. Material and methods

4.1 Airborne laser scanning data

This study used ALS-based Digital Elevation Model (DEM) raster of 1 m resolution and a canopy cover raster of 30 m resolution. The Taita Hills were laser scanned in February 2014 and 2015 and the lowland areas in March 2014. The mean pulse density in the highland scannings was 3.1 pulses/m^{-2} and mean return density 3.4 returns/m^{-2}, for the lowlands the pulse density was 1.04 pulses/m^{-2}. The pre-processed point clouds of the hills were processed by Adhikari et al. (2017) who produced the DEM, and the canopy cover raster was produced and provided by Adhikari (2017). The ALS data used in this study was the same as in Adhikari et al. (2017) and partially in Heiskanen et al. (2015b).

DEM was utilized to derive topographic factors to be used in the analysis of the satellite image. DEM was resampled to 30 m resolution to fit the Landsat 8 scene and to improve computer processing efficiency. ArcGIS Pro spatial analyst tools were used to derive slope degree (°) and slope aspect (°). Aspect pixels were then classified to eight classes: 0-22.5 ° as north, 22.5–67.5 ° as northeast, 67.5–112.5 ° as east, 112.5–157.5 ° as southeast, 157.5–202.5 ° as south, 202.5–247.5 as southwest, 247.5–292.5 ° as west, 292.5–337.5 ° as northwest and 337.5–360 ° as north.

4.2 Microclimate sensors

4.2.1 TOMST TMS-4 sensors

Twenty TOMST TMS-4 soil sensors were installed in the Taita Hills area during field work in May-June 2019. The TMS logger is a dagger-shaped and sized sensor that is placed in the soil surface at about 10 cm depth (Wild, et al., 2019). It measures soil temperature at three different levels: air temperature (T_{air}) at 15 cm above ground, surface temperature ($T_{surface}$) at 2 cm above ground and soil temperature (T_{soil}) at 6 cm depth. They also have soil moisture sensors. The sensors log temperature and moisture every 15 minutes. During the period of this study, one sensor was damaged shortly after installation and could not be used, leaving the total number of TMS sensors to 19. The study period was 28 days, from June 13 to July 10, 2019.

The location of each sensor was measured as UTM coordinates using Garmin Etrex GPS data logger. Elevations recorded by the GPS device were used in the analysis. At each site, slope angle and aspect were measured using an inclinometer and a compass. The sensor data was

collected with a laptop and a TOMST adapter, which was connected to the laptop with a USB portal. The procedure of attaching the sensor to the adapter and downloading the data took only a few seconds. The data was saved as .xlsx table format.

4.2.2 Study sites

The criteria for determining the site for TMS logger was the following: it represented the desired canopy cover; the site was as homogenous as possible; it was as flat as possible; it was safe; and the access was easy. The canopy cover raster by Adhikari (2017) of Taita Hills was the basis for choosing the locations for the TMS loggers. The 30-meter raster was generalized to 100-meter resolution to match the cell size of the Landsat 8 LST image. The tropical mountainous areas of Taita Hills are very heterogeneous in the scale of 100 meters. In order to find the most homogeneous sites, standard deviation of canopy cover was calculated for each new 100-meter square based on the 30-meter pixels to assist to find the most representative pixels. After this, canopy cover was classified into seven different classes based on Jenks's natural breaks. The reasoning for seven classes was that there were in total twenty TMS sensors and seven classes gave room to put three sensors in almost every class. The classes (%) were 0–5, 5–16, 16–27, 27–40, 40–55, 55–74 and 74–100. The new raster values were the canopy cover classes (Figure 6). The goal was to have at least two sensors to represent every class, preferably both in the highlands and in the lowlands. In many cases safety and accessibility had to be considered first, since many places that seemed perfect on the map were impossible to access or had high safety issues. All microclimate sensors were covered with a cage and in risky areas also other measures were conducted to protect the sensors (Figure 7). The safety of the person to go retrieve data had to be considered as well. Ideally, every class would have been represented in both lowlands and highlands, but suitable sites for medium canopy cover classes were lacking in the lowlands.

The final 19 sites are listed in Table 1. The analysis based on the original canopy cover of the site and not the classification. One site (Mwatate riverine forest) was lying outside the ALS area, meaning there is no ALS-based canopy cover computed and canopy cover based on hemispherical photography (from hereafter CC_{ALS} and CC_{HP}) has been indicated to that plot instead, except in the comparison between CC_{ALS} and CC_{HP}, where the site was left out completely. The Mwatate riverine site was needed in order to have two closed canopy forest sites in the lowlands.

Table 1. Microclimate sensor sites.

Site	Canopy cover (%)	Altitude (m a.s.l.)	Description
Ngerenyi campus	44	1572	Macadamia forest
Dembwa	13	1083	Agroforestry
Mlima wa simba	8	923	Bushland
Sarova grassland	0	900	Grassland
Saghaighu	16	1611	Terrace field
Bura riverine forest	79	880	Riverine forest
Wesu maize field	0	1562	Maize field
Wundanyi	31	1372	Close to river and buildings
Werugha	8	1613	Macadamia, agroforestry
Ngangao indigenous forest	94	1775	Indigenous forest
Ngangao eucalyptus forest	77	1778	Eucalyptus forest
Wesu	53	1642	Forest edge
Wuchichi	36	1595	Agroforestry
Sarova enclosure	0	901	Bushland
Chawia	97	1562	Indigenous forest
Mwatate riverine forest	63	884	Riverine forest
Bura	68	1095	School campus
Mwanda	2	1653	Bushland behind school
Maktau	19	1044	Bushland

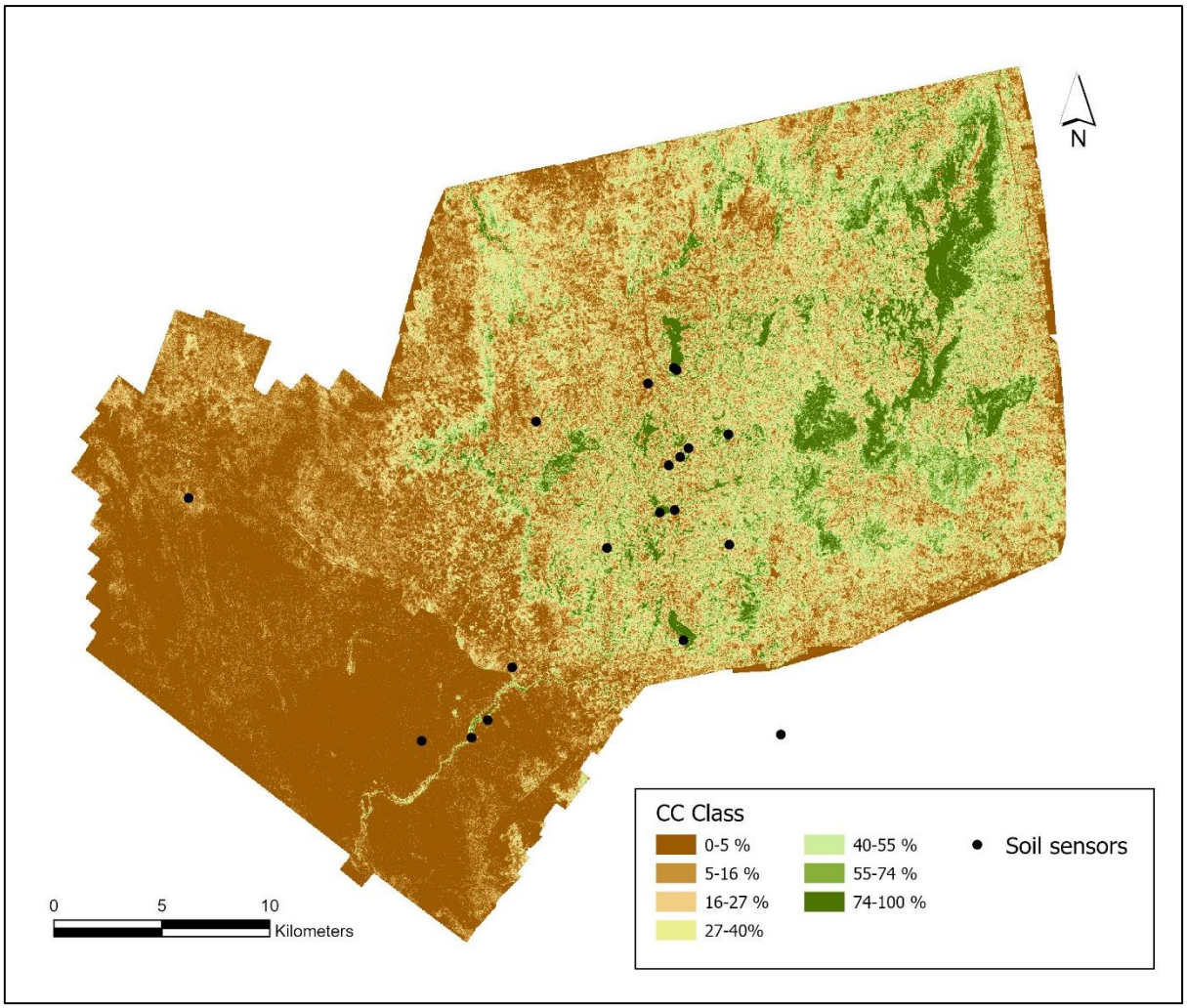

Figure 6. Classified ALS-based canopy cover in Taita Hills. Original canopy cover raster by Adhikari (2017).

Figure 7. Safety measures to protect the TOMST TMS-4 sensors. A) Bura riverine forest sensor was surrounded with stones to protect it from elephants. B) Contact details written on top of Wundanyi sensor. C) Elephant protection in Sarova grassland site.

4.2.3 Field data processing

The field data from the TOMST TMS-4 loggers was processed with R programming language in the open software RStudio. The script for the reading of data was by Maeda (2019) and modified to fit the data collected in this study. The data was filtered both for the date of the satellite overpass (July 4, 2019) and for the full measuring period of 28 days when there was data available for all sensors. Daytime aggregates were generated to be used in the analysis, meaning data collected between sunrise and sunset, local time 06.30–18.30 UTC + 3h. Maxima were calculated as the mean of daily maxima. Minimum temperatures were calculated as the mean of minimum temperatures based on the 24-hour cycle.

4.2.4 Topographic correction

Topography's effect on temperature was quantified and later removed to highlight canopy cover's impact on microclimate. Topographic variables considered in this study were altitude (m), slope (°) and aspect. Aspect was a categorical variable with nine classes indicating compass points, one class being flat ground. The relationships between the variables were studied first with Pearson's correlation. Small sample size made the inclusion on aspect in the analysis

unreasonable, hence it was finally left out of. The explanatory variables altitude (Figure 8), slope and canopy cover were fit in a multiple regression model. Altitude and canopy cover were the only statistically significant variables ($p < 0.001$). The variance inflation factor (VIF) for slope was 4.93, indicating multicollinearity in the model. Because the VIF was almost 5, which is considered as the limit for acceptable VIF values (Akinwande, et al., 2015), only altitude and canopy cover were included in the final model. This increased the adjusted R^2 from 0.821 to 0.829 (T_{soil}), 0.879 to 0.886 ($T_{surface}$) and 0.911 to 0.914 (T_{air}). Finally, the daytime mean temperatures for the full study period were corrected according to the altitudinal lapse rates, which were 7.26 °C/km (T_{soil}), 8.09 °C/km ($T_{surface}$) and 8.06 °C/km (T_{air}). In the case of diurnal comparison of canopy cover's cooling power, separate lapse rates were applied for each hour of day and varied from 6.1 °C to 8.2 °C/km in T_{soil}, 3.8 °C to 10.4 °C/km in $T_{surface}$ and 3.3 °C to 10.2 °C/km in T_{air}.

4.2.5 Statistical analysis

Statistical analysis, including descriptive statistics, linear regression and Pearson's correlation, were conducted to find the relationships between temperature, canopy cover and topographic variables. The focus of descriptive statistics was on mean, maximum and minimum temperatures computed for the full study period. Temporal analysis explored the variation in daily mean temperatures as well as for the hourly means. Pearson's correlation was computed to see if field temperatures correlated with canopy cover and if the correlation was statistically significant. The coefficient of determination (R^2) describes the explanatory power of a model and was used to study how much of the temperature variations could be explained with canopy cover and topographic factors. R^2 of T_{soil}, $T_{surface}$ and T_{air} were compared to explore if canopy cover affected temperatures differently at soil and air level. Standard deviation describes the variation occurring in the data set and was calculated to study the temperature variations in the sites. The results were compared between the different canopy covers.

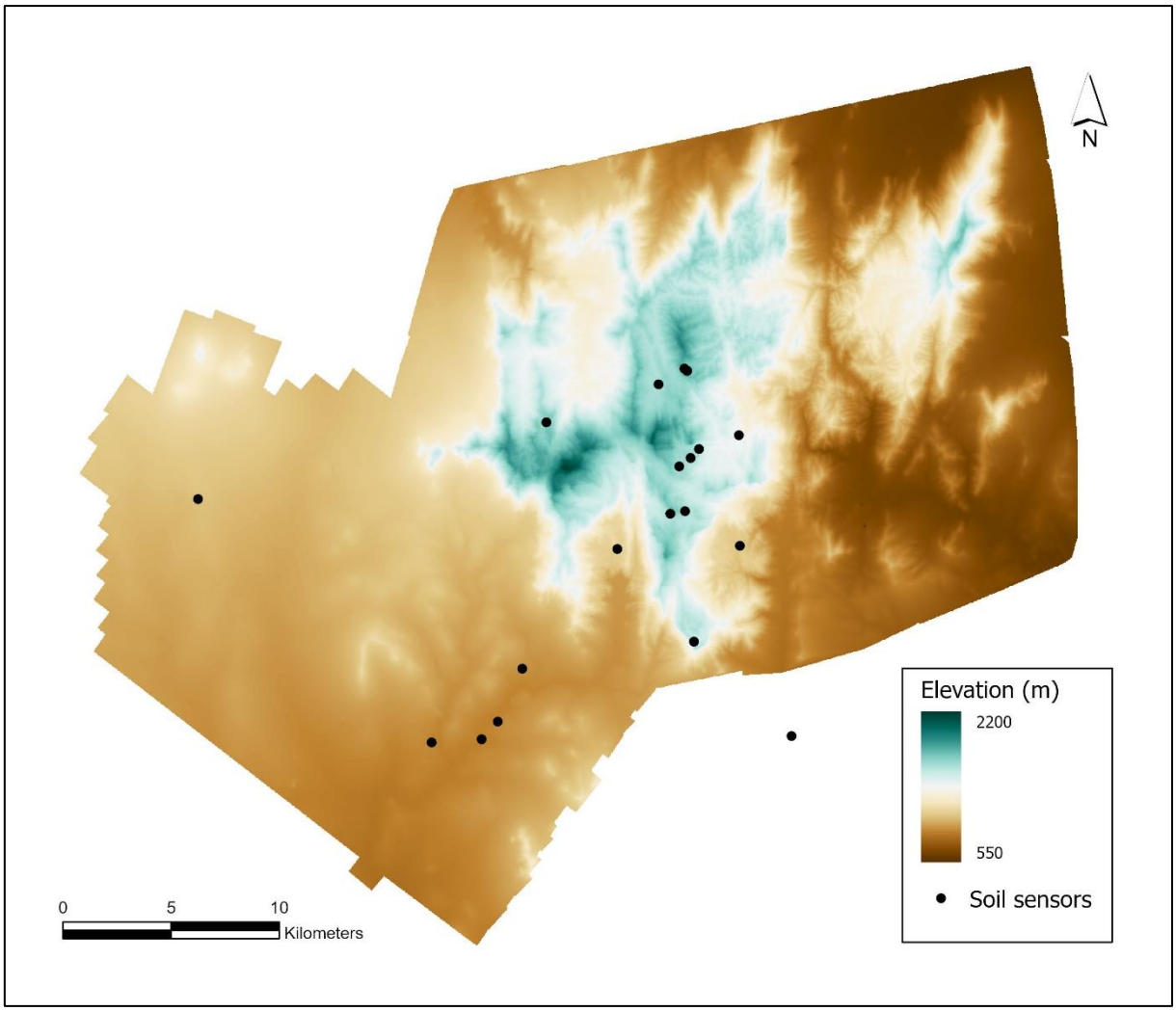

Figure 8. Elevation map of Taita Hills with microclimate sensor locations. DEM by Adhikari et al. (2017).

4.3 Hemispherical photographs

4.3.1 Data collection

Hemispherical photographs (Figure 9) were taken at every microclimate sensor site. The purpose of the images was to calculate canopy cover at the sites for the validation of CC_{ALS}, which was computed years earlier than this study was conducted. The camera in use was Nikon D5000 DSLR and the lens Sigma 4.5 mm F2.8 EX DC HSM Circular Fisheye. The camera was attached to a tripod during the taking of photographs. The photographs were taken at two different heights: as close to the actual sensor level as possible, meaning the lowest possible tripod adjustment, which was around 60 cm, and at eye-level around 130 cm. Photographs were taken at eye-level also to every intercardinal direction 15 meters away from the sensor. The camera was adjusted looking upward with the top of the camera pointing north. Two images at every height and direction were taken with different settings: first image on Program mode with automatic aperture and shutter speed, and the second on Manual mode with the rest of the settings staying the same as in picture one except shutter speed was reduced to half of the first mage. The ISO value was set as constant 500. The purpose of the smaller shutter speed was to reduce the impact of light conditions that were not optimal, meaning direct sunlight that causes overexposure of images which in turn makes them difficult to analyze. Optimally, the photographs should be taken under constant cloud cover or at the dawn or dusk (Pellikka et al., 2000), however due to the timetable, waiting for better light conditions at some sites was not possible, thus some images were overexposed.

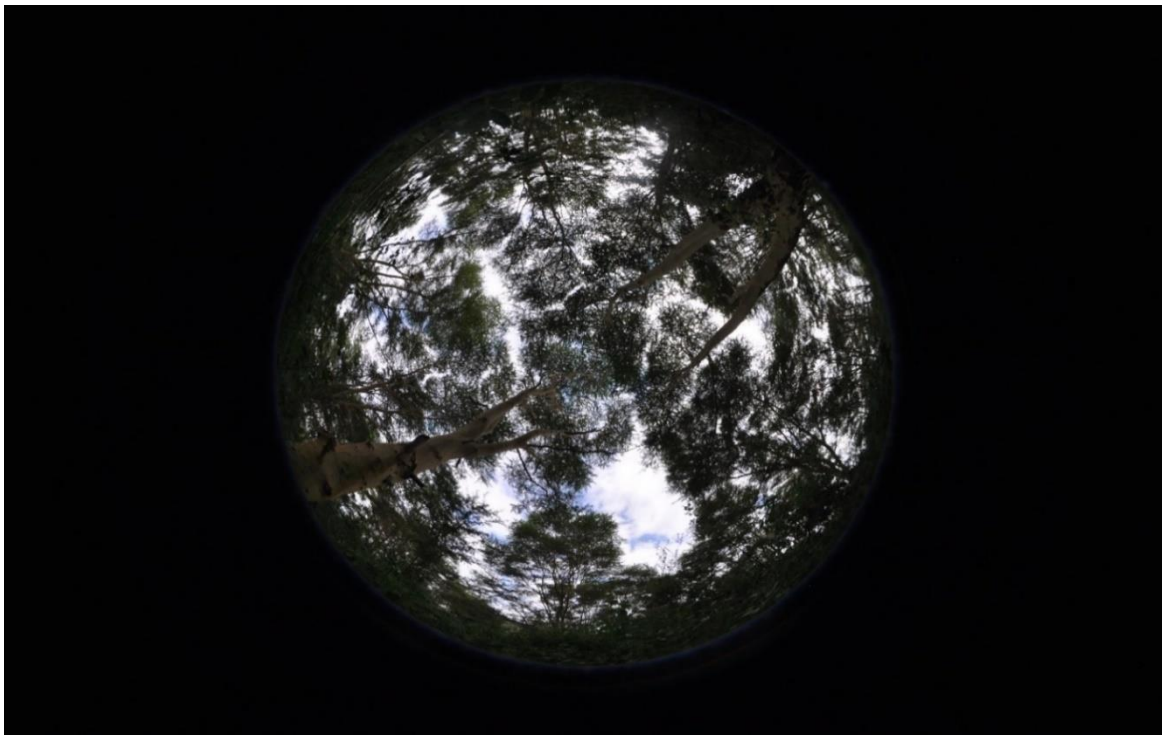

Figure 9. Hemispherical photograph taken in the Mwatate riverine forest site on June 10, 2019.

4.3.2 Canopy cover

The hemispherical photographs were analyzed in the software Hemisfer (WSL; version 2.2) (Schleppi, et al., 2007; Thimonier, et al., 2010). From the two images the less exposed one was used in the analysis. For the calculation of canopy cover, the images taken from eye-level were used since they were more comparable to the ALS-based canopy cover and the photographs in cardinal directions were all taken at eye-level. The image pixels were classified to sky and canopy by determining a threshold value to separate dark and light pixels in the image. For most images, the automatic threshold method by Nobis and Hunziker (2005) was used. In the case of some images, the algorithm was clearly producing errors due to overexposure and direct sunlight, therefore the algorithm by Ridler and Calvart (1978) was applied or a manual threshold was determined. Only the blue band was used in the analysis, apart from photographs where the classification was failing and using all the bands produced the best result (Heiskanen, et al., 2015a). The gamma correction was $\gamma = 2.2$. Only the zenith angle range of 0-15° was analyzed since errors in canopy cover accuracy increase with larger angles (Paletto & Tosi, 2009). The canopy cover was computed by calculating an average of 1-gap fraction of the five measurements and this gave a plot-wise canopy cover (Heiskanen, et al., 2015b). Finally, CC_{HP} and CC_{ALS} were compared using Pearson's correlation and a Student's t-test.

4.4 Satellite image

4.4.1 Landsat 8 scene

To observe canopy cover's effect on LST in the whole area of Taita Hills, a Landsat 8 OLI TIRS satellite image was analyzed. Landsat 8 provides thermal data in a resolution of 100 m but it is resampled to 30 m to fit the OLI images. The image used in the study is a Level-1 scene obtained July 4, 2019 at approximately 10:30 UTC + 3h. Level-1 images are radiometrically and geometrically corrected. The projection for terrain correction is UTM-WGS84 coordinate system and the orthorectification is carried out with ground control points and DEM. The sun azimuth angle was 45.6° and sun elevation 52.1° and were retrieved from the metadata**.** The reasoning for choosing the image was that it was the only cloudless scene for the study area for the study period, and still the total cloud cover of the scene was 11.67 %. The image was downloaded from Earth Explorer by USGS free of charge.

The workflow in Figure 10 follows the methodology of Ndossi and Avdan (2016), who developed an experimental QGIS plugin for LST retrieval. The plugin works in the QGIS version 2. The processing was done in RStudio with the raster-package. An LST map of the results was created in ArcGIS Pro.

4.4.2 Data pre-processing

The Landsat 8 scene was clipped and radiometrically and atmospherically calibrated. The image is a raster file that is comprised of digital numbers (DN) that represent the different radiance values. To convert the DN to meaningful physical units, they were first converted to at-sensor spectral radiance with Equation 1:

$$L_\lambda = M_L Q_{cal} + A_L \quad (1)$$

L_λ = At-sensor spectral radiance (W sr^{-1} m^{-2} μm^{-1})

M_L = Radiance multiplicative scaling factor for the band from the metadata

A_L = Radiance additive scaling factor for the band from the metadata

Q_{cal} = Level-1 pixel value in DN

The digital numbers were also converted to top of atmosphere brightness temperatures. For TIRS band 10, the Equation 2 was used:

$$T_{sen} = \frac{K_2}{ln\,(\frac{K_1}{L_\lambda})+1} \quad (2)$$

T_{sen} = At sensor brightness temperature (K)

L_λ = TOA spectral radiance (Watts/(m^2 * srad * μm))

K_1 = Band-specific thermal conversion constant from the metadata

K_2 = Band-specific thermal conversion constant from the metadata

4.4.3 Single channel method

The single channel method by Jiménez-Muñoz and Sobrino (2003) was used in this study because it needs only one thermal infrared channel and LSE and water vapor content as parameters. The SC formula is as follows (Eq. 3–5):

$$T_s = \gamma \left[\frac{1}{\varepsilon}(\Psi_1 L_{sen} + \Psi_2) + \Psi_3\right] + \delta \tag{3}$$

$$\gamma = \frac{T_{sen}^2}{b_\gamma L_{sen}} \tag{4}$$

$$\delta = T_{sen} - \frac{T_{sen}^2}{b_\gamma} \tag{5}$$

T_s = LST

γ = Parameter depending on Equation 4

δ = Parameter depending on Equation 5

ε = Land surface emissivity

L_{sen} = TOA spectral radiance (W sr^{-1} m^{-2} μm^{-1})

b_γ = 1324 K for Landsat 8 band 10

T_{sen} = At sensor brightness temperature (K)

The atmospheric parameters Ψ_1, Ψ_2 and Ψ_3 were obtained with Equation 6:

$$\begin{bmatrix}\Psi_1\\ \Psi_2\\ \Psi_3\end{bmatrix} = \begin{bmatrix}c_{11}\ c_{12}\ c_{13}\\ c_{21}\ c_{22}\ c_{23}\\ c_{31}\ c_{32}\ c_{33}\end{bmatrix}\begin{bmatrix}\omega^2\\ \omega\\ 1\end{bmatrix} \tag{6}$$

According to by Jiménez-Muñoz, et al. (2014) the coefficients for atmospheric parameters for Landsat 8 TIRS are as follows (Eq. 7):

$$c = \begin{bmatrix}0.04019 & 0.02916 & 1.01523\\ -0.38333 & -1.50294 & 0.20324\\ 0.00918 & 1.36072 & -0.27514\end{bmatrix} \tag{7}$$

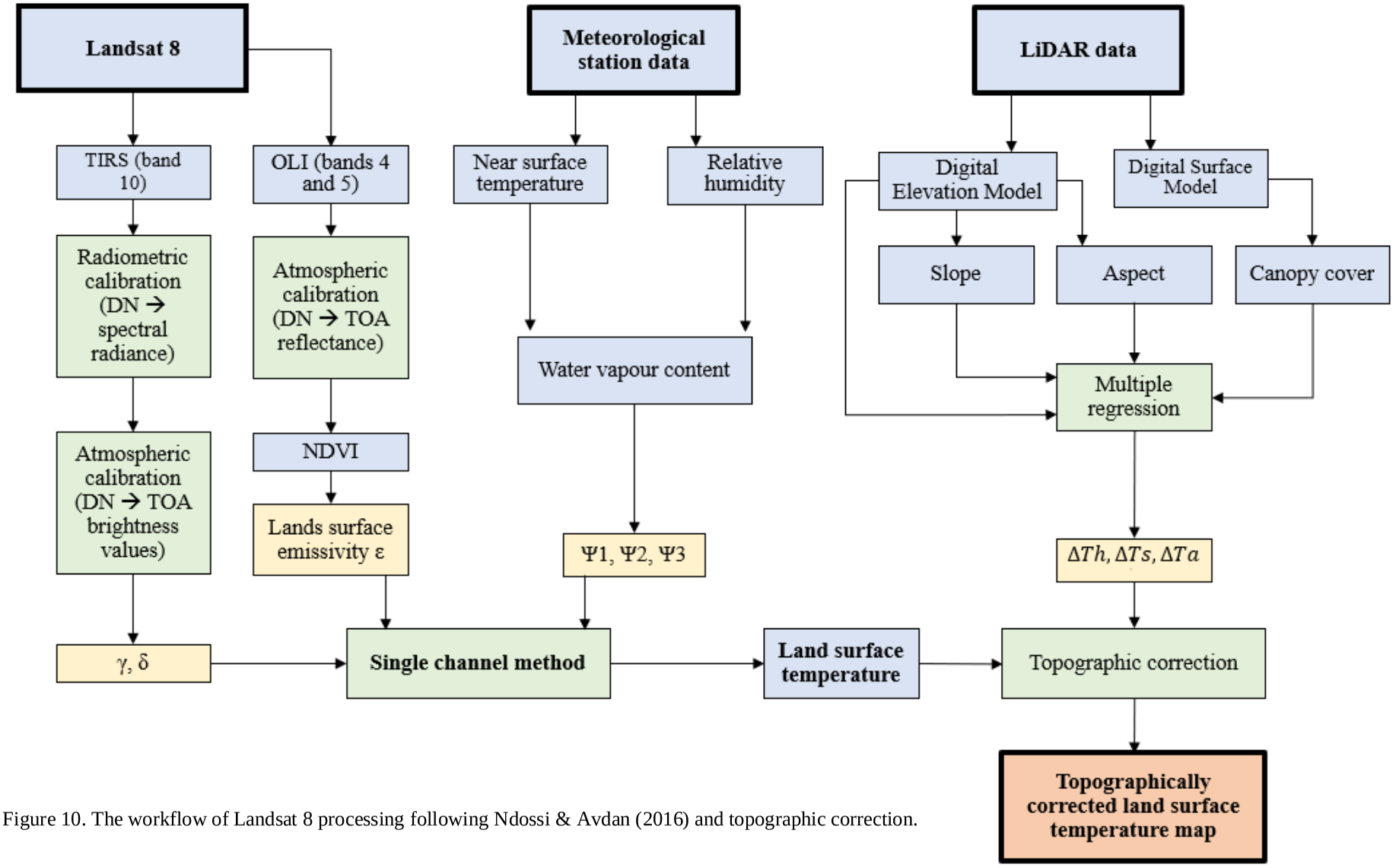

Figure 10. The workflow of Landsat 8 processing following Ndossi & Avdan (2016) and topographic correction.

4.4.4 Determination of water vapor content

The water vapor content was determined from the meteorological station data from satellite overpass time. The weather station is located in Maktau at 1070 m a.s.l. and is managed by Taita Research Station of the University of Helsinki. To obtain water vapor from relative humidity and near surface air temperature, the same equation (Eq. 8) was used as by Ndossi and Avdan (2016) in the QGIS plugin:

$$\omega = 0.0981\left\{10 * 0.6108 * exp\left[\frac{17.27*(T_0-273.15)}{237.3+(T_0-273.15)}\right] * RH\right\} + 0.1679 \quad (8)$$

ω = atmospheric water vapor

T_0 = near surface air temperature (K)

RH = relative humidity

4.4.5 Determination of land surface emissivity

As discussed in section 2.2.1, the emissivity of an object affects the proportion of the radiation that it emits and is recorded by a thermal infrared sensor. The estimation of emissivity is crucial for the correct LST retrieval (Van de Griend & Owe, 1993). Different surfaces have different emissivity due to physical and chemical reasons. NDVI can be used to separate between different land surface types (Jensen, 2007). In this study, the determination of emissivity was based on NDVI, because the study area is highly vegetated and has little urban areas or water bodies. The NDVI-based method by Ndossi and Avdan (2016) was chosen. It is a modification on the NDVI based LSE algorithm by Van de Griend and Owe (1993) and Zhang et al. (2006). NDVI was calculated using the atmospherically corrected OLI bands 4 and 5 with Equation 9:

$$NDVI = \frac{(NIR-R)}{(NIR+R)} \quad (9)$$

NDVI = Normalized Difference Vegetation Index

NIR = Landsat 8 OLI band 5

R = Landsat 8 OLI band 4

The estimation of emissivity is conducted by classifying each pixel based on their NDVI value and given an emissivity value that depends on the class they fall into. The classification by Ndossi and Avdan (2016) is shown in Table 1.

Table 2. NDVI-based emissivity by Ndossi and Avdan (2016).

NDVI	*LSE*
NDVI < -0.185	0.995
-0.185 ≤ NDVI ≤ 0.167	0.985
0.157 ≤ NDVI ≤ 0.727	1.0094 + 0.047 * ln(NDVI)
NDVI > 0.727	0.990

4.4.6 Land surface temperature and temperatures measured in the field

Correlations between LST and field temperatures on the satellite overpass date and their means were calculated for the comparison of the two measuring methods. The differences in means were examined using Student's t-test to determine if the difference was statistically significant. The result indicated whether LST and raw T give on average the same readings. R^2 of LST from the satellite image was compared with the results from microclimate analysis.

4.4.7 Topographic correction

Topography's effect on LST in the satellite image is demonstrated in Figure 11, where altitude and aspect significantly affect LST. Similar topographic correction was conducted with the Landsat image as with microclimate sensors to reduce the effect of topography for the sake of sensible comparison. The LST raster was clipped to fit the ALS area. All the topographic variables (altitude, slope and aspect), canopy cover and LST were included in a multiple regression model, where LST was the dependent variable and the rest independent variables. Aspect classes were treated as dummy variables due to their categorical nature. Following Wanderley, et al. (2019), the topographically corrected LST was calculated with Equation 10:

$$LST' = T - \Delta Th - \Delta Ts - \Delta Ta \quad (10)$$

LST' = topographically corrected LST

T = raw LST

ΔTh = difference of T to the reference LST at altitude of 880 m a.s.l.

ΔTs = difference of T to the reference LST at slope of 0 °.

ΔTa = difference of T to the reference LST in the aspect class "north"

Based on the corrections made in Equation 10, a topographically corrected LST map was produced in ArcGIS Pro.

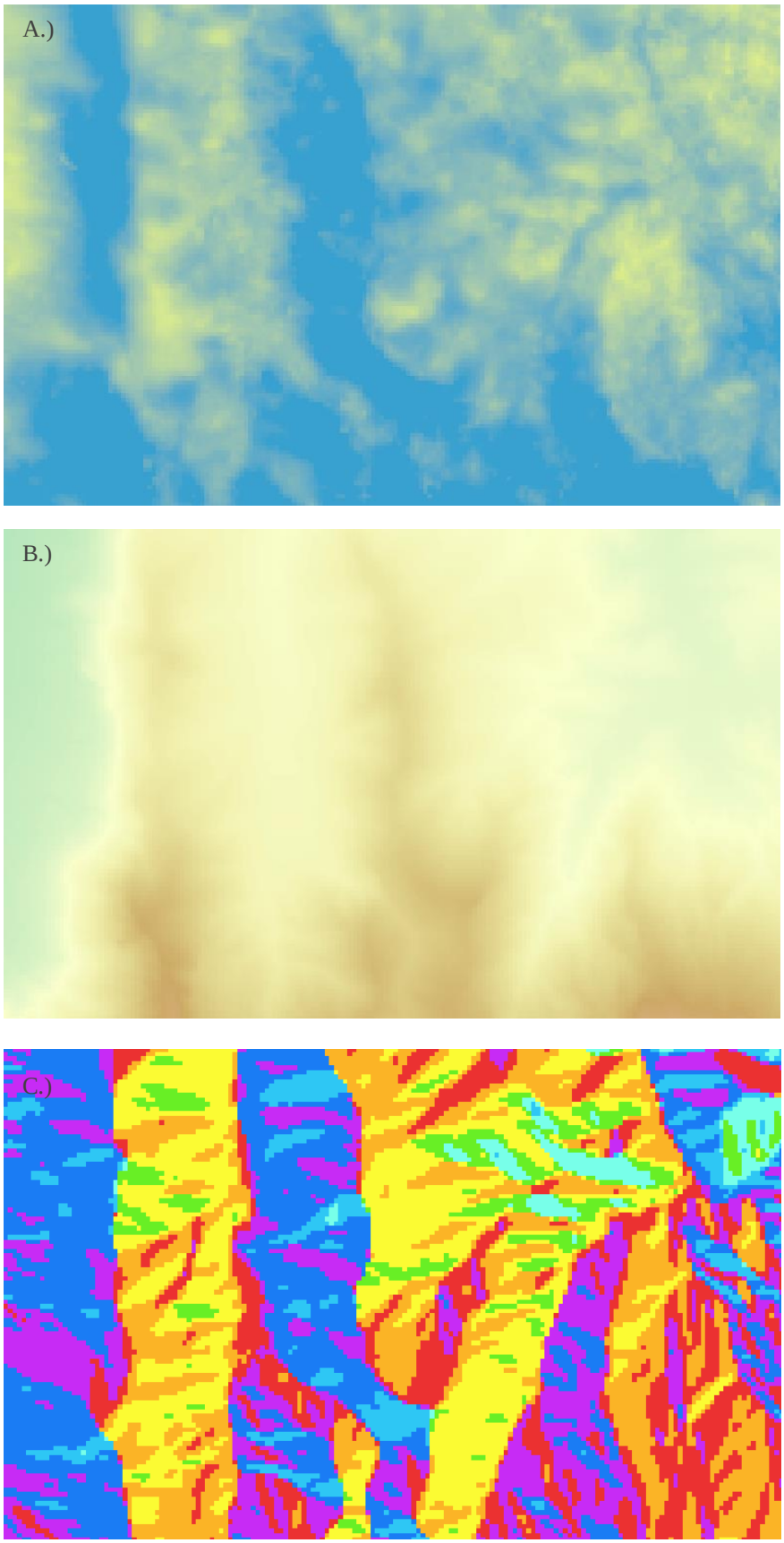

Figure 11. The relationship between LST (A), elevation (B) and aspect (C). A) The cooler LST is marked with blue color and warmer LST with red. B) The lower altitudes are presented in light brown and green color and high altitudes with dark brown. C) North = red, northeast = orange, east = yellow, southeast = green, south = cyan, southwest = light blue, west = dark blue, northwest = violet.

4.4.8 Linear regression models

Linear regression was used to study how much canopy cover percentage affects microclimate and LST. This was done by using topographic variables (Eq. 10) as controllers. The estimated model was as follows (Eq. 11):

$$T = \beta_0 + \beta_1 C + \gamma Z + \varepsilon \quad (11)$$

T = temperature

β_0 = intercept term

β_1 = coefficient of C

C = canopy cover (%)

Z = control variable vector

γ = parameter vector

ε = independently and identically distributed mean zero error term

In total, four different models were estimated for LST. The basic model (model 1) included canopy cover, elevation, slope and aspect classes. In the second model (model 2), canopy cover's cooling impact in different altitudes was studied by adding interaction terms to the model between canopy cover and dummy variables that reclassified the pixels to three altitudinal zones: below 1000 m, 1000–1500 m and above 1500 m. Model 3 added to the basic model an interaction term between the continuous variable altitude and canopy cover. In model 4, the relationship between aspect and canopy cover was studied by adding further interaction terms to model 2. Lastly, the cooling power in different altitudes was demonstrated by reclassifying the data to 8 classes: below 800 m, 800–1000 m, 1000–1200 m, 1200–1400 and comparing R^2 between topographically corrected LST and canopy cover in each class.

5 Results

5.1 Canopy cover derived from hemispherical photography and ALS

The correlation coefficient of CC_{HP} and CC_{ALS} was 0.93 and $p < 0.001$ (Figure 12). CC_{HP} gave in average lower canopy covers than CC_{ALS}. Differences in the estimations are highest in the intermediate canopy covers and less in low canopy covers and high canopy covers. The mean difference between CC_{HP} and CC_{ALS} was -0.89 % and according to Student's t-test not statistically significant, meaning the estimates were consistent enough for CC_{ALS} to be fit for further usage. The analysis of temperatures and canopy cover was proceeded using CC_{ALS} only.

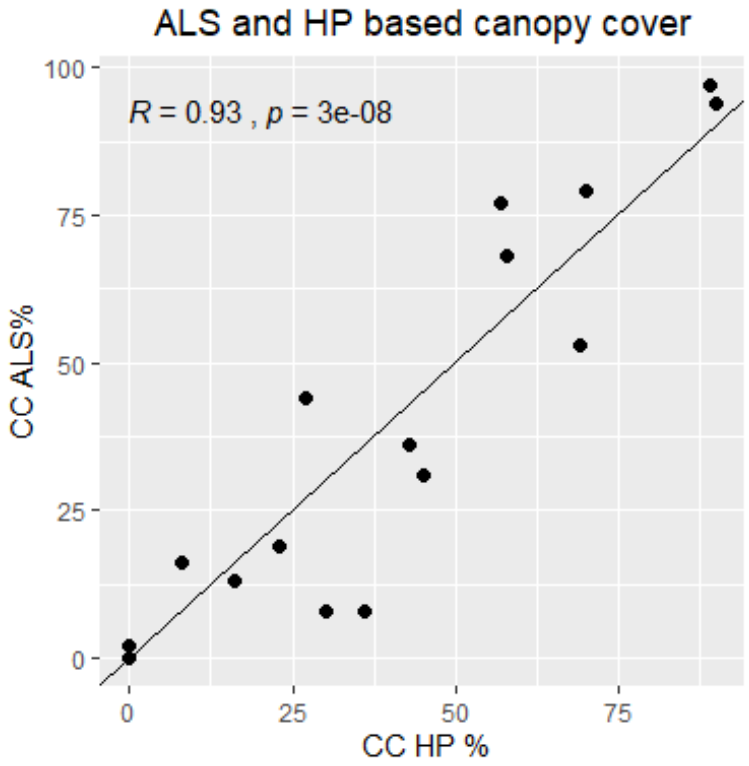

Figure 12. Comparison of CC_{ALS} and CC_{HP} in the soil sensor sites, with line of identity.

5.2 Impact of topography on microclimate

Daytime raw temperatures are highly correlated with altitude (r = 0.78 and p < 0.001) (Figure 13 A–C). Also slope affects the temperatures (Figure 14). Elevation and slope are highly correlated in the study area (r = 0.87, p <0.001), meaning that the steepest slopes are found in the mountains. The small sample size did not allow a comprehensive assessment of aspect's influence on microclimate, which is demonstrated in Figure 15. The presumption was that south-facing slopes would have had the lowest temperatures, and flat and north-facing slopes the highest temperatures, which however was not the case. This indicates that also other factors are affecting the results.

Regression using only topographic variables altitude and slope produced R^2 = 0.64 in T_{soil}, 0.7 in $T_{surface}$ and 0.76 in T_{air}. Before topographic correction, R^2 between canopy cover and T_{soil} was 0.4, $T_{surface}$ 0.43 and T_{air} 0.36 and p = 0.004, 0.002 and 0.006, respectively. The objective of topographic correction was to diminish the differences caused by altitudinal differences. The results of elevational lapse rate correction are shown in Figure 13 D-F.

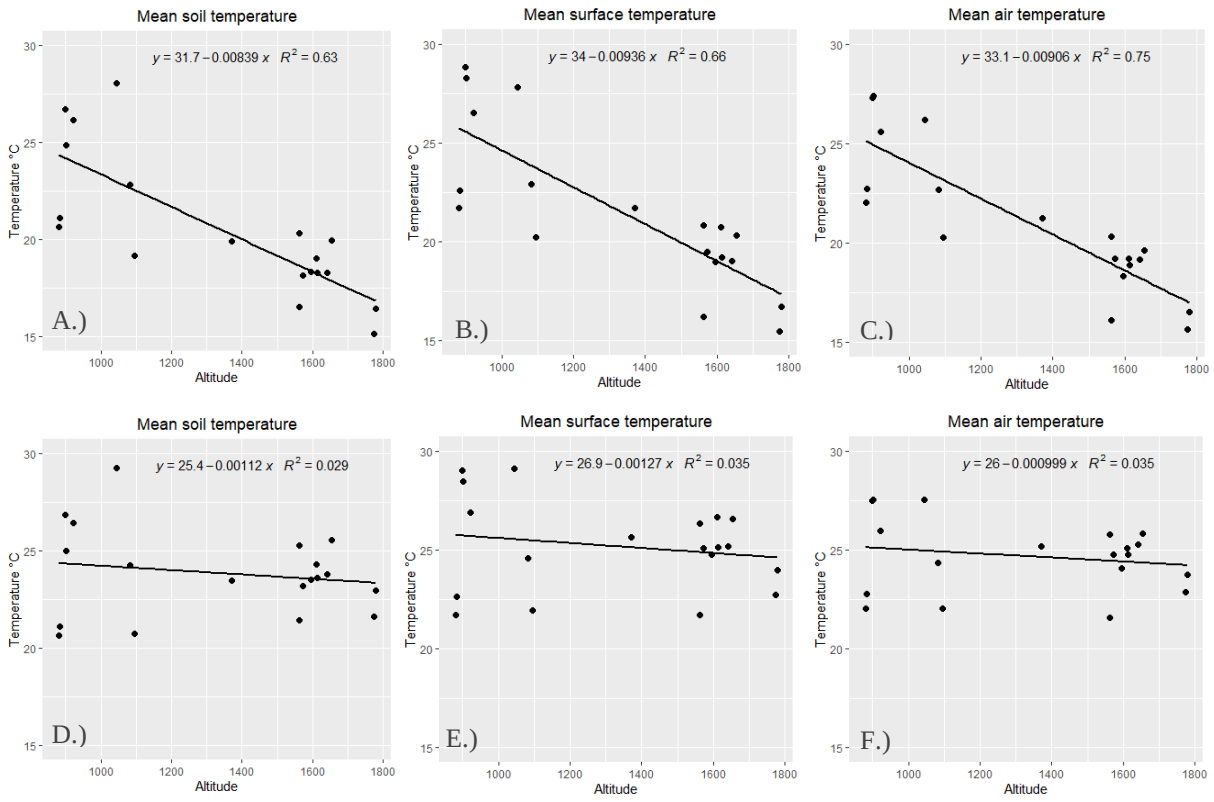

Figure 13. Mean temperatures in the TOMST-TMS4 microclimate sensor sites before (A-C) and after (D-F) altitudinal lapse rate correction of 7.26 °C/km for T_{soil}, 8.09 °C/km for $T_{surface}$ and 8.06 °C/km for T_{air}.

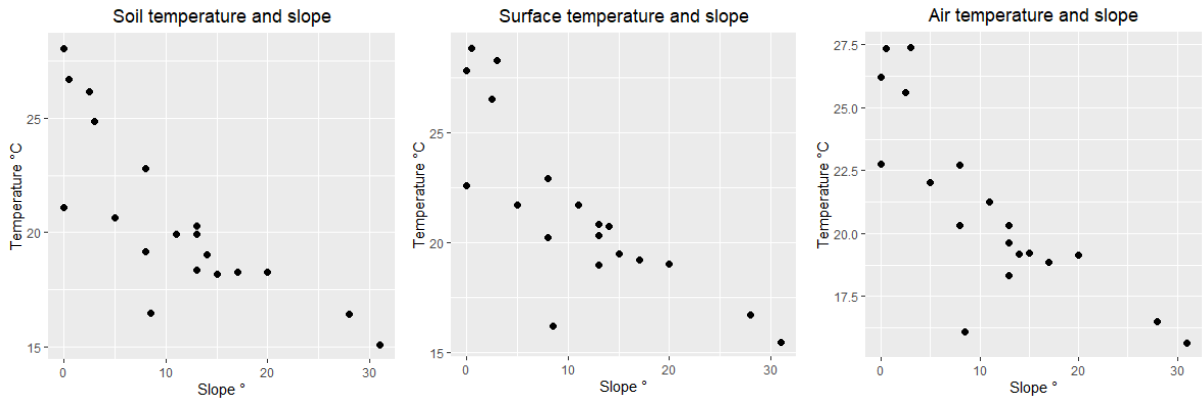

Figure 14. The effect of slope on mean temperatures in the microclimate sensor sites.

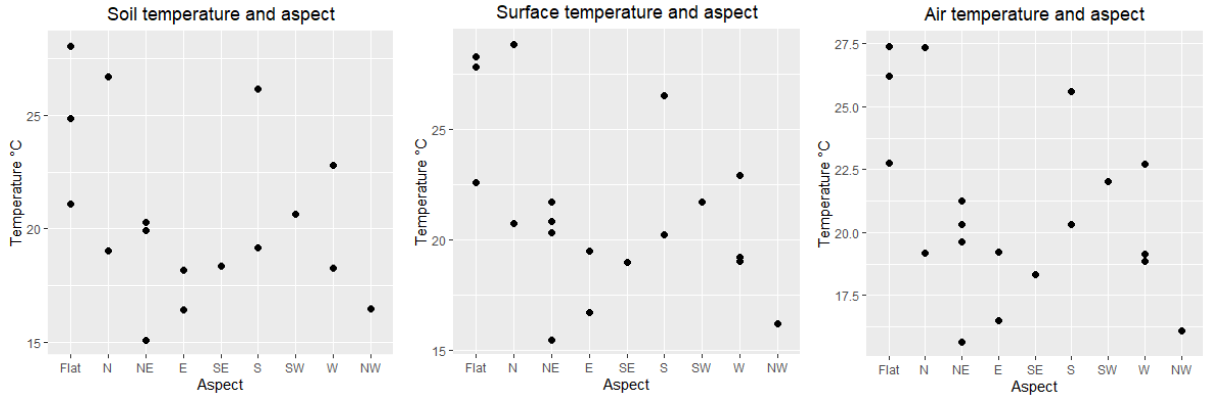

Figure 15. The relationship between aspect and mean temperatures in the microclimate sensor sites.

5.3 Canopy cover and microclimate

5.3.1 Temporal variation

The daily variation in topographically corrected (marked as T') daytime means is presented in Figure 16. Four hotter day streaks van be separated in the study period between June 13 and July 10, which continued from three to seven days. Landsat 8 overpass took place during one of the hottest periods on July 4. July 6 shows a clear drop in $T'_{surface}$ and T'_{air} but in T'_{soil} the temperature decreases only slightly. Daytime mean temperatures show greatest variation in $T'_{surface}$ and T'_{air}. T'_{air} and T'_{soil} have the lowest T' records, but T'_{soil} clearly exhibits less variation between days than T'_{air}, coolest sites remaining at stable 20 °C. Highest temperatures are measured in $T'_{surface}$, where average temperature of 30 °C is exceeded on each hot-day streak. The highest means of T'_{soil} are observed in Maktau (19 % CC), which separates clearly from the other sites. Maktau reaches 30 °C on the hottest period around Landsat overpass, while the rest of the sites stay below it. In $T'_{surface}$ and T'_{air} Maktau is not an outlier anymore.

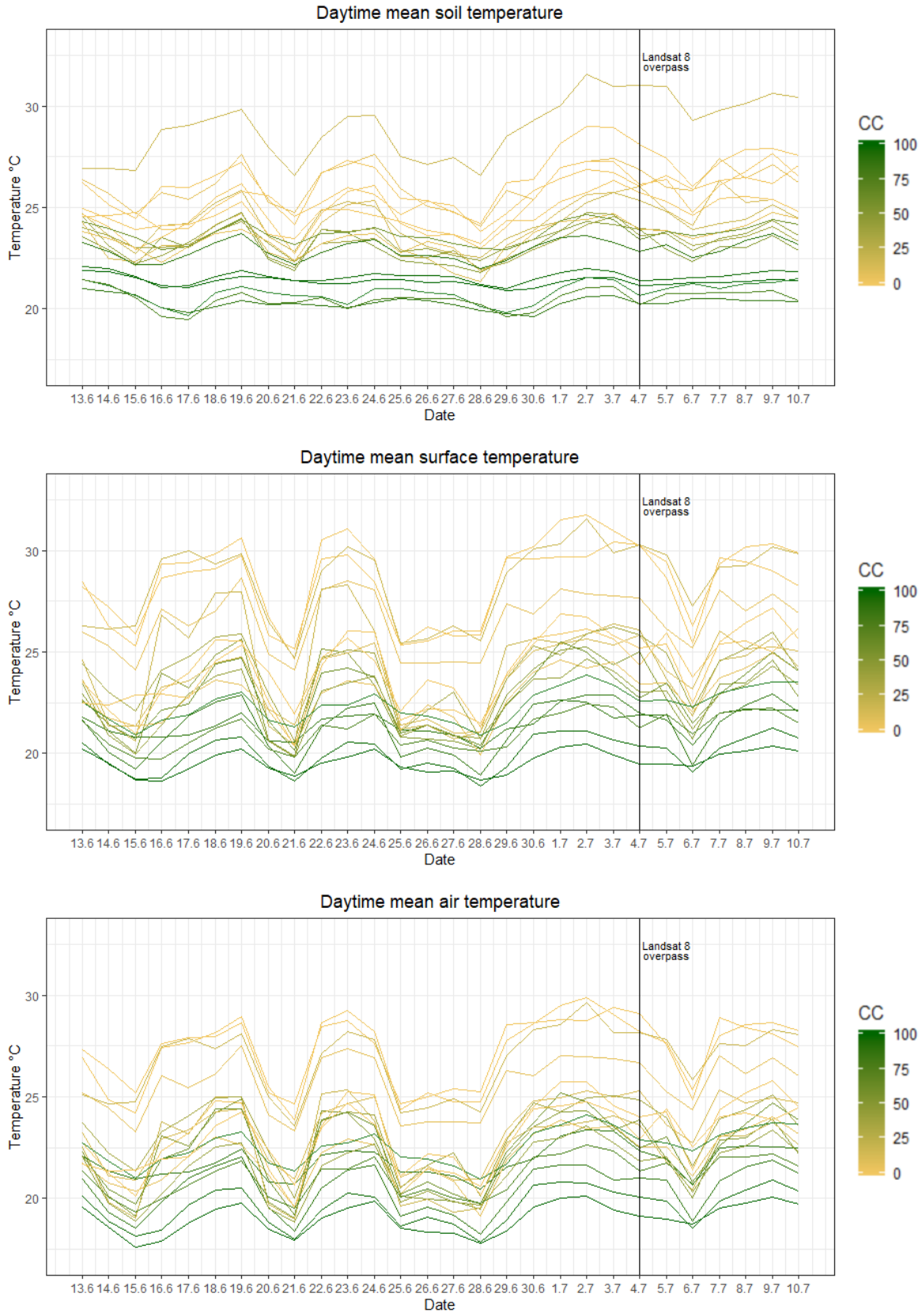

Figure 16. Daily variation in daytime (6.30-18.30) mean temperatures in the field plot sites between June 13 and July 10, 2019 measured with TOMST TMS-4 sensors. Line color indicates CC_{ALS} percentage.

Daily mean temperatures are low in high canopy covers. The highest temperatures are measured in low canopy covers, yet some low canopy cover sites exhibit relatively low temperatures as well. On the hottest days, T' difference between hottest and coolest sites is almost 11 °C in T'_{soil} and 10 °C in $T'_{surface}$, whereas the difference is less with T'_{air}, being approximately 7.3 °C. Even on the coolest days, for instance on June 25–28, the T' are around 5 °C lower in high canopy cover sites than at low canopy covers. Canopy cover shows to impact also temperature variation: T'_{soil} for the highest canopy covers remain relatively stable from day to day showing little fluctuation even on the hot day streaks, differences remaining even less than 1 °C between hottest and coolest days. In T'_{air}, differences between canopy covers are smaller than with $T'_{surface}$. $T'_{surface}$ and T'_{air} have more variation than T'_{soil} in all canopy covers. The daily peaks and drops are higher for low canopy covers than high at all three levels. In Figure 17 mean T' of each day is plotted separately, showing how on the coolest days the T' are relatively similar despite different canopy covers, while the cooling effect is evident on the hottest days.

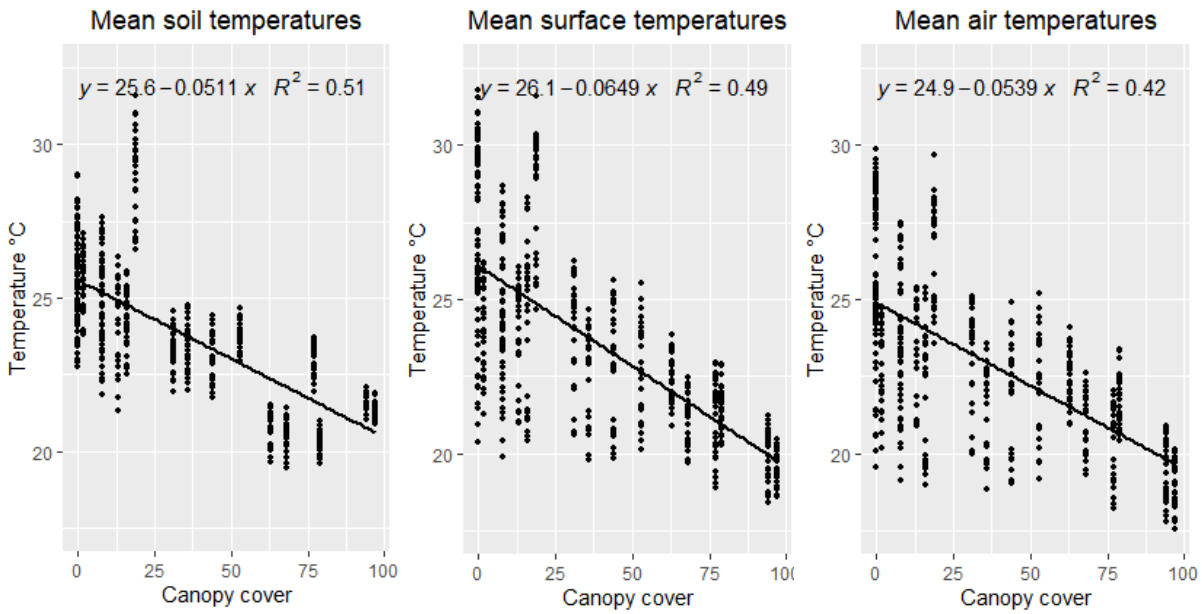

Figure 17. Mean temperatures measured with the microclimate sensors between June 13 and July 10, 2019 and CC_{ALS} percentage.

Daily T' variation is demonstrated in Figure 18 that shows standard deviation of temperatures for each site along the canopy cover gradient. T' variation decreases straightforwardly as canopy cover increases, especially in T'_{soil} (R^2 = 0.67), $T'_{surface}$ and T'_{air} having more scattered deviations (R^2 = 0.59 and 0.53, respectively). The standard deviations in $T'_{surface}$ and T'_{air} are also higher compared to T'_{soil}. T' fluctuations are smallest at soil level, where standard deviation is 1.5 C° at maximum, for $T'_{surface}$ maximum standard deviation rises to 2 C° and even above 2.5 C°.

Variation in daily maximum temperatures (Figure 19) shows similar relationship with canopy cover as mean temperatures in T'_{soil}. The standard deviation decreases linearly with canopy cover (R^2 = 0.7), but in $T'_{surface}$ and T'_{air} the relationship is weaker (R^2 = 0.37 and 0.23, respectively). As was the case in T' means, the variation in T' maxima is greater in $T'_{surface}$ and T'_{air} than T'_{soil}.

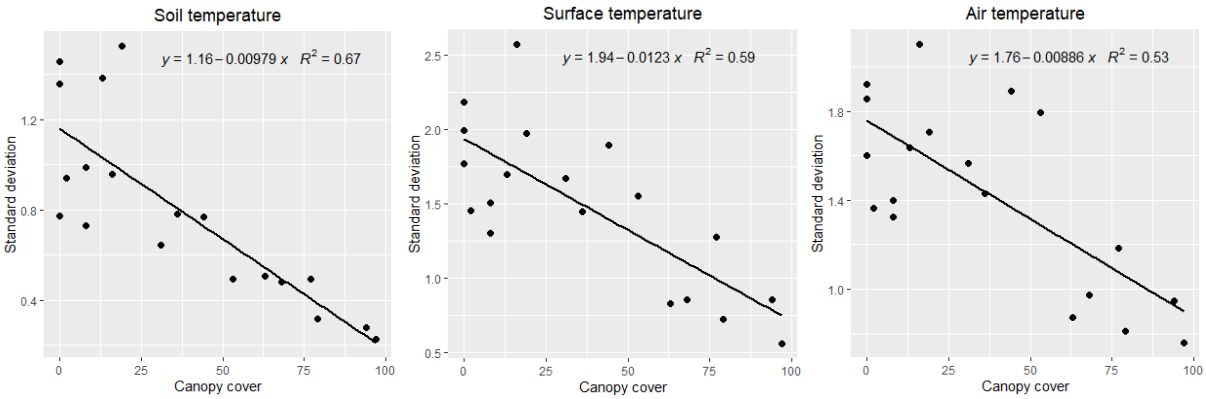

Figure 18. Standard deviation of mean temperatures measured with the TOMST-TMS4 microclimate sensors in different CC_{ALS} between June 13 and July 10, 2019.

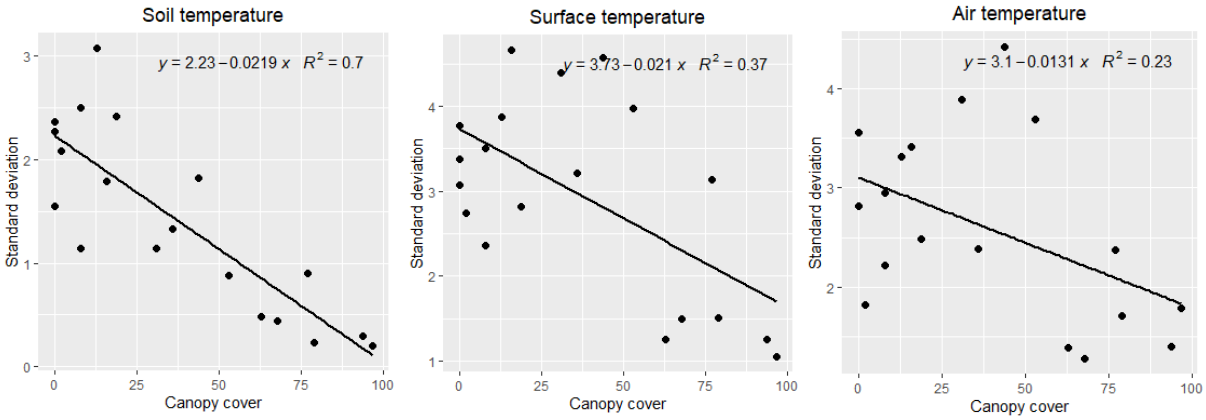

Figure 19. Standard deviation of maximum temperatures measured with the TOMST TMS-4 microclimate sensors in different CC_{ALS} between June 13 and July 10, 2019.

Figure 20 shows the 28-day diurnal temperature means. The curve for T'_{soil} is smoother than for $T'_{surface}$ and T'_{air} that show higher temperature peaks and drops. Between 6:00 and 8:00, temperatures start rising rapidly after the night, reaching highest readings between 11:00 and 15:00 in $T'_{surface}$ and T'_{air}, and between 15:00 and 17:00 in T'_{soil}. There is also great variation between sites. After peaking, temperatures descrease before stabilizing around the 20th hour in $T'_{surface}$ and T'_{air}, in T'_{soil} before midnight. $T'_{surface}$ exceeds 35 °C between 11:00 and 14:00 in Sarova enclosure (0 % CC) and Maktau. Sarova grassland (0 % CC), Mlima wa simba (13 % CC) and Wundanyi (31 % CC) are the next hottest sites. The same sites appear hottest in T'_{air}, the highest measurement being 34.7 °C in Sarova enclosure between 12:00 and 13:00. Lowest $T'_{surface}$ and T'_{air} around noon are 22.5 °C and 23.0 °C, both measured in Bura riverine forest site (79 % CC). Wesu site (53 % CC) does not follow the hourly trend: $T'_{surface}$ first rises above 27.7 °C in the 11th hour, then decreases to approximately 27.4 °C and rises again in the 16th hour to 29.9 °C. Same occurrence repeats in T'_{air}, except that the peaks hit 28 °C and 30 °C. Most considerable differences between the coolest (Bura riverine forest) and hottest (Sarova enclosure) sites at noon are 13.7 °C in $T'_{surface}$ and 11.6 °C in T'_{air}.

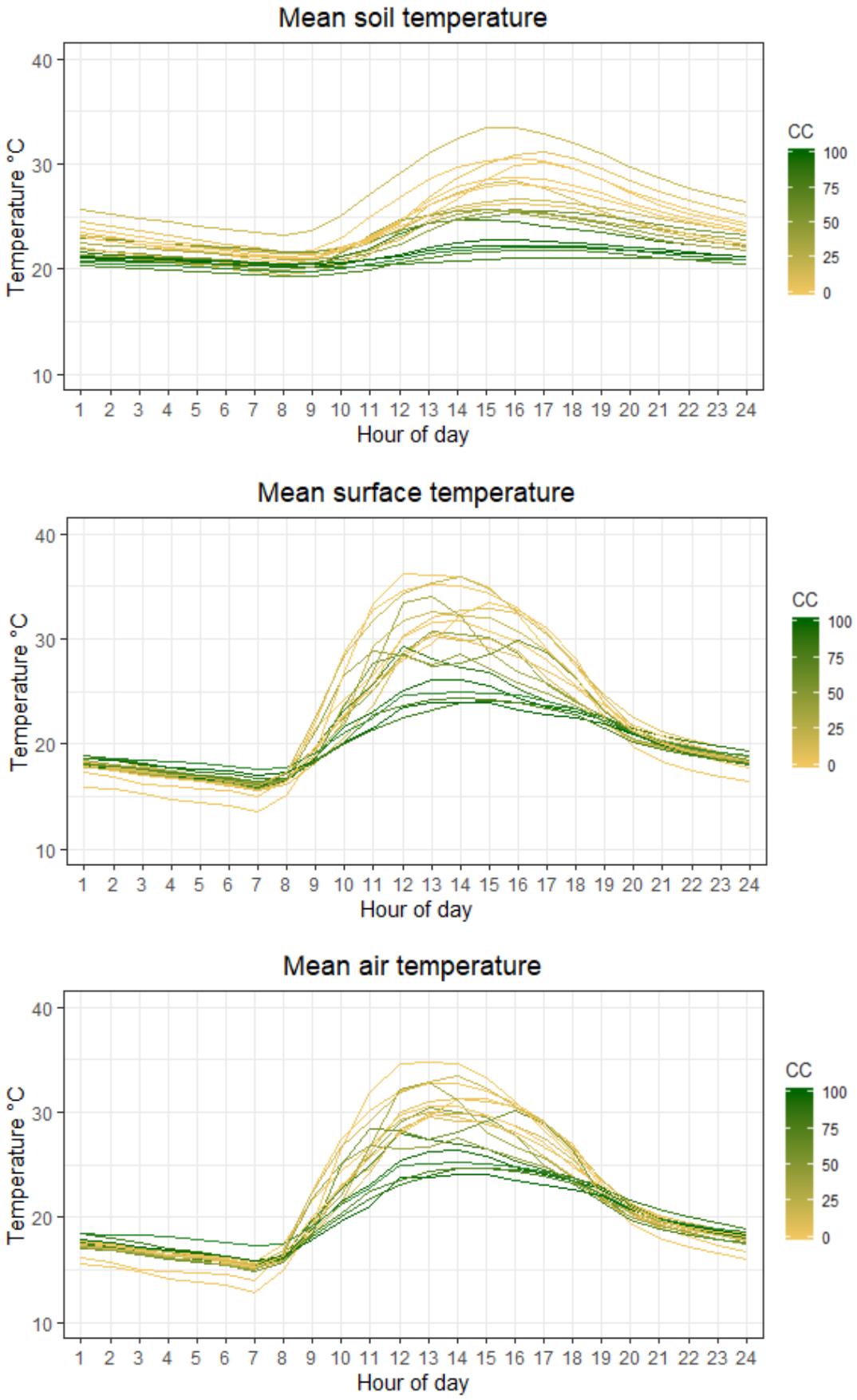

Figure 20. Diurnal mean temperatures measured with the microclimate sensors between June 13 and July 10, 2019. Line color indicates CC_{ALS} canopy cover percentage. Hour refers to ordinal number of hour, e.g. 1 means 00:00-01:00.

T'_{soil} in most sites peaks a few hours later than $T'_{surface}$ and T'_{air}, between 15:00 and 17:00. Highest T'_{soil} of 33.5 °C is measured in Maktau, where the temperatures remain the highest throughout the 24-hour period. Maktau, Mlima wa simba, Sarova grassland and Mwanda (2 % CC) reach 30 °C, Maktau being distinguishable from other sites. The lowest T'_{soil} at the hottest time is 21 °C, measured in Bura riverine forest. Between 15:00 and 16:00, the difference between Maktau and Sarova is 12.5 °C. The intermediate canopy cover sites fall somewhere between the forests and open areas, some having very high temperatures and some even lower than the highest canopy cover sites.

Lowest temperatures are recorded between 6:00 and 8:00 in all levels. During the night, $T'_{surface}$ and T'_{air} drop below 20 °C in each site when T'_{soil} stays mostly above 20 °C, except sites Dembwa (13 % CC), Bura (2 % CC) and Mwatate riverine forest (63 % CC), where T'_{soil} decreases to just above 19 °C. In two 0 % canopy cover sites the night temperatures are clearly lower than in the rest of the sites: in Sarova enclosure and Sarova grassland, $T'_{surface}$ drop to 13.4 °C and 15 °C, T'_{air} to 12.8 °C and 13.9 °C, respectively. These sites are the ones to also have the hottest $T'_{surface}$ and T'_{air} during the day. During the night, forest sites Chawia (97 % CC), Mwatate and Bura riverine forests have the highest $T'_{surface}$ and T'_{air} around 15.5–17.5 °C, $T'_{surface}$ being slightly higher. In the night hours, T' differences between sites decrease notably and canopy cover's effect dissolves. For low canopy cover sites, diurnal T' variation can rise above 20 °C in $T'_{surface,}$ the amplitude being a little smaller in T'_{air} while in T'_{soil} the difference between night and day does not stretch to more than 10 °C. In the higher end of canopy cover, T'_{soil} remains almost static throughout the day, temperatures varying between 20.1 C° and 22.8 C° for sites with 79–97 % canopy cover. The amplitude in $T'_{surface}$ and T'_{air} is higher, 6.9–11.1 C°.

Canopy cover's impact on temperatures is lowest in the morning as is demonstrated in Figure 21 where correlation between canopy cover and T' is studied. The figure looks very different for T'_{soil} compared to $T'_{surface}$ and T'_{air}. In T'_{soil}, temperatures correlate negatively with canopy cover throughout the day and the correlation decreases to -0.4 only between 7:00 and 8:00 when the minimum temperatures are reached. Correlation of < -0.8 exists in the afternoon hours. $T'_{surface}$ and T'_{air} seem to be affected by canopy cover mostly in the afternoon with $r < -0.8$. During the night, canopy cover's effect is inverse compared to T'_{soil} as the correlation becomes positive in the 20^{th} and 21^{st} hours. The correlation stays around 0.4 until the 7^{th} and 8^{th} hour for T'_{air} and $T'_{surface}$, respectively. $T'_{surface}$ seems to lag one hour behind and the correlation coefficient increases slower than T'_{air}, but the general pattern of are looks similar.

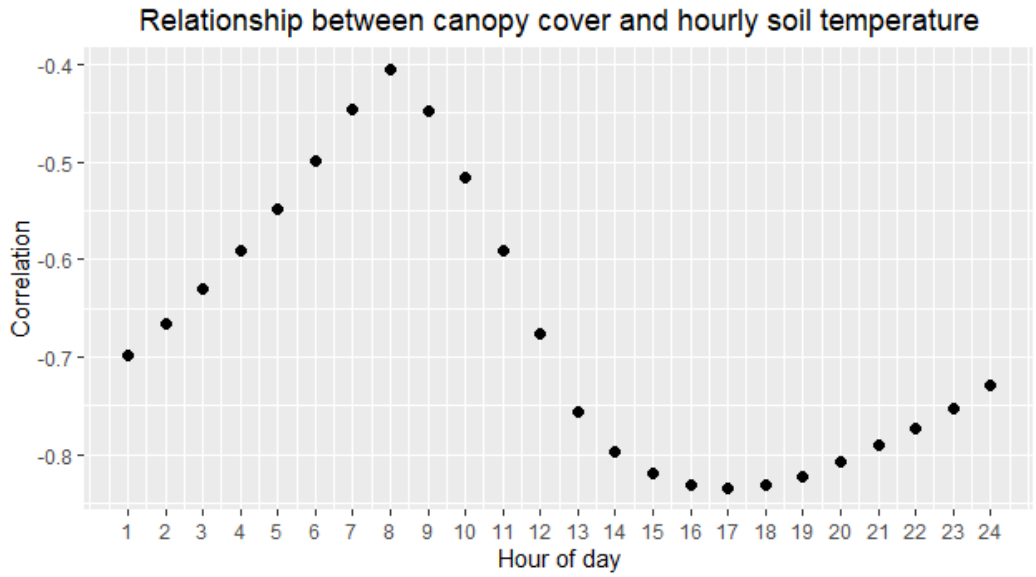

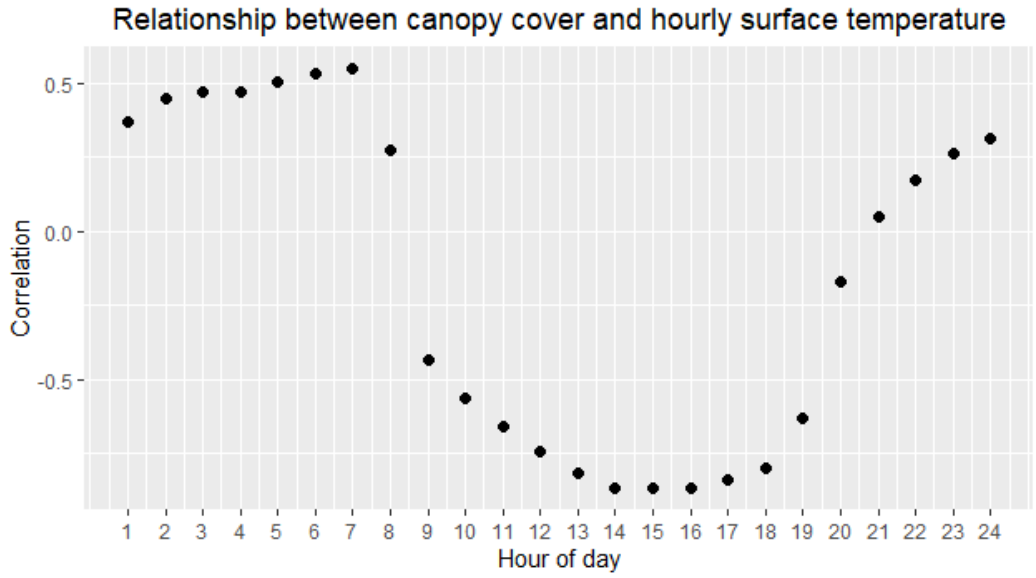

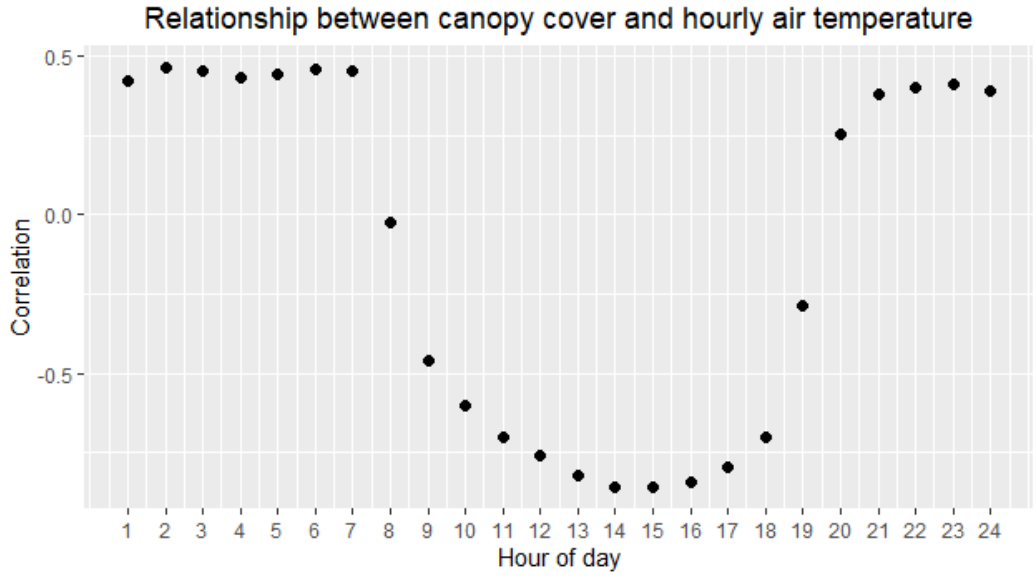

Figure 21. Correlation between temperature and CC_{ALS} at different times of the day based on diurnal mean temperatures between June 13 and July 10, 2019 in the microclimate sensor sites.

5.3.2 Impact of canopy cover on mean, maximum and minimum temperatures

The descriptive statistics and the result of the linear regression of T' are compiled in Table 3. Mean temperatures at all T' levels have statistically significant negative correlation with canopy cover, in $T'_{surface}$ and T'_{air} r = -0.84, and in T'_{soil} r = -0.78. Based on the linear regression, increase from 0 % to 100 % canopy cover decreases temperatures by 5.18 C° in T'_{soil}, (R^2 = 0.6), 5.86 C° in $T'_{surface}$ (R^2 = 0.71) and 4.61 C° in T'_{air} (R^2 = 0.71).

In Figure 22, T' mean aggregates are plotted against canopy cover. Highest T'_{soil} of 29.3 C° is measured in Maktau, which is clearly an outlier. This was visible also in the scatterplot earlier in Figure 17. Second highest mean T'_{soil} is 26.9 C° in Sarova grassland site. Lowest T'_{soil} of 20.6 C° is calculated in Bura riverine forest. In sites with 0–2 % canopy cover, mean T'_{soil} are 25–26.8 C°. In the sites with highest canopy covers, namely Chawia and Ngangao indigenous forest, T'_{soil} means are 21.5–21.6 C°.

$T'_{surface}$ and T'_{air} are in general higher than T'_{soil}. Temperature differences are as expected: lowest $T'_{surface}$ and T'_{air} are computed in the highest canopy covers and highest in low canopy covers. Maktau has similar T'_{soil} and $T'_{surface}$ means (29.3 C° and 29.2 C°), while T'_{air} is 1.6–1.7 C° lower, behaving against the general trend of cooler T'_{soil}.

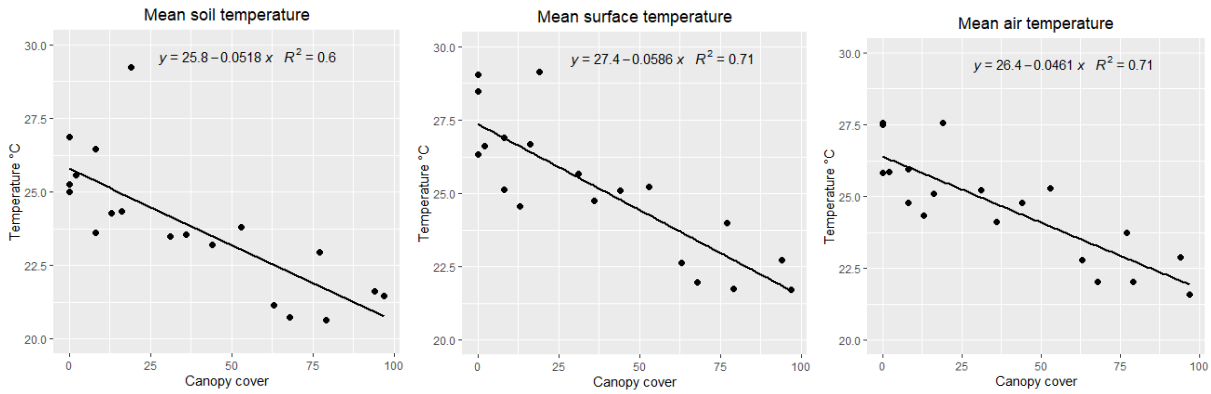

Figure 22. Mean daytime temperatures and CC_{ALS} in the microclimate sensor sites between June 13 and July 10, 2019.

Table 3. Summary statistics of T' mean, maximum and minimum of the full study period between June 13 and July 10, 2019. Name and canopy cover of sites with highest and lowest values of the relative statistics are presented right to the value.

		Max (C°)	Site and CC	Min (C°)	Site and CC	Coef	R^2	r	p-value
Mean	T'_{soil}	29.3	Maktau 19 %	20.6	Bura riverine forest 79 %	-0.0518	0.604	-0.777	<0.001 ***
	$T'_{surface}$	29.2	Maktau 19 %	21.7	Chawia 97 %	-0.0586	0.711	-0.843	<0.001 ***
	T'_{air}	27.6	Sarova enclosure 0 %	21.6	Chawia 97 %	-0.0461	0.710	-0.842	<0.001 ***
Max	T'_{soil}	33.3	Maktau 19 %	20.8	Bura riverine forest 79 %	-0.0895	0.693	-0.832	<0.001 ***
	$T'_{surface}$	38.8	Sarova enclosure 0 %	22.9	Chawia 97 %	-0.121	0.742	-0.862	<0.001 ***
	T'_{air}	37.4	Sarova enclosure 0 %	23.8	Chawia 97 %	-0.096	0.686	-0.828	<0.001 ***
Min	T'_{soil}	23.0	Maktau 19 %	19.2	Bura 68 %	-0.0032	0.083	-0.289	0.2312
	$T'_{surface}$	19.5	Chawia 97 %	12.9	Sarova enclosure 0 %	-0.0237	0.189	0.435	0.0628
	T'_{air}	19.3	Ngangao eucal. 77 %	12.3	Sarova enclosure 0 %	-0.0228	0.149	0.386	0.1023

Maximum T' are higher in $T'_{surface}$ and T'_{air} than T'_{soil} (Figure 23). Maktau is an outlier in T'_{soil} like with mean temperatures, but not in the two other levels. R^2 are higher with maximum T' than mean T', except in T'_{air}. The lowest $T'_{surface}$ and T'_{air} maxima of 22–25 C° are measured in the highest canopy covers, as expected. The highest $T'_{surface}$ and T'_{air} are measured in Maktau and the 0 % canopy cover sites, where maximum T' average between 30 C° and 38.5 C°. Canopy cover has the biggest impact on $T'_{surface}$. Results from the linear regression analysis showed that increasing canopy cover from 0 % to 100 %, maxima in T'_{soil} decrease 9 C°, $T'_{surface}$ 12.1 C° and T'_{air} 9.6 C° (Table 3). The coefficients for maximum T' are bigger than with the mean temperatures. Pearson's correlation of T' maxima increases in T'_{soil} and $T'_{surface}$ compared to mean T', in T'_{air} it decreases slightly.

The hottest day in $T'_{surface}$ and T'_{air} was July 9, when difference in $T_{surafce}$ between the coolest site (Chawia forest) and hottest site (Sarove enclosure) was 18.4 C°, and in T'_{air} 16.7 C° between Ngangao indigenous forest and Sarova enclosure. In T'_{soil}, the hottest day was July 2 and T' difference was 12.8 C° between Bura riverine forest and Maktau. Maximum T' and slope are highest on soil surface compared to the other measuring heights.

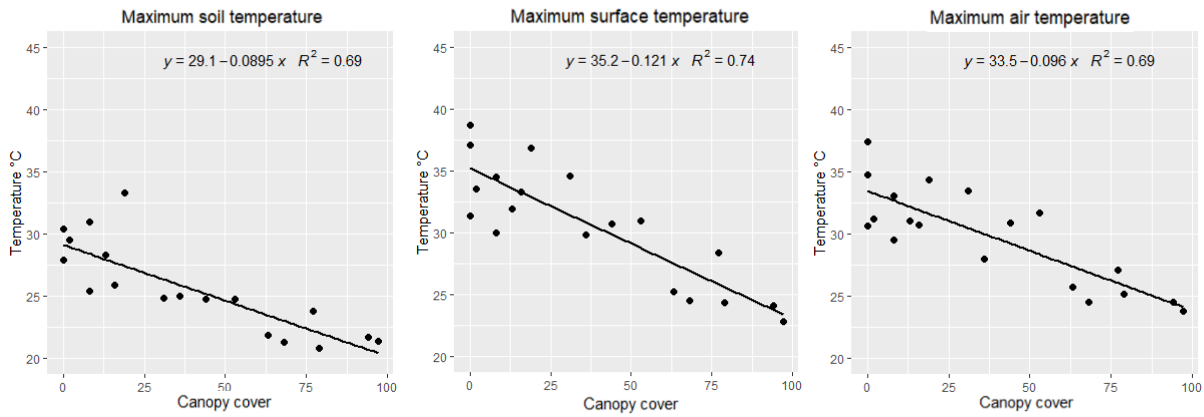

Figure 23. Average maximum temperatures and CC_{ALS} in the microclimate sensor sites between June 13 and July 10, 2019.

Minimum T' are shown in Figure 24. There is no explicit relationship between canopy cover and microclimate records, and sites with similar canopy covers have high variability in minimum temperatures. R^2 are low (< 0.2) in all levels (Table 3). The lowest minimum $T'_{surface}$ and T'_{air} are in the high canopy cover sites Chawia and Ngangao eucalyptus forest, and the lowest minimum is in the 0 % canopy cover site Sarova enclosure. In $T'_{surface}$, the connection between the variables is weak. T'_{soil} are notably higher than $T'_{surface}$ and T'_{air}. Correlation between T' and canopy cover for each level was statistically insignificant.

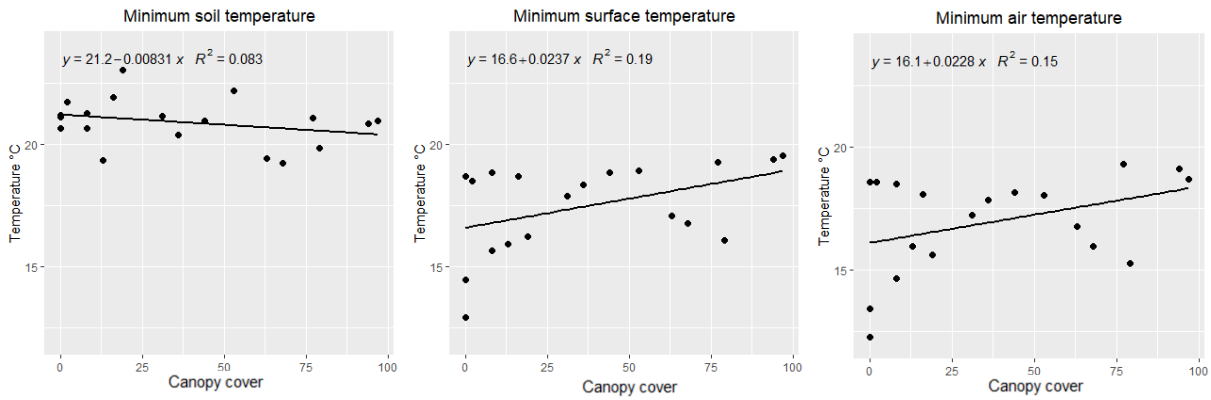

Figure 24. Average minimum temperatures and CC_{ALS} in the microclimate sensor sites between June 13 and July 10, 2019.

5.4 Landsat 8 land surface temperature

5.4.1 Land surface temperature and temperatures measured in the field

Comparison of LST and raw field temperatures (T) was done both with the mean records of the study period and with the temperatures from the exact satellite overpass time. Temperatures recorded by the microclimate sensors have statistically significant correlation with LST at the satellite overpass time, July 4 at 10:30 (Figure 25). T_{air} has the highest coefficient of correlation of 0.84, T_{soil} 0.82 and $T_{surface}$ 0.79. In 18 sites out of 19, LST is higher than T_{soil}. With both $T_{surface}$ and T_{air}, LST is higher than T in 10 sites. Mean difference was 4.1 °C with T_{soil}, -0.03 °C with $T_{surface}$ and 0.57 °C with T_{air}. The difference was statistically significant with 95 % confidence level with T_{soil}, but not with $T_{surface}$ and T_{air}. Based on this data, $T_{surface}$, T_{air} and LST do not produce regularly different values, but T_{soil} and LST clearly do.

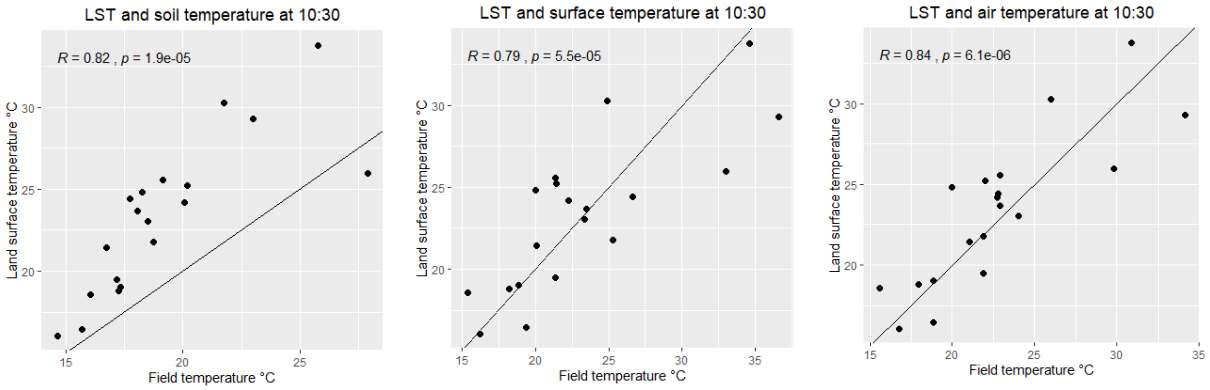

Figure 25. Landsat 8 LST and temperatures measured in the field at the satellite overpass time July 4, 2019 at 10:30, with line of identity.

LST shows even higher correlation with the mean T of the 28 days than the exact Landsat visiting time (Figure 26). $T_{surface}$ has the highest correlation coefficient of 0.92, T_{air} 0.91 and T_{soil} 0.88. In 17 sites, LST exceeds T_{soil}. $T_{surface}$ and T_{air} show again similar results where LST is higher than T in 15 sites. In most sites, LST and microclimate temperature means stay below 26 °C.

Mean difference was 2.74 °C for T_{soil}, 1.79 °C for $T_{surface}$ and 2.28 °C for T_{air}. Mean difference with T_{soil} was statistically significant as was the case with temperatures measured at 10:30. With $T_{surface}$ and T_{air}, the differences were not statistically significant. Generally, LST produced higher temperatures than the microclimate sensors, but based on this data the variation between LST and field T above the ground surface level was not systematic.

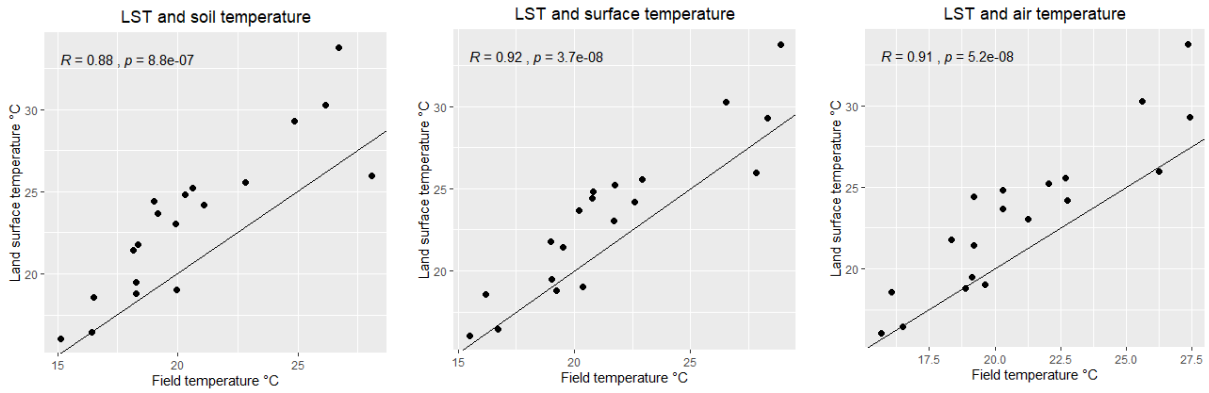

Figure 26. Landsat 8 LST and mean daytime temperatures measured in the field on the satellite overpass date July 4, 2019, with line of identity.

5.4.2 Impact of topography on land surface temperature

LST showed statistically significant correlation of -0.78 with altitude, as hypothesized, with R^2 = 0.61. Altitude and LST are plotted in the density scatter plot in Figure 27. At the same elevations, the temperature range could exceed 20 °C. LST and slope showed a significant correlation of -0.59 and R^2 = 0.35. Slope and altitude had correlation coefficient of 0.48 (p < 0.001).

In the tropics close to the equator, the effect of aspect on LST is smaller than in the higher latitudes, for example, but the phenomenon was distinguishable in Taita Hills as well (Figure 28). Highest temperatures were measured in north-eastern slopes with a 3.5 °C difference to south-facing areas. The temporal perspective on aspect's impact is evident as at 10:30 the sun has not yet reached its highest position but is shining from northeast at this time of the day (azimuth angle 45.6°). Minimums in turn do not show any relationship with aspect.

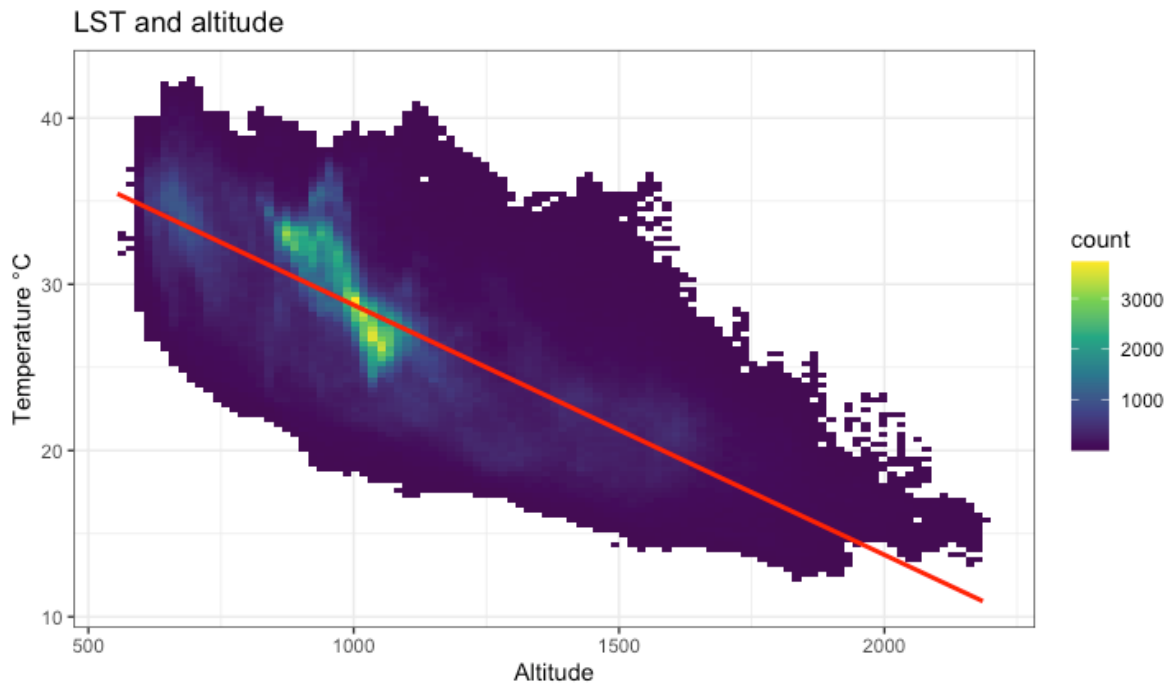

Figure 27. Density scatter plot of raw LST along the elevation gradient with linear regression line.

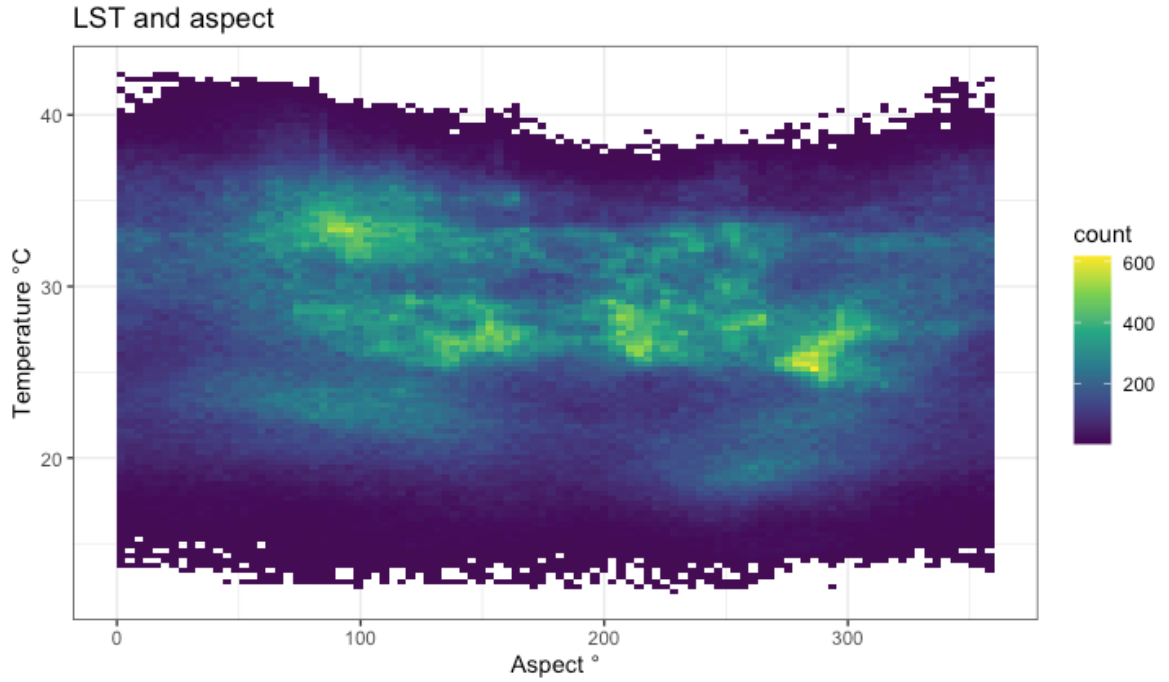

Figure 28. LST and ALS-based aspect in the study area. 0-22.5° = north, 22.5-67.5° = northeast, 67.5-112.5° = east, 112.5-157.5° = southeast, 157.5-202.5° = south, 202.5-247.5° = southwest, 247.5-292.5° = west, 292.5-337.5° = northwest and 337.5-360° = north.

5.4.3 Impact of canopy cover on land surface temperature

Correlation between raw LST and canopy cover for the whole area is -0.37 ($p < 0.001$) and R^2 = 0.14. After the topographic correction based on the multiple regression analysis, the correlation coefficient became -0.42 and R^2 = 0.18. All the variables in model 1 showed statistical significance ($p < 0.001$) and the model produced an adjusted R^2 = 0.74. VIF were < 2.6, expressing no severe multicollinearity. Topographically corrected LST (from hereafter LST') based on model 1 in Figure 29 shows the clear declining pattern of temperature as canopy cover increases. The smallest temperatures do not show any decreasing along the canopy cover gradient, but the hottest records decrease distinctly with increasing canopy cover. Based on the regression analysis, generally the increase from 0 % to 100 % in canopy cover decreases LST with 5 °C.

Results of the four linear regression models including all the explanatory variables are presented in Table 4. Adding the elevation zones to the model increased the adjusted R^2 from 0.74 to 0.77 in model 2, demonstrating a notable difference in canopy cover's cooling power depending on to which altitude zone the pixel belonged. At elevations below 1000 m, canopy cover's cooling effect was -6.6 °C going from 0 % canopy cover to 100 % canopy cover. In 1000–1500 m the effect was -3.2 °C , and above 1500 m the effect was -2.8 °C . Roughly, the cooling impact of canopy cover decreases to half when moving from lowlands to highlands. A considerable dividing line for canopy cover's effect was noticed at the elevation of 1000 m.

Replacing the interaction term of canopy cover and elevation zones with canopy cover and the continuous variable altitude (model 3) produced an adjusted R^2 = 0.74. The coefficient for the interaction term was 0.00005, indicating that 1000-m increase in elevation decreases canopy cover's effect with 0.05 °C. The model performed poorer compared to using the elevation zones. In summary, including either of the elevation factors in the model showed that altitude affects canopy cover's cooling power significantly, having two times higher impact in the lowlands compared to the hills. According to the results from model 4, the magnitude of aspect's influence on canopy cover's cooling power was mostly insignificantly small, except in the cases of northeast, east and southeast, as canopy cover's coefficient decreased by roughly 0.01 °C in these directions. Model 4 had the highest adjusted R^2 = 0.77.

The dependence of canopy cover's impact on elevation is demonstrated in Figure 30 using eight elevation classes. Canopy cover's coefficients decreased with increasing altitude (Figure 30A) after 1000 m, yet increased again in the class 1200–1400 m to roughly the same as in the

lowlands. Smallest effect was found in altitudes above 2000 m. Figure 30B shows R^2 between canopy cover and LST', R^2 being highest in the lowlands in 800–1000 m and in altitudes above 2000 m. Figure 31 represents LST' and canopy cover in different altitudes, the slope being steepest in elevations below 1000 m.

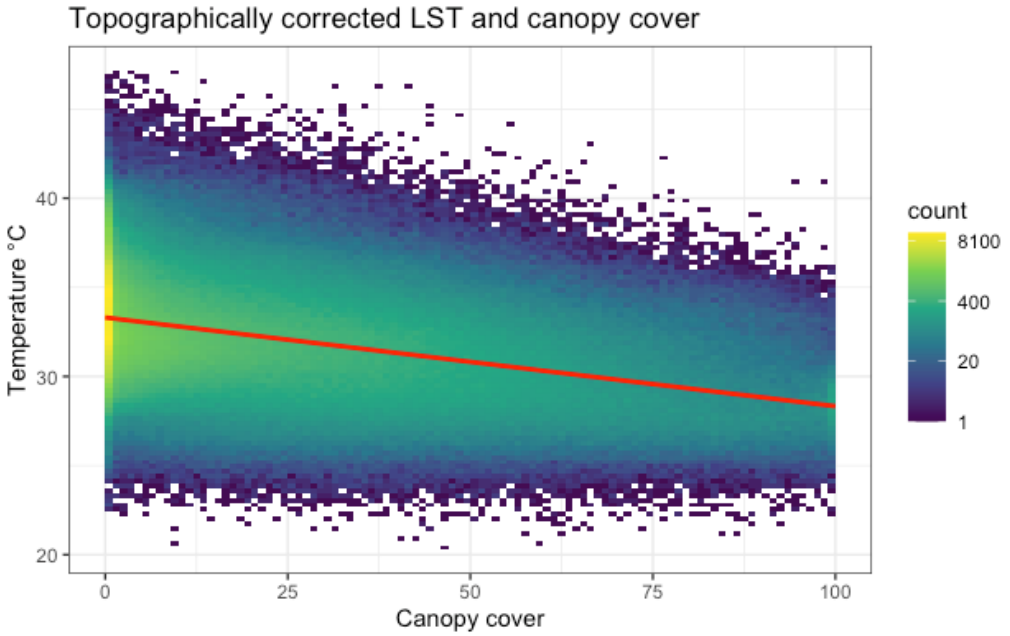

Figure 29. Topographically corrected LST based on model 1 and CC_{ALS} in the whole study area, with regression line.

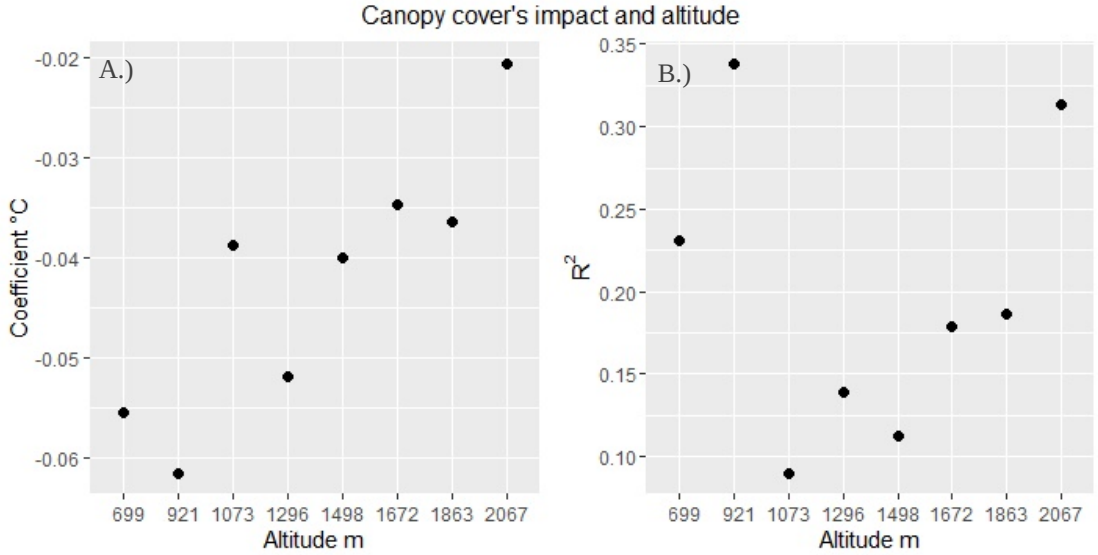

Figure 30. CC_{ALS}'s impact on topographically corrected LST and altitude. Altitude describes the mean elevation of the eight altitude classes. A) CC_{ALS}'s coefficient and altitude. B) R^2 between CC_{ALS} and LST' in different altitude classes.

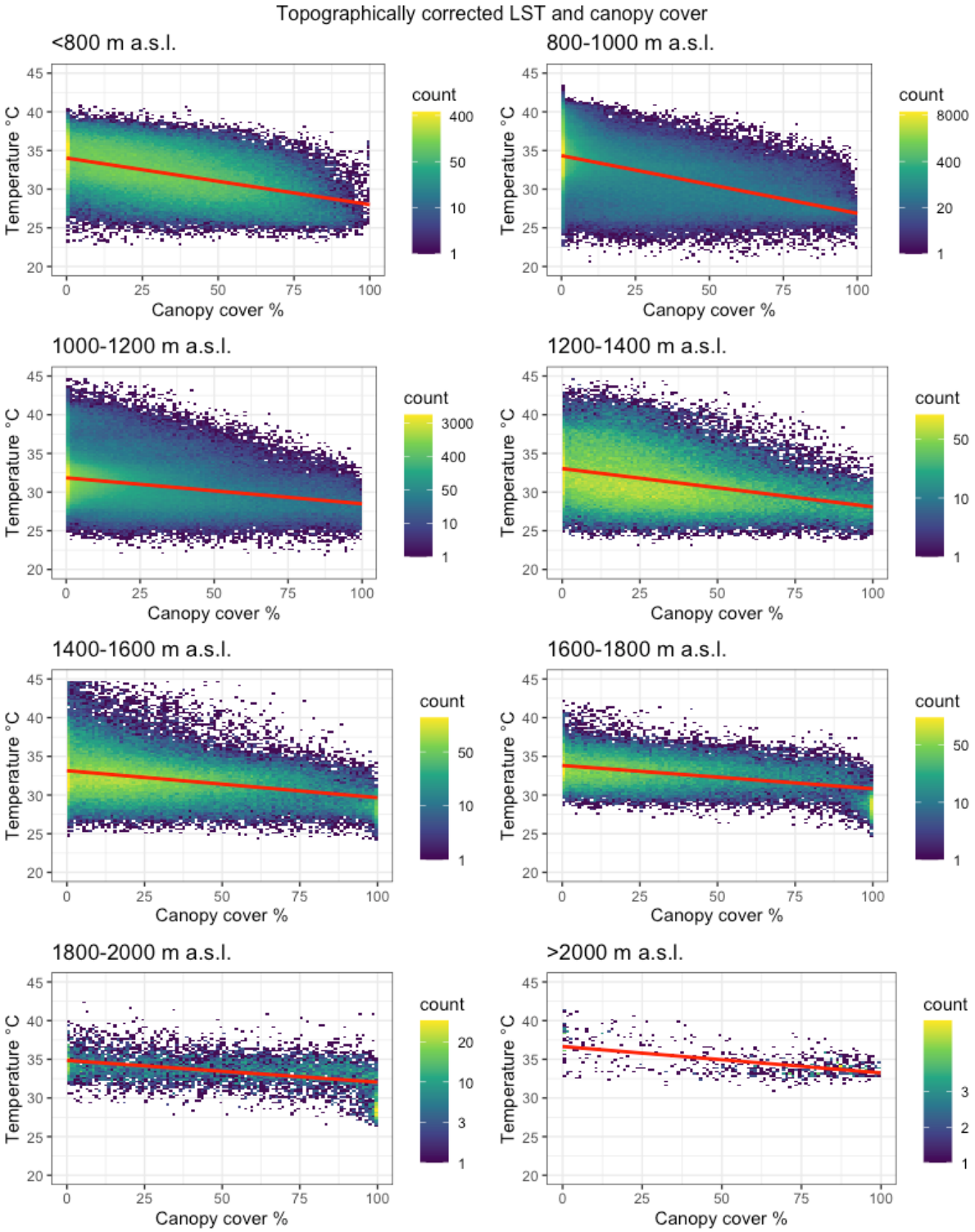

Figure 31. CC_{ALS} and topographically corrected LST in eight elevation classes, with regression line.

Table 4. Summary of regression coefficients in the analysis of LST. The first row refers to the results from the basic multiple regression (model 1), the second row after the inclusion of interactions between elevation zones and canopy cover (model 2), the third row after the inclusion of altitude's and canopy cover's interaction term (model 3), and fourth after the inclusion of interaction terms between canopy cover and elevation zones and canopy cover and aspect (model 4).

Predictor	**Coef**	**Std. Error**	**T-Value**	**P-Value**
Constant	44.79	0.01348	3323.99	<0.001***
	44.24	0.01923	2300.90	<0.001***
	46.71	0.0181	2580.25	<0.001***
	44.38	0.02071	2142.49	<0.001***
Altitude	-0.01305	0.00001	-1241.36	<0.001***
	-0.01128	0.00002	-577.164	<0.001***
	-0.01486	0.00002	-954.59	<0.001***
	-0.01130	0.00002	-579.331	<0.001***
Slope	-4.061	0.01846	-219.95	<0.001***
	-3.806	0.01771	-214.873	<0.001***
	-3.723	0.01841	-202.26	<0.001***
	-3.781	0.01778	-212.625	<0.001***
Canopy cover	-0.04979	0.00001	-419.04	<0.001***
	-0.06816	0.00015	-449.144	<0.001***
	-0.1091	0.00040	-274.65	<0.001***
	-0.07294	0.00035	-207.992	<0.001***
NE	0.1766	0.01105	15.98	<0.001***
	0.08377	0.01036	8.083	<0.001***
	0.1567	0.01094	14.32	<0.001***
	-0.2152	-0.01534	-14.03	<0.001***
E	-0.02963	0.01023	-28.97	<0.001***
	-0.428	0.00960	-44.586	<0.001***
	-0.352	0.01013	-34.73	<0.001***
	-0.7662	0.01388	-55.219	<0.001***
SE	-1.447	0.01033	-140.06	<0.001***
	-1.509	0.00970	-155.612	<0.001***
	-1.529	0.01024	-149.29	<0.001***
	-1.733	0.01361	-127.303	<0.001***
S	-2.095	0.01106	-189.42	<0.001***
	-2.132	0.01039	-205.246	<0.001***
	-2.186	0.01096	-199.41	<0.001***
	-2.166	0.01413	-153.325	<0.001***
SW	-2.441	0.01062	-229.97	<0.001***
	-2.554	0.00998	-256.010	<0.001***
	-2.527	0.01052	-240.07	<0.001***
	-2.538	0.01365	-185.911	<0.001***
W	-2.293	0.01045	-219.46	<0.001***
	-2.254	0.00980	-229.872	<0.001***
	-2.332	0.01035	-225.45	<0.001***
	-2.195	0.01381	-158.998	<0.001***
NW	-1.38	0.01089	-126.8	<0.001***
	-1.205	0.01022	-117.852	<0.001***
	-1.379	0.01078	-127.93	<0.001***
	-1.196	0.01461	-81.864	<0.001***

Table 4 cont.

Predictor	Coef	Std. Error	T-Value	P-Value
1000-1500 m	. -2.667 . -2.678	. 0.007687 . 0.007684	. -346.893 . -348.528	. <0.001*** . <0.001***
>1500 m	. -2.03 . -2.006	. 0.01825 . 0.01823	. -111.218 . -109.998	. <0.001*** . <0.001***
Canopy cover:1000–1500 m	. 0.03083 . 0.03161	. 0.000206 . 0.000206	. 149.695 . 153.501	. <0.001*** . <0.001***
Canopy cover:>1500m	. 0.02758 . 0.03780	. 0.000311 . 0.000311	. 120.662 . 121.574	. <0.001*** . <0.001***
Altitude:canopy cover	. . 0.00005402 .	. . 0.0000003 .	. . 156.31 .	. . <0.001*** .
Canopy cover:NE	. . . 0.0111	. . . 0.0004329	. . . 25.647	. . . <0.001***
Canopy cover:E	. . . 0.01295	. . . 0.0003976	. . . 32.572	. . . <0.001***
Canopy cover:SE	. . . 0.009617	. . . 0.0004015	. . . 23.952	. . . <0.001***
Canopy cover:S	. . . -0.0001076	. . . 0.0004511	. . . -0.238	. . . 0.812
Canopy cover:SW	. . . -0.003497	. . . 0.0004376	. . . -7.99	. . . <0.001***
Canopy cover:W	. . . -0.003214	. . . 0.0004127	. . . -7.788	. . . <0.001***
Canopy cover:NW	. . . -0.0004983	. . . 0.0004311	. . . -1.156	. . . 0.248

5.4.4 Land surface temperature maps

LST map of Taita Hills based on the single channel method is shown in Figure 32. This map does not include topographic correction. LST ranges from 12.4 °C to 43.6 °C. After the topographic correction (Figure 33) based on model 1 described in the previous chapter, canopy cover's effect is emphasized which is particularly visible in thick forests such as Ngangao or Chawia. The Bura riverine forest is also clearly decreasing LST.

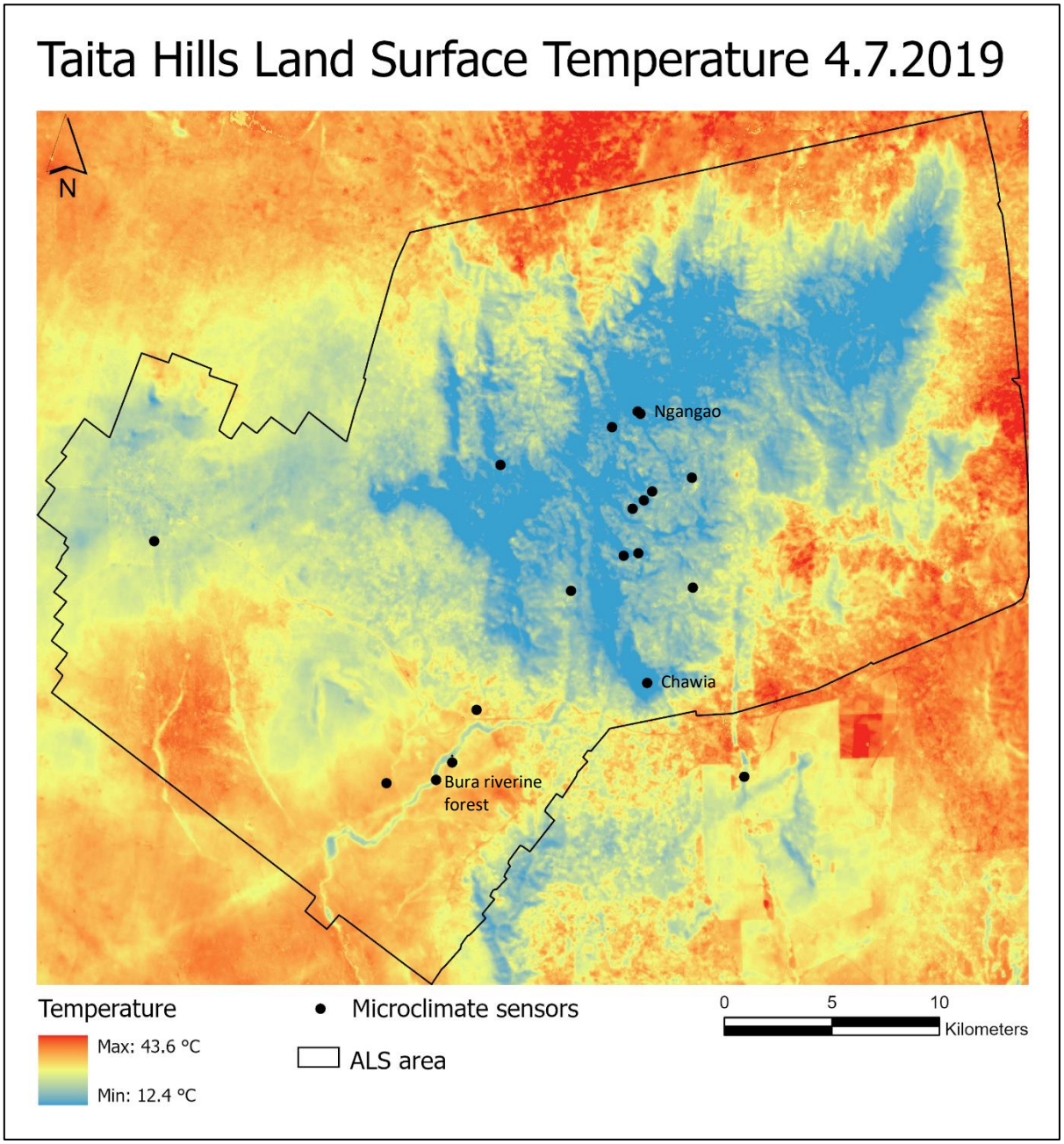

Figure 32. Landsat 8 LST on July 4, 2019, based on the single channel method with no topographic corrections applied.

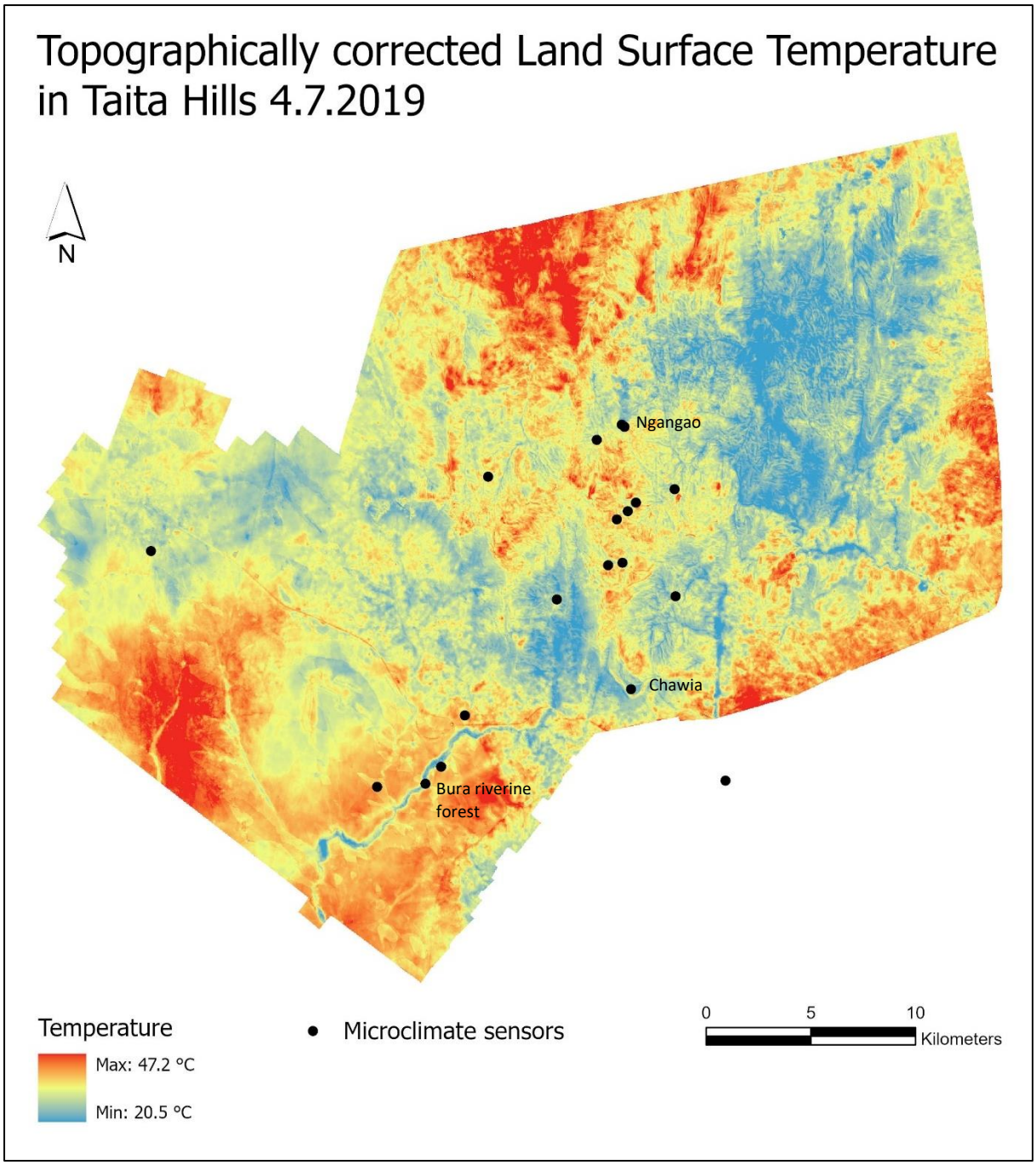

Figure 33. LST map after topographic correction based on model 1. The computed temperatures indicate the situation if the whole area was flat and located in 880 m a.s.l.

6 Discussion

6.1 Assessment of results

6.1.1 Impact of canopy cover on microclimate and land surface temperature

The objective of this study was to find out tree canopy cover's effect and its magnitude on temperatures recorded both at microclimate level as well as based on satellite observations of LST. Canopy cover is not the only factor controlling temperatures, thus the other variables had to be recognized and analyzed to better understand how much canopy cover contributes to temperature variations. Other variables considered in this study were topographic: altitude, slope and aspect. Factors such as the presence of water bodies or buildings were not considered separately. Based on the results, most of the temperature variation could be explained by the topography of the area. This applies both for microclimate and LST and conforms the results by Jucker et al. (2018), He et al. (2019) and Maeda and Hurskainen (2014). The topographic coefficients were similar to the lapse rates and aspect corrections in Maeda and Hurskainen (2014) in Mount Kilimanjaro. The topography can hardly be modified by people, but maintaining or destroying tree cover can impact the temperatures to a significant amount. Climate change is considered a megatrend in Africa (Pellikka & Hakala, 2019), where LULCC are major drivers of climate warming (IPCC, 2018; Abera, et al., 2020). Deforestation and tree cover loss are problems Africa (Fearnside, 2000; FAO, 2016), and in Taita Hills, only 1 % of the original forest cover is remaining (Pellikka, et al., 2009). The goal of this study was to quantify the cooling impact of various canopy covers to find out the extent to which trees can modify the temperatures.

Canopy cover seems to affect surface temperature the most: the mean and maximum computed for microclimate sensors showed highest slopes in $T'_{surface}$. The slope for LST, which can be considered to be closest to $T'_{surface}$, was also higher than it was for T'_{air}. Despite the measuring height of T_{air} being only 13 cm above $T_{surface}$, the effect of canopy cover was notably weaker in T_{air} and is in line with previous studies, where the temperature of the planetary boundary was less affected than LST by the removing of forest cover (Luyssaert, et al., 2014). In this study, temperature change caused by LULCC was not considered, but the results of such comparisons are still directional also in the case of prevalent canopy cover.

The results in this study are in accordance with those by Belsky et al. (1989), who recorded soil temperatures to be 5–11 °C lower under tree canopies compared to open grassland in a savanna

environment. Soil surface showed differences of up to 20 °C. Temperatures were measured and compared based on distance to the single tree under investigation, in contrast to this study, where the focus was on the total canopy cover of pixels sized 30 m x 30 m. In Taita Hills area, differences in mean T'_{soil} and maximum T'_{soil} between 0 % and 100 % canopy cover sites were 5.2 °C and 9 °C, respectively. The slope in maximum $T'_{surface}$ did not rise to as high as in Belsky et al. (1989) and was 12.1 °C. However, the maxima were computed as the average of maximum temperatures for the full study period, including the cooler days, applying the general lapse rates. Observations on the hottest day of the study period showed up to 18 °C differences in T'_{air} and 16 °C in $T'_{surface}$ between the coolest and warmest sites. In this study, dense canopies decreased the mean temperatures close to the ground surface with 4.6–5.9 °C. The results from the satellite image analysis support the findings, as the slope was 5 °C for LST. The effect of trees on climate is usually studied solely based on comparison between open land and forest (De Frenne, et al., 2019), neglecting the intermediate canopies and their significance, despite the fact that human action is mostly focused in areas with trees outside forests. This study showed that temperature and canopy cover have a liner relationship, pointing out that full canopy cover is not needed for a sensible cooling effect.

The diurnal temperature variations observed in the microclimate sensor sites follow the results from previous studies (Chen, et al., 1999). The maxima in the study sites were reached in the afternoon, and minima around sunrise. Similar results were found by Bouka Biona et al. (2001). The diurnal variation in temperatures was smallest under dense canopies, which has been found to be the global trend (e.g. Jin & Dickinson, 2011). Soil diurnal temperatures are expected to be lower than air temperatures and decrease exponentially with soil depth, reaching the maximum a few hours later than air temperature. During the night, air temperatures usually decrease below soil temperatures (McIntosh & Sharratt, 2001). In the tropics in general, forests have been discovered to have a slight cooling effect on minimum temperatures during the night (Li, et al., 2016b; Li, et al., 2015), which is utilized for example in coffee cultivation in Ethiopia (Hailu, et al., 2015). In Mount Kilimanjaro, Tanzania, vegetation cover had no effect on nocturnal LST (Maeda & Hurskainen, 2014). In this study, there existed a positive correlation between canopy cover and night temperatures at surface and air levels. However, the relationship was not as strong as during daytime: smallest variation between the study sites was observed at dawn. Fluctuations were considerably smaller in night temperatures compared to daytime temperatures. The nocturnal LST was not examined but night temperatures were solely studied with the microclimate sensors.

The altitudinal differences of trees' cooling impact were studied using the satellite image, and it was found that the cooling effect of trees is relative to altitude. In Taita Hills, a critical dividing line in 1000 m a.s.l. was observed where the cooling effect of trees decreased remarkably to around half compared to the lowlands. The result indicates that trees' importance in controlling temperatures increases in hot environments. The LST image was from a sunny, cloudless day in July and does not represent the year-round situation in the study area that experiences two annual rainy seasons. In the hills, cloudy and misty conditions are experienced throughout the year (Pellikka, et al., 2009; Helle, 2016). Based on the results from the microclimate sensors, during the cooler days, which indicate overcast conditions, canopy cover's cooling effect decreases and the temperature differences between low and high canopy cover sites are smaller. This further reaffirms that the cooling effect is relative to the prevalent temperatures. Plant evapotranspiration rates are relative to the solar radiation and ambient temperatures (Allen, et al., 1998), which is likely one reason behind the phenomenon. The discovery is meaningful, since agricultural expansion in the area is predicted to take place predominantly in the lowlands (Erdogan, et al., 2011; Maeda, et al., 2010a), where the temperatures are very high. Increasing tree cover on farmlands could thus be of considerable benefit in controlling the temperatures, especially in the lowlands. The impact of canopy cover on temperature is also most likely different on different days and different times of the year. For instance, Maeda et al. (2014) found that land cover's influence on LST in Mount Kilimanjaro was stronger in July compared to February.

6.1.2 Comparison of land surface temperature and microclimatological measurements

LST produced higher temperatures compared to field measurements both at the exact overpass time as well as compared to the mean temperature of the day, yet the differences in $T_{surface}$ and T_{air} were not statistically significant. $T_{surface}$ mean of the overpass date showed highest correlation with LST as expected, but at the time of the satellite overpass, T_{air} had the results closest to LST. This is in accordance with Mildrexler et al. (2011) who found Aqua/MODIS LST_{max} to be constantly higher than T_{max} measured in 1.5 m. In Mallorca, *in situ* measured LST produced 3–18 °C higher daytime temperatures than air temperature at 2 m height (Simó, et al., 2018). This thesis did not examine the universally used air temperature measured in 1.5 m or LST_{max}, thus the results are not completely comparable, yet they follow the same trend of satellite LST's higher estimates compared to *in situ* measurements. However, the temperatures recorded with the microclimatological measurements were surprisingly similar to those of LST. The low measuring height could explain the results. T_{soil} in turn showed constantly lower values

than LST, which can most likely be explained by dry surface soil's poor transmission of radiation in hot days (Simó et al., 2018).

6.1.3 Trees' cooling benefits and ecosystem services in facing climate change

Canopy cover can contribute to buffering the microclimate warming. An increase of 2 °C of the global temperature as a consequence of enhanced greenhouse effect can have detrimental impacts on the most vulnerable ecosystems (IPCC, 2018). Since the time span of local changes in temperatures due to LULCC is much shorter than in the global climate change, the regional and local consequences can be of even higher extent (Chen, et al., 1999). Due to the debts of species' adaptation capabilities to climate warming, changes in the microclimate temperatures may be fatal for flora and fauna occupying very narrow thermal niches. This may further impact biodiversity and consequently the crucial ecosystem services provided by forests that take place close to ground surface (Chen, et al., 1999; Zellweger, et al., 2020). For instance, soil evapotranspiration affects the availability of water to plants, which in turn affects plant growth (Breshears, et al., 1998). On the other hand, temperature rise may increase the biological activity in soils, which leads to enhanced decomposition of organic matter and the loss of soil carbon (Chapman, 2012). The thermal environments of forests are controlled by canopies to a high extent, which was reaffirmed in this study.

Fragmentation decreases a tropical forest's ability to buffer climate change (Ewers & Banks-Leite, 2013), but on regional scale even smaller forests moderate LST (Mildrexler, et al., 2011). Tree cover on farms has the same effect on local temperatures as forests despite the smaller scale and can hence help in conserving the biodiversity, as was the case in Costa Rica where farm trees were found to increase notably the number of tree and plant species (Mendenhall, et al., 2016). This study showed how the relationship of canopy cover and temperatures is linear and how sites with agroforestry trees and moderate canopy cover were already experiencing both lower mean and maximum temperatures than the open sites. Maintaining a moderate canopy cover may buffer against the impacts of climate change (De Frenne, et al., 2019). Most of the canopy cover in Taita Hills comprises of trees not classified as forests, occurring on farms and human settlement. Based on the results in this study, TOF may have substantial effect on regional LST as well as local microclimates. This conforms the findings of Mildrexler et al. (2011) about small forest patches' potential in moderating regional LST, and based on this study, even TOF have the same effect.

6.1.4 Agroforestry and food security

The Agriculture (Farm Forestry) Rules 2009 requires that at least 10 % forest cover should be mainatined on farms, and in Taita Hills an addition in carbon stocks since 2003 was reported by Pellikka et al. (2018). Based on this study, even 10 % canopy cover decreases temperatures. Soil and air temperatures affect crop productivity, as plants have optimal thermal ranges where their growth is maximized. In general, increasing temperatures make plant growth more efficient, but this is the case only as long as the increase occurs within the thermal limits of the plant's tolerance (Muimba-Kankolongo, 2018). As extreme heat and precipitation events are becoming more common with climate change (MoALF, 2016; IPCC, 2018), the negative effects of warming will become notable in the area. This further threatens the area's food security, especially as the most common crop in the area, maize, is one of the most vulnerable crops in terms of climate change in Africa. As maize residuals are also fed to cattle, the reduction in yields will affect livestock as well in addition to water scarcity and heat stress (Niang, et al., 2014). The implication of agroforestry practices especially in the lowlands could help in mitigating extreme weather events and moderating better thermal conditions for crops, as the results from this study showed that even moderate tree cover decreases temperatures and that the cooling impact is highest in hot environments. Changes in microclimatic conditions affect also pollinators, whose habitats are at high risk of degradation due to climate change and LULCC (Potts, et al., 2010). The reduction of pollinators may affect the yields and results in food insecurity. Trees provide both cooling of temperatures and maintain habitats for pollinators.

In addition to improved microclimates, other factors can prompt the adoption of agroforestry. Soil degradation is an alarming problem in sub-Saharan Africa (Garrity, et al., 2010). Soil erosion is a consequence of conversion of natural vegetation to farmland and in Taita Hills a problem that is expected to become worse in the future (Erdogan, et al., 2011; Maeda, et al., 2010b). Agroforestry has been widely documented to decrease soil erosion and degradation (Kuyah, et al., 2019). Trees on farms may increase soil fertility through increased amounts of leaf litter, which returns nutrients back to the soil in the process of decomposition, and depending on the tree species, possibly also through nitrogen fixation (Chander, et al., 1998; Garrity, et al., 2010). Even the indigenous forests contribute to the food security in the area, since cloud forests on the hills act as a water tower for the farms in the foothills and lowlands (Pellikka, et al., 2013). It is already observed that the hills cannot provide sufficient amounts of irrigation water to the lowland farms (Maeda, et al., 2011). The pressure on tropical forests in

sub-Saharan Africa is caused mostly by the collection of fuelwood (Abdelgalil, 2004), and could be relieved with increasing the tree cover on farms (Unruh, et al., 1993).

Trees on farms need to be planned and managed properly in order not to compromise yield. Bad design and management may lead to the transpiration of trees to increase to such high volumes that the soil moisture becomes very low and leads to the suffering of crops. In these cases, the microclimatic benefits are outweighed by the negative impacts of high transpiration (Ong, et al., 2006; Kuyah, et al., 2019). Water is scarce especially in the lowland areas, and trees' vast need for water must be taken into account. The phenomenon is paradoxical, since trees improve water cycles in general but are also consumers of high amounts of water (Ong, et al., 2006). In areas with water scarcity, trees' competition of water resources with crops, animals and people may be a limiting factor in the adoption of agroforestry practices.

6.2 Evaluation of methods

6.2.1 Canopy cover based on airborne laser scanning and hemispherical photography

The most important concept considered in this thesis was canopy cover, which was retrieved using two methods: ALS and hemispherical photography. The computed canopy cover value is only representing the reality, not the absolute and true canopy cover. In this study, CC_{ALS} and CC_{HP} were compared and CC_{ALS} was used in the temperature analyses. CC_{ALS} was obtained in 2014 and 2015, 4–5 years earlier than CC_{HP}. The scannings took place in February and March and hemispherical photographs are from May-June, which means that the canopy covers are computed during different seasons and phenology stages, consequently affecting the canopy cover. Another viewpoint is that the CC_{ALS} is in raster format and consists of 30-meter pixels, meaning they are not absolute plot-wise numbers but represent the whole pixel. The hemispherical photographs were not taken in the exact middle of the canopy cover pixels due to practical reasons, which means that the image plot may cover partly two or more pixels in CC_{ALS}. There can be significant differences in the canopy cover in the ALS scale of 30 meters, meaning that two adjacent pixels in the map can have very different values. Heiskanen et al. (2015a) conclude that CC_{HP} is accurate with the few photographs in the higher canopy covers, but scatters more as canopy cover decreases. This indicates that more photographs are likely needed for more accurate canopy cover computation in lower canopy covers. In this study, the sampling is smaller than in Heiskanen et al. (2015a), but a similar phenomenon was notable as the estimates were fairly similar in the canopy cover extremes. More photographs would probably have been needed for more accurate estimations, as in intermediate canopy covers the

location of photography sites affect the results in contrast to ALS. CC_{HP} produced lower estimates than CC_{ALS}, which can at least partly be explained by the fact that the method for canopy cover retrieval is based on the threshold method for canopy closure which includes canopy gaps (Korhonen, et al., 2006).

CC_{ALS} introduces the possibility of error in the analysis due to the time difference between the flight campaign and the temperature data in this study. Nevertheless, CC_{HP} showed that no significant change in canopy cover had occurred since 2013 and 2014 in the field plot sites, which makes the CC_{ALS} relatively reliable.

6.2.2 Microclimate

Local temperatures were studied with microclimate sensors recording temperature and soil moisture in three different levels near ground surface. The sensors provided data with high temporal resolution of 15 minutes. Soil moisture was not considered in this study but including it would have provided more useful information as moisture and temperature are closely related.

The sample size of soil sensor sites was small, only 19, which makes them susceptible for randomness. Topographic correction was applied on the microclimate data and was calculated based on elevation only. For aspect correction, there would have needed more sites to represent each class. In this case, the small amount of observations did not allow for calculation of aspect impact, which is however expected to exist based on the results from the LST analysis. Results from the comparison between microclimate temperatures and aspect showed that other factors, such as the other topographic variables, were affecting the temperatures more than aspect. Due to the topographic manipulation of the temperatures, they did not represent the true values recorded, but made the temperatures comparable in terms of canopy cover. The actual measurements of each sensor are compiled in Appendices 1–3. There exists a need for studies in these scales (Jucker, et al., 2018) and this study has despite the limited number of observations provided information about a topic whose importance has only recently been recognized (De Frenne, et al., 2013; Zellweger, et al., 2020).

6.2.3 Land surface temperature

As has been documented in several studies, spaceborne TIR remains an uncertain method for accurate LST retrieval (Simó, et al., 2018; Li, et al., 2013). Li et al. (2013) list the main problems related to LST: the mathematically unsolvable problems with unknown factors regarding the retrieval, the inaccuracies proposed by noise and atmospheric correction, the coupling of LSE to LST, complicatedness of atmospheric corrections, physical interpretation

of LST and the validation of satellite-derived LST. After all, LST is an indirect measurement and the results of complicated mathematical processing requiring knowledge of several components, where error in any of them causes inaccuracies in LST (Simó, et al., 2018). Estimation of LSE is determinant in the correct LST retrieval, yet highly difficult to measure and prone to error. Landsat 8 TIRS band 11 was not used in this study due to the stray light problem, which exposes the LST to higher possibility of inaccuracy. Wang, et al. (2019) recommend the use of SW for Landsat 8, but as long as the use of band 11 is not recommended by USGS and in the waiting of more scientific evidence on the effectiveness of stray light correction, using Landsat 8 band 11 remains questionable. However, Wang, et al. (2019) concluded that the SC is a valid method for Landsat 8 and produces results on accuracy high enough for most purposes. In this study, no systematic validation of LST was performed.

Since the major interest was in canopy cover's effect on temperature, the results based on SC method were topographically corrected, which further caused the LST not to represent the reality but made the temperatures comparable. Moreover, in dense canopies the signal constitutes mostly of the upper canopy and does not necessarily capture the temperatures on the forest floor, which does not make them representative of understory conditions (Bense, et al., 2016; Zellweger, et al., 2019).

Previous research about vegetation and LST have been often conducted in much lower spatial resolutions and used less accurate topographic correction (Li, et al., 2015). This study used a DEM of 30 m acquired with ALS over the precise study area, making more accurate topographic corrections possible. This kind of high-resolution data about topographic and canopy variables is more suitable for local and regional studies, especially if moving to even smaller scale as to microclimates.

6.3 Improvements and future research

Including soil moisture, air temperature and more field plots would have provided more useful information about the sites and their differences. A greater sample size would have made also more accurate topographic corrections possible. As the field plots in this study were under 20, unknown factors and coincidence may affect the results and conclusions cannot me drawn in a very large scale. The study could also be expanded to cover more months or even years since the variation in temperatures is not expected to be stable (Maeda & Hurskainen, 2014). The elevational differences discovered in canopy cover's cooling power should be explored more

thoroughly in the future for instance by including analyses of mean temperatures, evapotranspiration and NDVI in different elevation zones.

Agroforestry's potential in climate change mitigation and adaptation has been recognized. Not all trees are of equal benefits in agroforestry, and future research could be targeted to the comparison of different agroforestry species' cooling potential as well as plantation forests. It is also important to separate the different resolutions: satellite-derived LST does not necessarily describe the microclimate very well, but microclimate scale does not tell about the temperatures of a whole region (Li, et al., 2013; Jucker, et al., 2018). Both satellite observations and field measurements of microclimate are needed in the studies tackling climate change since both scales are relevant.

ALS is not yet been commonly used in studies about microclimates. As more scannings will take place in an increasing number of places, the knowledge gap of spatial differences about microclimates and factors affecting them will shrink. As 3D data will become more common, also regional studies in wider scales with high-resolution spatial data about topography and canopies as well as other factors can be conducted. More spatially specific information would also make modelling of impacts more accurate.

7 Conclusions

This study demonstrates a consistent but heterogeneous influence of canopy cover on the microclimate of highly diverse tropical ecosystems. Temperatures correlate inversely with canopy cover, the effect being strongest on surface temperatures. During the hottest days, the difference between sites of high and low canopy covers becomes most notable. The cooling effect does not exist only with high canopy cover, but even intermediate canopy cover buffers the highest temperatures. This study agrees with previous research that trees have potential in decreasing particularly the temperature maxima. However, various other factors play a part in determining the temperature of a given area.

LST is affected by canopy cover in similar manner as microclimate. Increase in canopy cover does not need to be high in order to decrease the local LST, but the relationship is linear and any change in canopy cover will influence the temperatures. Therefore, tree canopies do not only affect the local microclimates but impact LST as well, proposing that the impact is wider than only the immediate surroundings.

The most important finding of this study was that canopy cover's cooling power decreases with increasing altitude. In the highlands, the cooling power is roughly the half compared to the lowlands. This highlights trees' role in cooling the temperatures of warm areas compared to areas with mild temperatures. In the plains where dense tree cover is scarce, adopting agroforestry practices could improve the microclimates and decrease the local and regional LST as well. However, the viewpoint of water availability must be considered, and may be a limiting factor in implementing agroforestry.

This study provided valuable information about trees' potential in climate change adaptation and mitigation in a tropical environment. Including more sample plots and variables would have made this study even more comprehensive. Remote sensing technologies like ALS and TIRS should be utilized more in research due to their many advantages and possibilities in examining tree cover's impact on climate in many resolutions.

8 Acknowledgements

This thesis was conducted as part of Smartland project (Environmental sensing of ecosystem services for developing a climate-smart landscape framework to improve food security in East Africa, decision no. 31864) funded by Academy of Finland.

I would like to thank everyone who has helped and supported me during this project. Special thanks to Mwadime Mjomba who helped me during my field work by being my driver and assistant and offering me endless support and encouragement. My thanks to also everyone working in the Taita Research Station for taking such good care of me during my stay in Kenya. I am also deeply grateful to Agnes Mwangombe, Ali Ndizi, Mrs. Mwamburis, Mrs. Nyatta, Cathrine Mwakesi, Simon, Moses Onyimbo and Dalmas moka secondary school, Jason Collette and Teita Sisal Estate, St. Mary's Teachers' Training College, and Taita Taveta University Ngerenyi campus for letting me keep the soil sensors on their lands and assisting during the installations as well as protecting the sensors from harm. Chawucha!

I want to express my gratitude to my supervisors Prof. Petri Pellikka for offering me this opportunity to work in Kenya with such an interesting topic and for all the guidance along the way, Dr. Eduardo Maeda for the initial idea for this thesis and the valuable comments on the work, and Dr. Janne Heiskanen for the help with R and the encouragement I have received. Moreover, I would like to thank Dr. Petteri Muukkonen for his help during this work, Dr. Matti Räsänen for provision of weather station data and Dr. Hari Adhikari for the canopy cover data.

Lastly, I want to thank my student colleagues, friends and family for the love, support and patience with me during this journey. I want to thank particularly my brother Eljas for teaching me R and statistics during late-night Zoom-meetings.

9 References

Abdelgalil, E. A. (2004). Deforestation in the drylands of Africa: Quantitative modelling approach. *Environment, Development and Sustainability, 6*, 415-427.

Abera, T. A., Heiskanen, J., Pellikka, P. K., Adhikari, H., & Maeda, E. E. (2020). Climatic impacts of bushland to cropland conversion in Eastern Africa. *Science of The Total Environment, 717*(137255).

Abera, T. A., Heiskanen, J., Pellikka, P., & Maeda, E. E. (2018). Rainfall–vegetation interaction regulates temperature anomalies during extreme dry events in the Horn of Africa. *Global and Planetary Change, 167*, 35-45.

Abera, T. A., Heiskanen, J., Pellikka, P., Rautiainen, M., & Maeda, E. E. (2019). Clarifying the role of radiative mechanisms in the spatio-temporal changes of land surface temperature across the Horn of Africa. *Remote Sensing of Environment, 221*, 210-224.

Adhikari, H. (2017). Canopy cover raster of Taita Hills and Maktau.

Adhikari, H., Heiskanen, J., Siljander, M., Maeda, E., Heikinheimo, V., & Pellikka, P. K. (2017). Determinants of Aboveground Biomass across an Afromontane Landscape Mosaic in Kenya. *Remote Sensing, 9*(8), 827.

Adhikari, U., Nejadhashemi, A. P., & Woznicki, S. A. (2015). Climate change and eastern Africa: a review of impact on major crops. *Food and Energy Security, 4*(2), 110-132.

Akinwande, M. O., Dikko, H. G., & Samson, A. (2015). Variance Inflation Factor: As a Condition for the Inclusion of Suppressor Variable(s) in Regression Analysis. *Open Journal of Statistics*(5), 754-767.

Akinyemi, F. O., Ikanyeng, M., & Muro, J. (2020). Land cover change effects on land surface temperature trends in an African urbanizing dryland region. *City and Environment Interactions, 4*.

Alexander, C., Moeslund, J. E., Bøcher, P. K., Arge, L., & Svenning, J.-C. (2013). Airborne laser scanner (LiDAR) proxies for understory light conditions. *Remote Sensing of Environment, 134*, 152-161.

Alkama, R., & Cescatti, A. (2016). Biophysical climate impacts of recentchanges in global forest cover. *Science, 351*(6273), 600-604.

Allen, R. G., Pereira, L. S., Raes, D., & Smith, M. (1998). *Crop evapotranspiration - Guidelines for computing crop water requirements.* Rome: Food and Agriculture Organization of the United Nations.

Baccini, A., Walker, W., Carvalho, L., Farina, M., Sulla-Menashe, D., & Houghton, R. A. (2017). Tropical forests are a net carbonsource based on abovegroundmeasurements of gain and loss. *Science, 358*(6360), 230-234.

Barbierato, E., Bernetti, I., Capecchi, I., & Saragosa, C. (2019). Quantifying the impact of trees on land surface temperature: a downscaling algorithm at city-scale. *European Journal of Remote Sensing, 52*(S4), 74-83.

Belsky, A. J., Amundson, R. G., Duxbury, J. M., Riha, S. J., Ali, A. R., & Mwonga, S. M. (1989). The Effects of Trees on Their Physical, Chemical and Biological Environments in a Semi-Arid Savanna in Kenya. *Journal of Applied Ecology, 26*(3), 1005-1024.

Bense, V. F., Read, T., & Verhoef, A. (2016). Using distributed temperature sensing to monitor field scale dynamics of ground surface temperature and related substrate heat flux. *Agricultural and Forest Meteorology, 220*, 207-215.

Boffa, J.-M. (1999). *Agroforestry Parklands in Sub-Saharan Africa. FAO Conservation Guide 34.* Rome: Food and Agriculture Organization of the United Nations.

Bouka Biona, C., Druilhet, A., Benech, B., & Lyra, R. (2001). Diurnal cycle of temperature and wind fluctuations within an African equatorial rain forest. *Agricultural and Forest Meteorology, 109*(2), 135-141.

Breshears, D. D., Nyhan, J. W., Heil, C. E., & Wilcox, B. P. (1998). Effects of Woody Plants on Microclimate in a Semiarid Woodland: Soil Temperature and Evaporation in Canopy and Intercanopy Patches. *International Journal of Plant Sciences, 159*(6), 1010-1017.

Brink, A. B., & Eva, H. D. (2009). Monitoring 25 years of land cover change dynamics in Africa: A sample based remote sensing approach. *Applied Geography, 29*(4), 501-512.

Chander, K., Goyal, S., Nandal, D. P., & Kapoor, K. K. (1998). Soil organic matter, microbial biomass and enzyme activitiesin a tropical agroforestry system. *Biology and Fertility of Soils, 27*(2), 168-172.

Chapman, P. J. (2012). Soil in the environment. In J. Holden (Ed.), *An Introduction to physical Geography and the Environment* (pp. 269-306). Pearson Education Limited.

Chen, J., Saunders, S. C., Crow, T. R., & Naiman, R. J. (1999). Microclimate in forest ecosystem and landscape ecology. *Bioscience, 49*(4), 288-297.

Das, A., Nagendra, H., Anand, M., & Bunyan, M. (2015). Topographic and Bioclimatic Determinants of the Occurrence of Forest and Grassland in Tropical Montane Forest-Grassland Mosaics of the Western Ghats, India. *PLoS One, 10*(6).

De Frenne, P., Rodríguez-Sánchez, F., Coomes, D. A., Baeten, L., Verstraeten, G., Vellend, M., . . . Verheyen, K. (2013). Microclimate moderates plant responses to macrocliamte warming. *PNAS, 110*(46), 18561-18565.

De Frenne, P., Zellweger, F., Rodríguez-Sánchez, F., Scheffers, B. R., Hylander, K., Luoto, M., . . . Lenoir, J. (2019). Global buffering of temperatures under forest canopies. *Nature Ecology & Evolution*(3), 744-749.

Deutsch, C. A., Tewksbury, J. J., Huey, R. B., Sheldon, K. S., Ghalambor, C. K., Haak, D. C., & Martin, P. R. (2008). Impacts of climate warming on terrestrial ectotherms across latitude. *PNAS, 105*(18), 6668-6672.

D'Odorico, P., He, Y., Collins, S., De Wekker, S. F., Engel, V., & Fuentes, J. D. (2013). Vegetation–microclimate feedbacks in woodland–grassland ecotones. *Global Ecology and Biogeography, 22*(4), 364-379.

Dollinger, J., & Jose, S. (2018). Agroforestry for soil health. *Agroforestry Systems, 92*, 213-219.

Ellison, D., Morris, C. E., Locatelli, B., Sheil, D., Cohen, J., Murdiyarso, D., . . . Sullivan, C. A. (2017). Trees, forests and water: Cool insights for a hot world. *Global Encironmental Change, 43*, 51-61.

Erdogan, H. E., Pellikka, P. K., & Clark, B. (2011). Modelling the impact of land-cover change on potential soil loss in the Taita Hills, Kenya, between 1987 and 2003 using remote-sensing and geospatial data. *International Journal of Remote Sensing, 32*(21), 5919-5945.

Ewers, R. M., & Banks-Leite, C. (2013). Fragmentation Impairs the Microclimate Buffering Effect of Tropical Forests. *PLoS ONE, 8*(3).

FAO. (2000). *Global Forest Resources Assessment 2000 (FRA 2000).* Food and Agriculture Organization of the United Nations.

FAO. (2015). *Forest Resources Assessment. Terms and definitions.* Rome: Food and Agriculture Organization of the United Nations.

FAO. (2016). *Global forets resources assessment 2015. How are the world's forests changing?* (2 ed.). Rome: Food and Agriculture Organization of the United Nations.

Fearnside, P. M. (2000). Global warming and tropical land-use change: greenhouse gas emissions from biomass burning, decomposition and soils in forest conversion, shifting cultivation and secondary vegetation. *Climatic Change, 46*, 115-158.

García-Santos, V., Cuxart, J., Martínez-Villagrasa, D., Jiménez, M. A., & Simó, G. (2018). Comparison of Three Methods for Estimating Land Surface Temperature from Landsat 8-TIRS Sensor Data. *Remote Sensing, 10*(9).

Garrity, D. P., Akinniesi, F. K., Ajayi, O. C., Weldesemayat, S. G., Mowo, J. G., Kalinganire, A., . . . Bayala, J. (2010). Evergreen Agriculture: a robust approach to sustainable food security in Africa. *Food Security, 2*(3), 197-214.

Gkatsopoulos, P. (2017). A Methodology for Calculating Cooling from Vegetation Evapotranspiration. *Procedia Environmental Sciences, 38*, 477-484.

Gonsamo, A., D'odorico, P., & Pellikka, P. (2013). Measuring fractional forest canopy element cover and openness – definitions and methodologies revisited. *Oikos, 122*(9), 1283-1291.

Griffin, A. M., Popescu, S. C., & Zhao, K. (2008). Using LIDAR and Normalized Difference Vegetation Index to remotely determine LAI and percent canopy cover. *SilviLaser*(17-19), 446-455.

Hailu, B. T., Maeda, E. E., Pellikka, P., & Pfeifer, M. (2015). Identifying potential areas of understorey coffee in Ethiopia's highlands using predictive modelling. *International Journal of Remote Sensing, 36*(11), 2898-2919.

He, J., Zhao, W., Li, A., Wen, F., & Yu, D. (2019). The impact of the terrain effect on land surface temperature variation based on Landsat-8 observations in mountainous areas. *International Journal of Remore Sensing, 40*(5-6), 1808-1827.

Heiskanen, J., Korhonen, L., Hietanen, J., & Pellikka, P. K. (2015a). Use of airborne lidar for estimating canopy gap fraction and leaf area index of tropical montane forests. *International Journal of Remote Sensing, 36*(10), 2569-2583.

Heiskanen, J., Korhonen, L., Hietanen, J., Heikinheimo, V., Schäfer, E., & Pellikka, P. K. (2015b). Comparison of field and airborne laser scanning based crown cover estimates across land cover types in Kenya. *The international archives of the photogrammetry, remote sensing and spatial information sciences, XL-7/W3*, 409-415.

Helle, J. (2016). *Lentolaserkeilaus ja hemisfäärikuvaus metsikkösadannan tutkimisessa Taitavuorilla Keniassa.* Bachelor's thesis, University of Helsinki.

IPCC. (2018). *Global Warming of 1.5°C. An IPCC Special Report on the impacts of global warming of 1.5°C above pre-industrial levels and related global greenhouse gas emission pathways, in the context of strengthening the global response to the threat of climate change, sustainable development, and efforts to eradicate poverty*. Intergovernmental Panel on Climate Change.

Jennings, S. B., Brown, N. D., & Sheil, D. (1999). Assessing forest canopies and understorey illumination: canopy closure, canopy cover and other measures. *Forestry, 72*(1), 59-73.

Jensen, J. R. (2007). *Remote Sensing of the Environment: An Earth Resource Perspective* (2 ed.). Prentice Hall.

Jiménez-Muñoz, J. C., Cristóbal, J., Sobrino, J. A., Sòria, G., Ninyerola, M., & Pons, X. (2009). Revision of the Single-Channel Algorithm for Land Surface Temperature Retrieval

From Landsat Thermal-Infrared Data. *IEEE Transactions on Geoscience and Remote Sensing, 47*(1), 339-249.

Jiménez-Muñoz, J. C., Sobrino, J. A., Skoković, D., Mattar, C., & Cristóbal, J. (2014). Land Surface Temperature Retrieval Methods From Landsat-8 Thermal Infrared Sensor Data. *IEEE Geoscience and Remote Sensing Letters, 11*(10), 1840-1843.

Jin, M., & Dickinson, R. E. (2010). Land surface skin temperature climatology: benefitting from the strengths of satellite observations. *Environmental Research Letters, 5*(4).

Juan, J.-M. C., & Sobrino, J. A. (2003). A generalized single-channel method for retrieving land surface temperature from remote sensing data. *Journal of Geophysical Research, 108*(D22).

Jucker, T., Hardwick, S. R., Both, S., Elias, D. D., Ewers, R. M., Milodowski, D. T., . . . Coomes, D. A. (2018). Canopy structure and topography jointly constrain the microclimate of human-modified tropical landscapes. *Global Change Biology, 24*, 5243-5258.

Kim, J.-P. (2013). Variation in the accuracy of thermal remote sensing. *International Journal of Remote Sensing, 34*(2), 729-750.

Kohli, A., & Saini, B. C. (2003). Microclimate modification and response of wheat planted under trees in afan design in northern India. *Agroforestry Systems, 58*, 109-118.

Korhonen, L., Korhonen, K. T., Rautiainen, M., & Stenberg, P. (2006). Estimation of Forest Canopy Cover: a Comparison of Field Measurement Techniques. *Silva Fennica, 40*(4), 577-588.

Korhonen, L., Korpela, I., Heiskanen, J., & Maltamo, M. (2011). Airborne discrete-return LIDAR data in the estimation of vertical canopy cover, angular canopy closure and leaf area index. *Remote Sensing of Environment, 115*, 1065-1080.

Kuyah, S., Whitney, C. W., Jonsson, M., Sileshi, G. W., Öborn, I., Muthuri, C. W., & Luedeling, E. (2019). Agroforestry delivers a win-win solution for ecosystem servicesin sub-Saharan Africa. A meta-analysis. *Agronomy for Sustainable Development, 39*(47).

Leakey, R. R., Tchoundjeu, Z., Schreckenberg, K., Schackelton, S. E., & Schackelton, C. M. (2005). Agroforestry Tree Products (AFTPs): TargetingPoverty Reduction and Enhanced Livelihoods. *International Journal of Agricultural Sustainability, 3*(1), 1-23.

Li, Y., De Noblet-Ducoudré, N., Davin, E. L., Motesharrei, S., Zeng, N., Li, S., & Kalnay, E. (2016a). The role of spatial scale and background climate in the latitudinal temperature response to deforestation. *Earth System Dynamics, 7*, 167-181.

Li, Y., Zhao, M., Mildrexler, D. J., Motesharrei, S., Mu, Q., Kalnay, E., . . . Wang, K. (2016b). Potential and Actual impacts of deforestation and afforestation on land surface temperature. *Journal of Geophysical Research: Atmosphere, 121,* 14372-14386.

Li, Y., Zhao, M., Motesharrei, S., Mu, Q., Kalnay, E., & Li, S. (2015). Local cooling and warming effects of forests based on satellite observations. *Nature Communications, 6*(6603).

Li, Z.-L., Tang, B.-H., Wu, H., Ren, H., Yan, G., Wan, Z., . . . Sobrino, J. A. (2013). Satellite-derived land surface temperature: Current status and perspectives. *Remore Sensing of Environment, 131*, 14-37.

Luyssaert, S., Jammet, M., Stoy, P. C., Estel, S., Pongratz, J., Ceschia, E., . . . Dolman, A. J. (2014). Land management and land-cover change have impacts of similar magnitude on surface temperature. *Nature Climate Change, 4*, 389-393.

Maeda, E. E. (2019). R-script for the retrieval of TOMST microclimate data.

Maeda, E. E., & Hurskainen, P. (2014). Spatiotemporal characterization of land surface temperature in Mount Kilimanjaro using satellite data. *Theoretical and Applied Climatology, 118*, 497-509.

Maeda, E. E., Clark, B. J., Pellikka, P., & Siljander, M. (2010a). Modelling agricultural expansion in Kenya's Eastern Arc Mountains biodiversity hotspot. *Agricultural Systems, 103*, 609-620.

Maeda, E. E., Pellikka, P. K., Clark, B. J., & Siljander, M. (2011). Prospective changes in irrigation water requirements caused by agricultural expansion and climate changes in the Eastern Arc Mountains of Kenya. *Journal of Environmental Management, 92*(3), 982-993.

Maeda, E. E., Pellikka, P. K., Siljander, M., & Clark, B. J. (2010b). Potential impacts of agricultural expansion and climate change on soil erosion in the Eastern Arc Mountains of Kenya. *Geomorphology, 123*(3-4), 279-289.

Malhi, Y., Meir, P., & Brown, S. (2002). Forests, carbon and global climate. *Philosophical Transactions of the Royal Society A: Mathematical, Physical and Engineering Sciences, 360*(1797), 1567-1591.

Martínez, P. G., Perera, A. H., Peterson, U., & Iverson, L. R. (2018). Ecosystem Services from Forest Landscapes: An Overview. In A. Perera, U. Peterson, G. Pastur, & L. Iverson (Eds.), *Ecosystem Services from Forest Landscape.* Cham: Springer.

Mbow, C., Van Noordwijk, M., Luedeling, E., Neufeldt, H., Minang, P. A., & Kowero, G. (2014). Agroforestry solutions to address food security and climate change challenges in Africa. *Current Opinion in Environmental Sustainability, 6*, 61-67.

McClatchey, J. (2012). Regional and local climates. In H. Joseph (Ed.), *An Introduction to Physical Geography and the Environment* (pp. 157-182). Pearson Education Limited.

McIntosh, G., & Sharratt, B. S. (2001). Thermal properties of soil. *The Physics Teacher, 39*, 258-460.

McMillin, L. M. (1975). Estimation of Sea Surface Temperatures From Two Infrared Window Measurements With Different Absorption. *Journal of Geophysical Research, 80*(36), 5113-5117.

Meijaard, E., Abram, N. K., Wells, J. A., Pellier, A.-S., Ancrenaz, M., Gaveau, D. L., . . . Mengersen, K. (2013). People's Perceptions about the Importance of Forests on Borneo. *PLoS ONE, 8*(9).

Mendenhall, C. D., Shields-Estrada, A., Krishnaswami, A. J., & Daily, G. C. (2016). Quantifying and sustaining biodiversity in tropical agricultural landscapes. *PNAS, 113*(51), 14544-14551.

Meng, X., Cheng, J., Zhao, S., Liu, S., & Yao, Y. (2019). Estimating Land Surface Temperature from Landsat-8 Data using the NOAA JPSS Enterprise Algorithm. *Remote Sensing, 11*(2).

Mildrexler, D. J., Zhao, M., & Running, S. W. (2011). A global comparison between station air temperatures and MODISland surface temperatures reveals the cooling role of forests. *Journal of Geophysical Research, 116*(G3).

MoALF. (2016). *Climate Risk Profile for Taita Taveta. Kenya County Climate Risk Profile Series.* Nairobi: The Kenya Ministry of Agriculture, Livestock and Fisheries (MoALF).

Montanaro, M., Gerace, A., & Rohrbach, S. (2015). Toward an operational stray light correction for the Landsat 8 Thermal Infrared Sensor. *Applied Optics, 54*(13), 3963-3978.

Muimba-Kankolongo, A. (2018). *Food Crop Production by Smallholder Farmers in Southern Africa.* Elsevier.

Mwalusepo, S., Massawe, E. S., Affognon, H., Okuku, G. O., Kingori, S., Mburu, P. D., . . . Le Ru, B. P. (2015). Smallholder Farmers' Perspectives on Climatic Variability and Adaptation Strategies in East Africa: The Case of Mount Kilimanjaro in Tanzania, Taita and Machakos Hills in Kenya. *Journal of Earth Science & Cimatic Change, 6*(10).

Naharuddin, R., Wulandari, R., & Paloloang, A. K. (2018). Surface runoff and erosion from agroforestry land use types. *The Journal of Animal & Plant Sciences, 28*(3), 875-882.

Ndossi, M. I., & Avdan, U. (2016). Application of Open Source Coding Technologies in the Production of Land Surface Temperature (LST) Maps from Landsat: A PyQGIS Plugin. *Remote Sensing, 8*(5), 413.

Nemani, R., Pierce, L., & Running, S. (1993). Developing Satellite-derived Estimates of Surface Moisture Status. *Journal of Applied Meteorology, 32*, 548-557.

Niang, I., Ruppel, O. C., Abdrabo, M. A., Essel, A., Lennard, C., Padgham, J., & Urquhart, P. (2014). Africa. In V. R. Barros, C. B. Field, D. J. Dokken, M. D. Mastrandrea, K. J. Mach, T. E. Bilir, . . . L. L. White (Eds.), *Climate Change 2014: Impacts, Adaptation, and Vulnerability. Part B: Regional Aspects. Contribution of Working Group II to the Fifth Assessment Report of the Intergovernmental Panel on Climate Change* (pp. 1199-1265). Cambridge and New York: Intergovernmental Panel on Climate Change.

Nobis, M., & Hunziker, U. (2005). Automatic thresholding for hemispherical canopy-photographs based on edge detection. *Agricultural and Forest Meteorology, 128*, 243-250.

Ong, C. K., Black, C. R., & Muthuri, C. W. (2006). Modifying forestry and agroforestry to increase water productivity. *CAB Reviews: Perspectives in Agriculture, Veterinary Science, Nutrition and Natural Resources, 1*(65).

Paletto, A., & Tosi, V. (2009). Forest canopy cover and canopy closure: comparison of assessment techniques. *European Journal of Forest Research, 128*(3), 265-272.

Pellikka, P. K., Clark, B. J., Gosa, A. G., Himberg, N., Hurskainen, P., Maeda, E., . . . Siljander, M. (2013). Agricultural Expansion and Its Consequences in the Taita Hills, Kenya. In P. Paron, D. Olago, & C. T. Omuto, *Developments in Earth Surface Processes, Vol. 16* (pp. 165-179). Amsterdam: Elsevier.

Pellikka, P. K., Heikinheimo, V., Hietanen, J., Schäfer, E., Siljander, M., & Heiskanen, J. (2018). Impact of land cover change on aboveground carbn stocks in Afromontane landscape in Kenya. *Applied Geography, 94*, 178-189.

Pellikka, P. K., Lötjönen, M., Siljander, M., & Lens, L. (2009). Airborne remote sensing of spatiotemporal change (1955–2004) in indigenous and exotig forest cover in the Taita Hills, Kenya. *International Journal of Applied Earth Observation and Geoinformation, 11*(4), 221-232.

Pellikka, P., & Hakala, E. (2019). Climate change. In I. Vastapuu, M. Mattlin, E. Hakala, & P. Pellikka, *Megatrends in Africa* (pp. 7-14). Ministry of Foreign Affairs of Finland.

Pellikka, P., Seed, E. D., & King, D. J. (2000). Modelling Deciduous Forest Ice Storm Damage Using Aerial CIR Imagery and Hemispheric Photography. *Canadian Journal of Remote Sensing, 26*(5), 394-405.

Potter, K. A., Woods, H. A., & Pincebourde, S. (2013). Microclimatic challenges in global change biology. *Global Change Biology, 19*, 2932-2939.

Potts, S. G., Biesmeijer, J. C., Kremen, C., Neumann, P., Schweiger, O., & Kunin, W. E. (2010). Global pollinator declines: trends, impacts and driver. *Trends in Ecology & Evolution, 25*(6), 345-353.

Prata, A. J., Caselles, V., Coll, C., Sobrino, A., & Ottlé, C. (1995). Thermal Remote Sensing of Land Surface Temperature From Satellites: Current Status and Future Prospects. *Remote Sensing Reviews, 12*, 175-224.

Qin, Z., Karnieli, A., & Berliner, P. (2001). A mono-window algorithm for retrieving landsurface temperature from Landsat TM data and its application to the Israel-Egypt border region. *International Journal of Remote Sensing, 22*(18), 3719--3746.

Ridler, T. W., & Calvard, S. (1978). Picture Thresholding Using an Iterative Selection Method. *IEEE Transactions on Systems, Man, and Cybernetics, SMC-8*(8), 630-632.

Robinette, G. O. (1972). *Plants and their environmental functions.* Washington, D.C.: U.S. Department of the Interior.

Rogan, J., Ziemer, M., Martin, D., Ratick, S., Cuba, N., & DeLauer, V. (2013). The impact of tree cover loss on land surface temperature: A casestudy of central Massachusetts using Landsat Thematic Mapper thermal data. *Applied Geography, 45*, 49-57.

Rozenstein, O., Qin, Z., Derimian, Y., & Karnieli, A. (2014). Derivation of land surface temperature for Landsat-8 TIRS using a split window algorithm. *Sensors, 14*, 5768-5780.

Schleppi, P., Conedera, M., Sedivy, I., & Thimonier, A. (2007). Correcting non-linearity and slope effects in the estimation of the leaf area index of forests from hemispherical photographs. *Agricultural and Forest Meteorology, 144*(3-4), 236-242.

Schnell, S., Kleinn, C., & Ståhl, G. (2015). Monitoring trees outside forests: a review. *Environmental Monitoring and Assessment, 187*(9).

Simó, G., Martínez-Villagrasa, D., Jiménez, M. A., & Cuxart, J. (2018). Impact of the Surface–Atmosphere Variables on the Relation Between Air and Land Surface Temperatures. *Pure and Applied Geophysics, 175*, 3939-3953.

Smith, R. C., & Choudhury, B. J. (1991). Analysis of normalized difference and surface temperature observations over southeastern Australia. *International Journal of Remote Sensing, 12*(10), 2021-2044.

Thimonier, A., Sedivy, I., & Schleppi, P. (2010). Estimating leaf area index in different types of mature forest stands in Switzerland: a comparison of methods. *European JOurnal of Forest Research, 129*, 543-562.

Tran, D. X., Pla, F., Latorre-Carmona, P., Myint, S. W., Caetano, M., & Kieu, H. V. (2017). Characterizing the relationship between land use land cover change and land surface temperature. *ISPRS Journal of Photogrammetry and Remote Sensing, 124*, 119-132.

Unruh, J. D., Houghton, R. A., & Lefebvre, P. A. (1993). Carbon storage in agroforestry: an estimate for sub-Saharan Africa. *Climate Research, 3*, 39-52.

USGS. (2017). *Landsat 8 OLI and TIRS Calibration Notices*. Retrieved 17.2.2020, from https://www.usgs.gov/land-resources/nli/landsat/landsat-8-oli-and-tirs-calibration-notices

USGS. (2019). *Landsat 8 (L8) Data Users Handbook. Version 5.0.* Sioux Falls, South Dakota: Department of the Interior: U.S. Geological Survey.

Valor, E., & Caselles, V. (1996). Mapping land surface emissivity from NDVI: Application to European, African and South American areas. *Remote sensing of Environment, 57*(3), 167-184.

Van de Griend, A. A., & Owe, M. (1993). On the relationship between thermal emissivity and the normalized difference vegetation index for natural surfaces. *International Journal of Remote Sensing, 14*(6), 1119-1131.

van Leeuwen, T. T., Frank, A. J., Jin, Y., Smyth, P., Goulden, M. L., van der Werf, G., & Randerson, J. T. (2011). Optimal use of land surface temperature data to detect changes in tropical forest fover. *Journal of Geophysical Research, 116*(G2).

van Noordwijk, M., Bayala, J., Hairiah, K., Lusiana, B., Muthuri, C., Khasanah, N., & Mulia, R. (2014). Agroforestry Solutions for Buffering Climate Variability and Adapting to Change. In J. Fuhrer, & P. Gregory (Eds.), *Climate Change Impact and Adaptation in Agricultural Systems* (pp. 216-232). University of Reading.

Wanderley, R. L., Dominigues, L. M., Joly, C. A., & da Rocha, H. R. (2019). Relationship between land surface temperature and fraction of anthropized area in the Atlantic forest region, Brazil. *PLoS ONE, 14*(12).

Wang, L., Lu, Y., & Yao, Y. (2019). Comparison of Three Algorithms for the Retrieval of Land Surface Temperature from Landsat 8 Images. *Sensors, 19*(22).

Weng, Q., Lu, D., & Schubring, J. (2004). Estimation of land surface temperature–vegetation abundance relationship for urban heat island studies. *Remote Sensing of Environment, 89*, 467-483.

Wild, J., Kopecký, M., Maeck, M., Sanda, M., Jankovec, J., & Haase, T. (2019). Climate at ecologically relevant scales: A new temperature and soil moisture logger for long-term microclimate measurement. *Agricultural and Forest Meteorology, 268*, 40-47.

Wilson, M. H., & Lovell, S. T. (2016). Agroforestry - The Next Step in Sustainable and Resilient Agriculture. *Sustainability, 8*(574).

Zellweger, F., De Frenne, P., Lenoir, J., Rocchini, D., & Coomes, D. (2019). Advances in Microclimate Ecology Arising from Remote Sensing. *Trends in Ecology & Evolution, 34*(4), 327-341.

Zellweger, F., De Frenne, P., Lenoir, J., Vangansbeke, P., Verheyen, K., Bernhardt-Römermann, M., . . . Coomes, D. (2020). Forest microclimate dynamics drive plant responses to warming. *Science, 368*, 772-775.

Zhang, J., Wang, Y., & Li, Y. (2006). A C++ program for retrieving land surface temperature from the data of Landsat TM/ETM+ band 6. *Computers & Geosciences, 32*(10), 1796-1805.

Ziter, C. D., Pedersen, E. J., Kucharik, C. J., & Turner, M. G. (2019). Scale-dependent interactions between tree canopy cover and impervious surfaces reduce daytime urban heat during summer. *PNAS, 116*(15), 7575-780.

Zomer, R. J., Neufeldt, H., Xu, J., Ahrends, A., Bossio, D., Trabucco, A., . . . Wang, M. (2016). Global Tree Cover and Biomass Carbon on Agricultural Land: The contribution of agroforestry to global and national carbon budgets. *Scientific Reports*(6).

Zomer, R. J., Trabucco, A., Coe, R., Place, F., van Noordwijk, M., & Xu, J. C. (2014). *Trees on farms: an update and reanalysis of agroforestry's global extent and socio-ecological characteristics. Working Paper 179.* Bogor, Indonesia: World Agroforestry Centre (ICRAF) Southeast Asia Regional Program.

Appendices

Appendix 1. TOMST TMS-4 microclimate data that were used in this study, sensors 1–8.

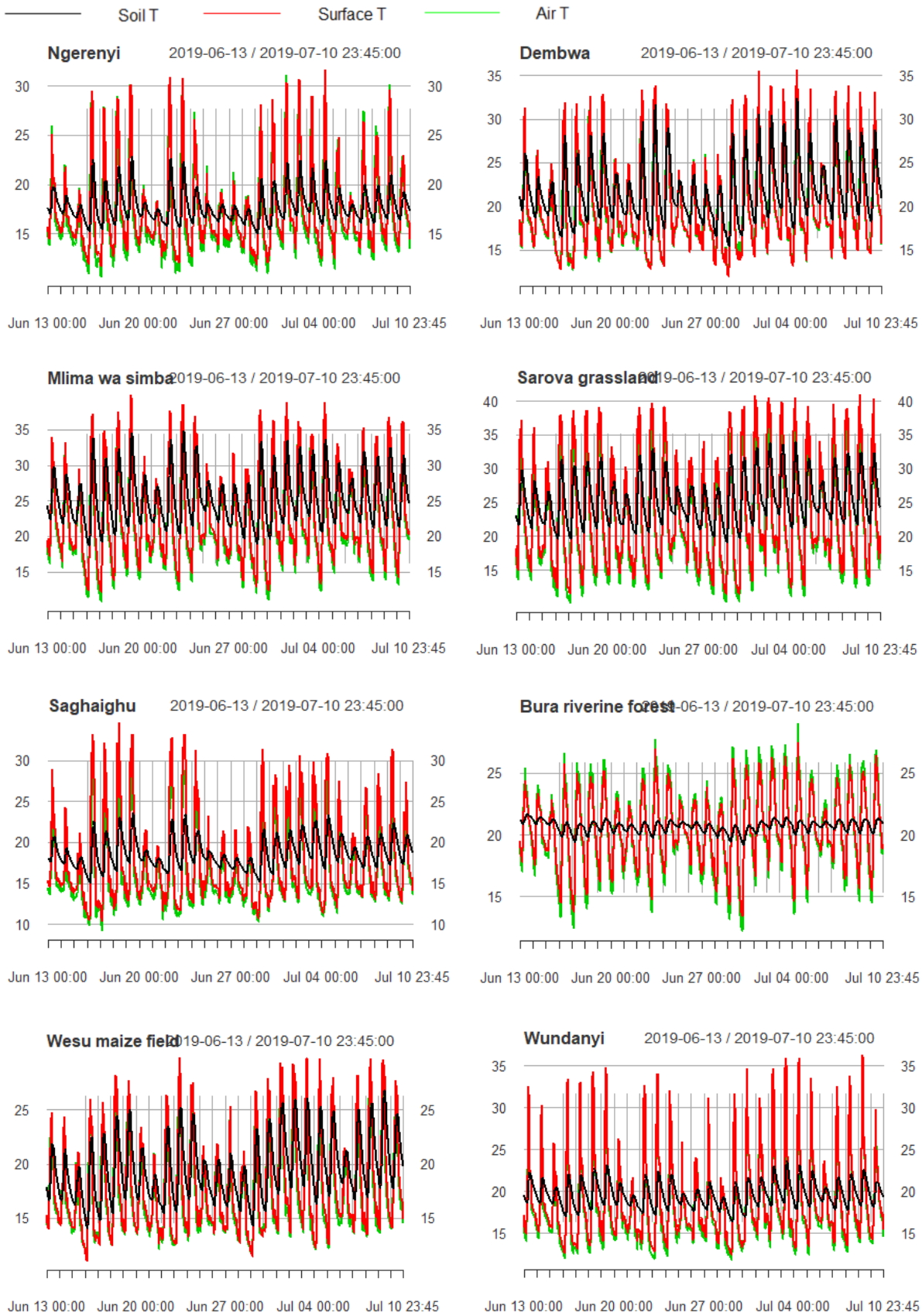

Appendix 2. TOMST TMS-4 microclimate data that were used in this study, sensors 9–16.

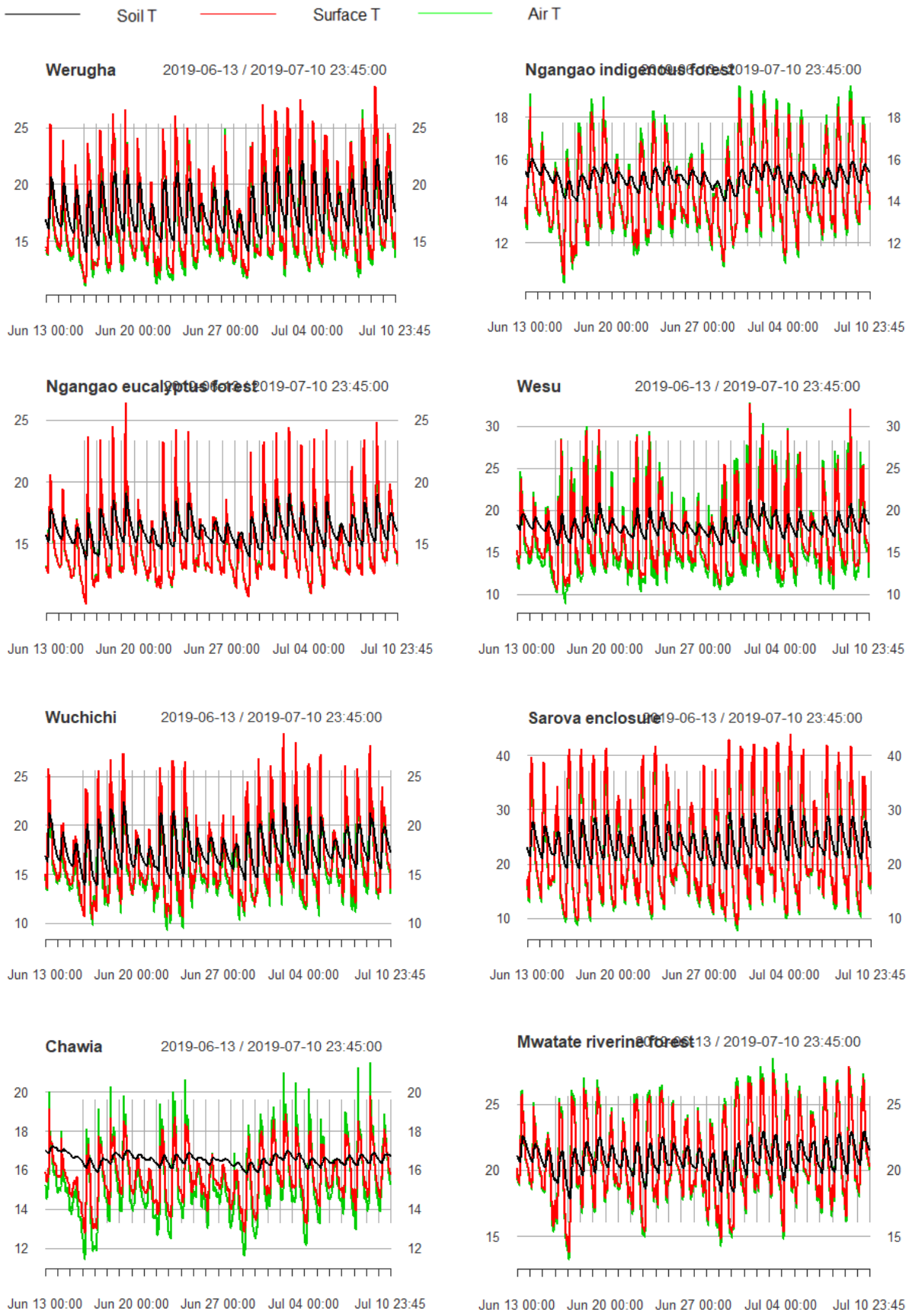

Appendix 3. TOMST TMS-4 microclimate data that were used in this study, sensors 17–19.